Extrudability of Particle-Reinforced Aluminium Metal Matrix Composites at Warm Working Temperatures (0.3 – 0.5 T_m)

Zizo Gxowa

Student number: 547981

A dissertation submitted to the Faculty of Engineering and the Built Environment, University of the Witwatersrand, in fulfilment of the requirements for the degree of Master of Science in Engineering**.**

Johannesburg, 2018

Declaration

I, Zizo Gxowa, declare that this is my own work and text that has been taken from other authors has been duly referenced. This work is being submitted for the degree Master of Science in Engineering (Metallurgy and Materials) to the University of the Witwatersrand, Johannesburg. It has not been submitted before for any degree or examination at any other university.

……..

Zizo Gxowa

January, 2018

Abstract

This work evaluates the warm temperature extrudability of aluminium Metal Matrix Composites (MMCs) and Metal Matrix Nano Composites (MMNCs) produced by powder metallurgy. Green and sintered compacts were produced by blending 2124-Al with Al_2O_3 (5 or 10 vol. %) or SiC (10 or 15 vol. %) powders in a high energy ball mill, cold *i.e.* ambient temperature compaction and sintering at 490°C for 1 hr. The deformation behaviour of unreinforced 2124-Al, MMC and MMNC green and sintered compacts was studied by performing uniaxial compression tests using a Gleeble 3500®, within the warm working temperature range (170 - 280°C). Strain rates of 0.01 and 5 s^{-1} were used and the total strain of 0.3 was kept constant. The Abaqus Finite Element modelling (FEM) programme was used to simulate an extrusion process using the results from the uniaxial compression tests as input data. The uniaxial compression test results and the FEM analysis were used to design a warm temperature extrusion process. These results were then validated by performing a laboratory scale extrusion experiment.

A more uniform distribution of reinforcing particles in the 2124-Al alloy matrix was achieved in the Al_2O_3 reinforced MMNCs than SiC reinforced MMCs. Cold compaction of the 2124-Al with 10 vol. % Al_2O_3 powder was unsuccessful as green compacts pressed from this powder fractured. This fracturing was attributed to poor bonding and plastic flow due to the higher density of Al_2O_3 particles on the surface of the 2124-Al powder. Alternate consolidation techniques, such as spark plasma sintering (SPS), were recommended for the 10 vol. % Al_2O_3 powder. Deformation behaviour improved significantly when sintered MMC compacts were uniaxially compressed at 280°C, a strain rate of 5 s^{-1} and a soaking time of 20 minutes. The best deformation, *i.e.* good ductility which is shown by a large plastic region and high flow stress, was achieved in the 2124-Al with 10 vol. % SiC MMC, as it plastically deformed at the highest stress (~153 MPa) up to the maximum strain of 0.3.

Extrudability of the unreinforced 2124-Al was good, while the 5 vol. % Al_2O_3 reinforced MMNC and SiC reinforced MMCs had poorer warm temperature extrudability, which was attributed to a lack of lubrication during extrusion. The MMCs and MMNC were more difficult to extrude than the unreinforced 2124-Al alloy because they have a higher resistance to deformation as a result of the harder, stiffer reinforcing particles which do not deform easily. The lack of lubrication could have made deformation of MMCs and MMNCs more difficult due to higher friction (increased resistance to deformation) and

reduced material flow. The desired good distribution of Al_2O_3 in 2124-Al achieved in blending was not maintained by cold compaction, uniaxial compression and extrusion. This indicated that an alternate processing route is required for the Al_2O_3 reinforced MMNCs. Distribution of SiC particles in 2124-Al with 10 vol. % SiC improved slightly due to uniaxial compression. It was observed that in some areas, SiC particles were reasonably dispersed inside slightly deformed 2124-Al grains; illustrating that deformation influenced the distribution of SiC particles in the aluminium alloy matrix. Analysis of small extruded portions of SiC reinforced MMCs showed that extrusion has the potential to improve distribution of SiC particles in 2124-Al grains. However, higher deformation is required to optimise the SiC distribution.

Dedication

This dissertation is dedicated to God and to my parents, Vuyisile and Zingisa Gxowa.

Acknowledgements

I would first of all like to acknowledge God for giving me strength and wisdom as I pursued this work. I am grateful for His grace that has been more than sufficient for me. His powerful hand was upon me at all times.

Thank you to the Council for Scientific and Industrial Research (CSIR) for affording me the opportunity to pursue a Master's degree, allowing me to use their lab facilities and for the financial support. I am truly grateful that I was chosen by the CSIR and that I was entrusted with this work. The opportunities to present my work to the staff as well as at conferences so that I could get constructive criticism also meant a lot and really helped me to improve my work. I am also grateful to the CSIR staff for all their support during the difficult times that I faced while pursuing this degree.

I really appreciate my supervisors, Dr L.H. Chown and Dr G. Govender, for their guidance and support. I am truly inspired by their work ethics, leadership styles and achievements. It was an honour to have been supervised by them. Their patience and willingness to help and advise at all times is much appreciated.

Thank you to Mr S.T. Camagu and Dr U.A. Curle for their support and assistance. Their willingness to help is truly appreciated. Thank you for always giving your very best to everything that I needed assistance with.

Thank you to the DST-NRF Centre of Excellence in Strong Materials for support, giving me access to the Gleeble when I needed it and all the learning opportunities through workshops and presentations that I was privileged enough to attend.

There are a lot of elements of this work that would not have been possible without the assistance of other people that were not directly involved in the project. Thank you to Miss L. Mahlatji for all the advice and assistance in the powder lab, and to Mr N. Mnguni for assistance with the cold compaction of the powders and training on use of the cold press. Thank you to Mr M. William for designing and overseeing the manufacturing of the compaction die. Thank you to Mr S. Masete for all the moral support and assistance with the hardness tester. Sincerest gratitude to Mr M. Bodunrin for his assistance with the uniaxial compression tests on the Gleeble. I am grateful that he took time out of his busy

schedule to assist me, especially his willingness to work with me even on weekends. Thank you to Mrs M. Jordaan for doing the Finite Element analysis (FEA). Thank you to Mr Filipe Pereira for designing and overseeing the manufacturing of the extrusion die. Thank you to Mr C. McDuling and Mr E. Guldenpfennig for carrying out the laboratory scale extrusion experiments. Finally, I would like to thank my family and friends for their support and encouragement.

Contributions from this study

1. Gxowa, Z., Camagu, S. T., Govender, G. & Pereira, M. F. (2015). Reinforcement of 2124-Al alloy with low micron SiC and nano Al_2O_3 via solid-state forming. In H. K. Chikwanda & S. Chikosha (Eds.), *Light Metals Technology Conference 2015* (pp. 172–178). Port Elizabeth, South Africa. TransTech Publications Ltd. http://doi.org/10.4028/www.scientific.net/MSF.828-829.172

2. Poster presentation titled: Solid-state forming of low micron SiC and nano Al_2O_3 MMCs and MMNCs at *CSIR 'Ideas that work' Conference* (October, 2015). This presentation was awarded the 'Best Master's Student Presentation' prize.

3. Gxowa, Z., Chown, L. H., Govender, G. & Curle, U. A (2016). Deformation behaviour of aluminium low micron MMCs and MMNCs at warm working temperatures (0.3- 0.5 T_m). *Journal of South African Institute of Mining and Metallurgy*, 116 (October), 963–968. http://doi.org/10.17159/2411-9717/2016/v116n10a11. The presentation of this paper at the *AMI Ferrous and Base Metals Development Network Conference*, Durban, 19-21 October 2016, was awarded the 'Runner-up for Best Student Presentation' prize.

4. Oral presentation at *annual DST-NRF Centre of Excellence (CoE) workshop* (May, 2017). Presentation title: Deformation of low micron MMCs and MMNCs at warm working temperatures (170-280°C), was awarded the 'Best Oral Presentation' prize.

5. Gxowa, Z., Chown, L.H. and Govender, G., Warm temperature (170-280°C) uniaxial compression of SiC reinforced 2124-Al MMCs. Full paper accepted for presentation at *MS&T 2017* conference in Pittsburgh, USA, October 2017.

Table of Contents

List of Figures

List of Tables

1 Introduction

Metal Matrix Composites (MMCs) are materials formed when an intermetallic compound, ceramic, metal or metallic alloy is embedded in a continuous metallic phase (Taya & Arsenault, 1989; Evans, *et al*., 2003). The metallic phase takes on the role of the ductile matrix and the phase embedded in it is the reinforcement (Tumanov & Portnoi, 1972). The matrix protects the reinforcement and keeps it in an established position, while the reinforcement enhances the mechanical and physical properties of the matrix (Agarwal *et al*., 2006). These mechanical and physical properties may include: hardness, strength and thermal stability (Srivatsan *et al*., 1991).

MMCs may be continuously reinforced with fibres, or discontinuously reinforced by dispersing particles or whiskers with higher hardness in the matrix (Tumanov & Portnoi, 1972; Tjong, 2000). In MMCs, the size of the reinforcement phase is in the micron-size range, *i.e.* >100 nm (Giannelis, 1992). When the size of the reinforcement is reduced to the nano-size range (*i.e.* 1-100 nm), the composite is referred to as a Metal Matrix Nano Composite or MMNC (Giannelis, 1992; Saravanan & Senthilvelan, 2015).

The techniques used to fabricate MMCs and MMNCs can be divided into two categories: solid state and liquid state techniques. The solid state techniques are powder metallurgy based processes, *e.g.* high energy ball milling and powder blending, and examples of liquid state forming of composites include infiltration and stirring techniques. Solid state techniques are more widely adopted due to the fact that a better distribution of reinforcing particles in the matrix is achieved. The major drawback with solid state techniques is high processing costs. Liquid state techniques are thought to be more economically viable when compared to solid state techniques due to fewer processing steps. The use of liquid state techniques as a fabrication method for MMCs and MMNCs has been hindered by poor distribution of reinforcing particles in the matrix due to poor wettability between the matrix and reinforcement (Aghajanian *et al*., 1991).

The automotive and aerospace industries took interest in MMCs and MMNCs due to the growing demand for lightweight and high performance materials (Mazen & Emara, 2004). MMCs and MMNCs have been considered as replacements for conventional metals and alloys because they have better stability at elevated temperatures, good strength-to-mass ratios, superior wear resistance, along with high stiffness and strength (Zhou *et al*., 1999).

Potential applications for MMCs and MMNCs in automotive and aerospace industries include: manufacturing of gudgeon pins, connecting rods, fan and compressor blades, cylinder linings, brake callipers, pistons and piston liners (Serafini *et al*., 1986; Moghadam *et al*., 2014). Research also shows that there is potential use for MMCs and MMNCs as packaging for electronics and in the manufacturing of bicycles and golf clubs (Sadanandam *et al*., 1992; Asadipanah & Rajabi, 2015). MMCs and MMNCs have potential use in various industries because their properties can be tailored for specific applications by altering parameters such as size, shape, distribution and amount of reinforcement in the matrix (Liu *et al*., 1994; Moghadam *et al*., 2014). The properties of composites are also influenced by the matrix microstructure and strength of interfacial bonds between the matrix and reinforcement (Park *et al*., 2001).

The mechanical properties of MMC and MMNC products are mainly influenced by the distribution of reinforcing particles in the matrix and the strength of the interfacial bonds between reinforcing particles and the matrix (Liang *et al*., 1992). Producing an even distribution of the reinforcement phase in the matrix is a challenge when fabricating both MMCs and MMNCs. In MMCs, the micron-sized reinforcing particles tend to settle on the grain boundaries and in MMNCs the nano-sized reinforcing particles form agglomerates (Borgonovo & Apelian, 2011; Casati & Vedani, 2014). In 2014, the Advanced Casting Technologies (ACT) research group from the Council for Scientific and Industrial Research (CSIR) successfully used a powder metallurgical processing route to fabricate MMCs (2124-Al with 10 or 15 vol. % SiC) and MMNCs (2124-Al with 5 or 10 vol. % Al_2O_3). The process was considered to be successful because metallographic evaluations showed that a fairly uniform distribution of reinforcing particles in the 2124-Al matrix was achieved. However, in this work, a few of the composites did not have a uniform distribution of the reinforcing particles in the matrix (Gxowa *et al*., 2015).

Secondary processing techniques, such as extrusion, may be used to improve the reinforcing particle distribution, thereby enhancing mechanical properties such as hardness and strength (Hirianiah *et al*., 2012). It is believed that the mechanism by which deformation processes improve the distribution of reinforcing particles in the matrix is plastic flow. During deformation, as plastic flow occurs, clusters of reinforcing particles may be broken up and the rearrangement of reinforcing particles may also take place since the reinforcing particles are embedded in the matrix and are therefore carried by the matrix as it flows (Campbell, 2010; Wang *et al*., 2010). Designing these secondary processing

techniques tends to be time consuming and costly, because the design phase encompasses experimental trials conducted in the laboratory and sometimes on an industrial scale (Wang *et al*., 2015). A thermomechanical simulator such as a Gleeble may assist with efficient and cost effective design of secondary processing techniques. A Gleeble can be used to understand the deformation behaviour of materials in bulk deformation processes and thus aid selection of process parameters such as temperature, strain, strain rate and load without having to carry out extensive laboratory or industrial scale experimental trials (Wang *et al*., 2015).

This work evaluates the warm temperature (170 - 280°C) extrudability of 2124-Al MMCs and MMNCs produced by powder blending in a high energy ball mill. The main focus is on the effective design of a warm temperature extrusion process using uniaxial compression tests performed on a Gleeble and how deformation achieved (in uniaxial compression and extrusion) affects distribution of reinforcing particles (Al_2O_3 or SiC) in the Al alloy matrix.

The main motivation for this work is that there are no MMC and MMNC industries in South Africa. The use of MMCs and MMNCs may be introduced to South Africa by demonstrating to industry that a reliable, robust and cost-effective fabrication process can be developed through careful selection of process parameters (Klimowicz, 1994).

1.1 Justification of the Research

The problem that this work considers is the non-uniform distribution of reinforcing particles in Metal Matrix Composites (MMCs) and Metal Matrix Nano Composites (MMNCs) produced by powder blending. The agglomeration of reinforcing particles is undesirable because it causes a non-uniform stress distribution in the composite, which leads to poor mechanical properties, including hardness, tensile strength and ductility (Hafizpour *et al*., 2011). The agglomerates are preferred sites for crack nucleation, making the composites susceptible to failure by intergranular or transgranular cracking (Sri *et al*., 2009). It is stated in literature that using a deformation process such as extrusion, can improve the distribution of the reinforcement in the matrix and strengthen the interfacial bonds between reinforcing particles and the matrix, ultimately enhancing mechanical properties such as hardness and strength (Tekmen *et al*., 2003). Extrusion is usually carried out at elevated temperatures (*i.e.* > 350°C) to increase plastic flow, and hence more deformation can be achieved (Saravanan & Senthilvelan, 2015). However, operating at

high temperatures has the disadvantages of high energy costs, reduced equipment and tool life, poor surface finish and low dimensional accuracy. These disadvantages mean that hot worked MMC and MMNC components are expensive and thus unattractive to industry.

Previous experimental work has been done by Gxowa *et al*. (2015) on extruding a MMC 2124-Al with 10% SiC compact at ambient temperature by reducing an initial diameter rod of 17 mm to 8 mm. The part failed before its entire diameter could be reduced. It was deduced that the mode of failure was intergranular cracking. The compact was partially extruded using a load of 250 kN, which was the maximum operating load of the press. This experiment showed that high loads are required to deform MMCs at ambient temperature, which may shorten the service life of the die set. Warm working (*i.e.* temperatures between 30 and 60% of matrix material melting point) has been shown to have some advantages over both cold and hot working (Rao *et al*., 1999; van Tyne, 2004).

Advantages of warm working over cold working include (Cavaliere, 2002):

- Less strain hardening – fewer annealing operations
- Increased plastic flow – lower loads are required
- Higher metal ductility.

Warm working has lower processing costs than hot working due to a lower energy requirement, longer equipment and tool life, and better dimensional accuracy and surface finish (Cavaliere, 2002). Hence, operating at warm working temperatures may lower processing costs while still producing high quality products (Jensrud, 1998). Therefore, this work explores the extrudability of 2124-Al MMCs and MMNCs at warm working temperatures (*i.e.* 30-60% of matrix phase melting point (Van Tyne, 2004))

Thermomechanical simulation and modelling can be used as a means to accurately simulate deformation processes such as extrusion. Important parameters such as temperature, strain and strain rate can be extracted from the simulation results and used to design, even optimize, deformation processes (Harris *et al*., 2004; Zhang *et al*., 2010). The costs incurred and errors made in experimental trials, on a laboratory and industrial scale, may be minimised if a thermomechanical simulator such as a Gleeble is used to evaluate the deformation behaviour of aluminium MMCs and MMNCs and also aid the study of the microstructural evolution which takes place during deformation (Harris et al., 2004). Metallographic evaluation is relevant because the final microstructure essentially determines mechanical and physical properties. Studying the deformation behaviour and

microstructural evolution which takes place during extrusion will make it possible to predict properties and also design MMCs (Ko & Yoo, 2000).

This work has practical and theoretical significance in that it may lead to successful warm temperature extrusion of MMCs and MMNCs, thus making MMC and MMNC products more attractive to industry. Moreover, it will improve the understanding of deformation behaviour of MMCs and MMNCs at warm working temperatures as well as show how deformation at warm working temperatures affects distribution of reinforcing particles in the Al alloy matrix.

1.2 Research Hypothesis

It is expected that aluminium MMCs and MMNCs produced by powder metallurgy can be extruded successfully at warm working temperatures when parameters such as temperature and strain rate are carefully selected with the assistance of a thermomechanical simulator such as a Gleeble 3500®.

1.3 Research Questions

1. Can Metal Matrix Composites (MMCs) and Metal Matrix Nano Composites (MMNCs) be extruded successfully at warm working temperatures?
2. What effects do temperature and strain rate have on the deformation behaviour of MMCs and MMNCs?
3. Which combination of deformation parameters (*i.e.* temperature and strain rate) will produce products with the best quality?
4. Can thermomechanical simulation using a Gleeble be used to successfully design an extrusion process with improved reinforcing particle distribution in the Al matrix?

1.4 Aims

The first aim of this work is to fabricate MMC (2124-Al + 10 or 15 vol. % SiC) and MMNC (2124-Al + 5 or 10 vol. % Al_2O_3) products with uniformly distributed reinforcing particles in the matrix. The second aim is to increase knowledge on the deformation characteristics of these MMCs and MMNCs within the warm working temperature range of 170 - 280°C.

1.5 Objectives

1. To use powder metallurgy to produce Metal Matrix Composite (MMC) and Metal Matrix Nano Composite (MMNC) compacts.
2. To use a Gleeble 3500® thermomechanical simulator to study the deformation behaviour of these MMCs and MMNCs and thus design a warm temperature extrusion process.
3. To use warm temperature extrusion to improve distribution of reinforcing particles in MMC and MMNC products.

1.6 Dissertation structure

This dissertation contains six chapters. The literature review is presented in Chapter 2 and is divided into three sections: Fabrication of MMCs and MMNCs via powder metallurgy, Extrusion of MMCs and MMNCs and Thermomechanical simulation. The experimental procedure is covered in Chapter 3. The results obtained are presented, analysed and discussed in Chapter 4. Conclusions drawn from this work are presented in Chapter 5 and recommendations are made in Chapter 6.

2 Literature Review

2.1 Overview

This chapter reviews literature pertaining to aluminium Metal Matrix Composites (MMCs) and Metal Matrix Nano Composites (MMNCs). It particularly focuses on the fabrication of MMCs and MMNCs using a powder metallurgical processing route, the extrusion of aluminium composites and the use of a thermomechanical simulator, such as a Gleeble 3500®, to study deformation behaviour.

The literature review shows that although extensive work has been done on aluminium composites produced by powder metallurgy, there are still some challenges in achieving a uniform distribution of reinforcing particles in the matrix. Many authors have reported the successful fabrication of aluminium composites, but none have been able to demonstrate repeatability and consistency of results by producing more than one successful blend of the same powder. This highlighted the need to demonstrate repeatability and blending consistency over a set of batches made from the same powders.

Most of the literature focuses on composites based on the 6000 series aluminium alloys. This illustrates that more work must be done on other types of aluminium alloy composites, particularly other heat treatable aluminium alloys such as the 2000 series aluminium alloys.

There is extensive literature on the extrusion of aluminium MMCs and MMNCs. However most of the extrusion processes were carried out at high temperatures, generally above 350°C where defects such as surface cracks were reported. Thus, there is a need to study the deformation behaviour of these composites at lower temperatures. In most of the studies, the extrusion process was preceded by heat treatment processes such as homogenisation, making experimental extrusion trials costly (Harris *et al*., 2004). Uniaxial compression tests performed on a Gleeble can be used to understand deformation behaviour of materials and thus assist in selecting suitable parameters to successfully deform the materials (Dieter, 1986). The use of a thermomechanical simulator such as a Gleeble to study deformation behaviour and then design an extrusion experiment was presented by Chen *et al*. (1996). They illustrated that the Gleeble allowed for quick studies on deformation behaviour to be done at lower cost and with less effort than if extrusion

trials had been performed. The results that they obtained from the Gleeble and extrusion experimental trials were comparable.

Overall, this literature review shows that while there is extensive knowledge on aluminium MMCs and MMNCs, there are still knowledge gaps to be filled, especially concerning the deformation behaviour of 2000 series aluminium alloy MMCs and MMNCs at warm working temperatures.

2.2 Fabrication of MMCs and MMNCs via powder metallurgy

2.2.1 Blending

Metal Matrix Composites and Metal Matrix Nano Composites can be manufactured by liquid, semi-solid or solid state processes (Lim *et al*., 1997; Koli, 2013). Vacuum filtration and ultrasonic-assisted casting are examples of liquid state processes (Borgonovo & Apelian, 2011). Casati & Vedani (2014) found that rheocasting can be used to fabricate MMCs and MMNCs via a semi-solid state processing route. Rheocasting is a casting process which utilises slurry materials (Lindroos & Talvitie, 1995). Powder metallurgy is the solid state technique that is used to fabricate composite materials (Liu *et al*., 1994). When liquid state and solid state techniques are compared it can be deduced that liquid state techniques may be less costly since they do not have as many process steps as solid-state techniques (Borgonovo & Apelian, 2011). Solid state processes are usually more complex and the powders are more difficult to handle but a better distribution of the reinforcement phase in the matrix is achieved with solid state techniques.

The powder metallurgy process can be divided into two stages: primary and secondary manufacturing (Liu *et al*., 1994). Koli (2013) viewed primary manufacturing as a three step process, where the first step is blending which is normally performed in a ball mill (Singh & Singh, 2014). Blending is followed by compaction and sintering. Compaction is normally done with a hot or cold isostatic press (Lu & Shi, 1994). Sintering conditions that have to be specified include atmosphere, temperature and time (Liu *et al*., 1994).

Extrusion is an example of secondary manufacturing (Liu *et al*., 1994). The uniform distribution of the reinforcement phase in the matrix contributes most to the properties of the composite (Nestler *et al*., 2011). The powder metallurgical processing route is recommended for its ability to achieve uniform distribution of the reinforcing particles in the matrix (Hirianiah *et al*., 2012).

Blending can be done wet or dry. Borgonovo & Apelian (2011) used a technique similar to wet milling to blend aluminium powder with 50 nm Al_2O_3 particles, while Liu *et al*. (1994) used a dry blending process in their work. In the wet blending process, Al_2O_3 was first mixed with pure ethanol to form a slurry, which was blended with the aluminium powder and dried at 150°C. Drying was followed by compaction and sintering at 620˚C (Borgonovo & Apelian, 2011). When the products from the wet blending process were analysed it was observed that there was significant agglomeration, which increased with a decrease in particle size (Borgonovo & Apelian, 2011). Liu *et al.* (1994) used SiC as the reinforcement where Borgonovo & Apelian (2011) used Al_2O_3. Liu *et al*. (1994) achieved a more uniform distribution of SiC particles in the aluminium matrix during the dry blending process than had been achieved by Borgonovo & Apelian (2011) using Al_2O_3.

The large amount of agglomeration that was encountered by Borgonovo & Apelian (2011) may have been due to poor wettability between Al_2O_3 and ethanol (Hashim *et al*., 1999), where the ethanol may have acted as a barrier causing poor wettability. It can be inferred that a dry blending process would achieve a better distribution of the ceramic particles in the matrix since there is direct contact between the powders, and the challenges associated with wettability are removed (Ravichandran & Dineshkumar, 2014).

We can deduce that the particle size plays a crucial role. A decrease in particle size increases the probability of forming agglomerates (Casati & Vedani, 2014), therefore giving the impression that there is an ideal particle size range.

The blending process is a crucial step in the fabrication of composites using solid state techniques (Yadav *et al*., 2012). The quality of the blend is dependent on parameters such as time, particle size distribution, size and proportion of grinding media in the mill as well as the speed that is used (Yadav *et al*., 2012). The blending process is driven by the amount of energy that is transferred by the grinding media to the powder (Yadav *et al*., 2012). These parameters have to be chosen carefully and monitored because they influence the energy transfer that takes place (Nestler *et al*., 2011).

Liu *et al*. (1994) supported the idea of manufacturing MMCs and MMNCs using a powder metallurgical processing route, and highlighted that certain factors had to be taken into consideration for the process to be successful:

- Powder selection.
- The size distribution and shape of the powder particles.

- Coating the reinforcement.

Powder selection is important because the quality of the starting powder ultimately affects the microstructure and thus the properties of the composite (Liu *et al*., 1994). The quality of the starting powder can be determined by looking at the shape and size of the particles. Spherical particles for the matrix powder are preferred over irregularly shaped particles because spherical particles can be processed with fewer difficulties. When compared to powders with spherical particles, powders with irregularly shaped particles have poorer compressibility and flowability, due to higher interparticle friction (Klar & Samal, 2007). Coarser particles are preferentially reduced and may also undergo plastic deformation as they come into contact with the grinding media (Nestler et al., 2011). This plastic deformation alters the shape of the particles (Yadav *et al*., 2012). From this we see how the size and shape work together as suggested by Liu *et al*. (1994).

Cold welding may also occur during blending, where particles adhere to one another and thus increase the relative size of the particles in the powder (Yadav *et al*., 2012). This may be a disadvantage because larger particles do not get embedded into the matrix as well as smaller particles (Nestler *et al*., 2011). It can also be argued that coarse particles may lead to a better distribution because they are less likely to form clusters and are more prone to fracture, resulting in finer particles after blending (Yadav *et al*., 2012). When selecting the powders it is also important to look at the chemical stability and cost of the powders (Liu et al., 1994). The wettability may be improved by coating the reinforcing particles with metals like titanium and nickel. This may, however, compromise the commercialisation of composite materials since added coatings increase the processing costs (Liu *et al*., 1994).

The good mechanical properties (*e.g.* hardness, strength and wear resistance) of MMCs and MMNCs can be attributed to strengthening mechanisms such as the load transfer effect (Casati & Vedani, 2014). The load transfer effect that is encountered in MMCs and MMNCs explains how they are able to withstand heavier loads than the unreinforced matrix (Casati & Vedani, 2014). According to the load transfer effect any external load that is applied to the MMC or MMNC is shared by the matrix and reinforcement (Ryu & Hong, 2000). The reinforcement is stiffer and stronger than the matrix and is thus expected to bear a larger proportion of the applied load.

The effect of reinforcement phase on hardness was investigated by Koli (2013) who used Al_2O_3 as the reinforcing material, and Singh & Singh (2014) who used 4 - 10% SiC in the

aluminium matrix. In both cases, a high energy ball mill was used but the grinding media differed: Al with Al_2O_3 powder was blended using tungsten balls while stainless steel balls were used for blending Al with SiC powder (Koli, 2013; Singh & Singh, 2014). Aluminium reinforced with Al_2O_3 was harder than unreinforced aluminium (Koli, 2013). Singh & Singh (2014) showed that hardness increased as the proportion of the SiC in the matrix increased.

The materials of the balls used for blending and their proportions in the ball mill jar are important as these affect the kinetics of the blending process (Yadav *et al*., 2012). It is preferable that the balls be made of dense materials such as tungsten carbide or steel for more efficient grinding. A ball to powder weight ratio of 10:1 was used by Yadav *et al*., (2012) for both ball materials. The proportion of the balls in the ball mill jar affects the quality of the resulting blend, so the correct amount of balls is required for good contact between the balls and the powder. If an excess number of balls is added, the balls will be too densely packed and will mostly collide with each other instead of the powder (Yadav *et al*., 2012) and may even contaminate the powder (Casati & Vedani, 2014).

In all the work that has been reviewed thus far, the matrix and reinforcement powders were mixed together before they were blended. A different approach was taken where aluminium powder (matrix material) was first milled in a high energy ball mill for five hours with stearic acid as a process control agent, with the Al_2O_3 reinforcement phase added at a later stage. The ball to powder ratio was 10:1 and a tungsten carbide grinding medium was used. Some micron-sized clusters formed, but the overall distribution of the Al_2O_3 particles in the aluminium matrix was satisfactory. There was also an 11% increase in hardness (Koli, 2013).

As cold welding is likely to occur during blending (Yadav *et al*., 2012) a process control agent such as stearic acid can be added to prevent cold welding (Casati & Vedani, 2014). Koli (2013) found that the uniform distribution of the reinforcement phase in the matrix could be attributed to the presence of stearic acid. The hardness may have been increased because the well-distributed Al_2O_3 particles hindered dislocation movement in the matrix (Casati & Vedani, 2014). With well-dispersed Al_2O_3 reinforcing particles there was more interaction between the Al_2O_3 particles and dislocations in the matrix (Koli, 2013).

Once the powders have been blended they can be consolidated into a desired shape using compaction (Ramesh & Senthilvelan, 2010).

2.2.2 Compaction

The primary stage of powder metallurgy has three steps: blending, compaction and sintering (Koli, 2013; Liu *et al.*, 1994). In all the work that has been reviewed and discussed thus far all three steps were used, but the focus has been on the influence of blending parameters on properties of the final product. It would also be beneficial to analyse compaction and sintering parameters and the effect that they have on the final product quality.

Once the powders have been blended they can be consolidated into the desired shape using compaction (Ramesh & Senthilvelan, 2010) by applying an external force (Kunin & Yurchenko, 1968). Uniaxial die compaction involves the use of rigid dies and a mechanical or hydraulic press to consolidate powder (Upadhyaya, 2002). Compaction may be performed at ambient temperature (cold compaction) while hot compaction is done at temperatures above ambient (Radomysel'skii & Serdyuk, 1970; Sundaresh, 2014).

The mass of powder to be compacted is poured into the die and the load is transmitted to the powder with the aid of a punch from a press. The powder consolidation occurs in stages during die compaction. The first stage involves particle rearrangement where powder particles slide past each other and move closer together due to the applied load (Yavuz, 1996). Interparticle distance decreases as particles continue to move and elastic deformation occurs as a result of the applied load. The yield point of the powder is exceeded due to continued application of the load and the particles are then plastically deformed. At the end of the compaction process the particles are bonded together mostly by plastic deformation, although some particles may still be elastically bonded to one another (Yavuz, 1996; Klar & Samal, 2007). The compacted parts are referred to as green compacts (Roy, 2014). The integrity of green compacts is influenced mainly by the pressing technique used, the presence of friction and powder characteristics (Rahman *et al.*, 2011).

There are two pressing techniques that can be used in die compaction; single- and double-action pressing. The major difference between these two techniques is the way the load is applied to the powder by the press (Oberacker, 2012), as illustrated in Figure 1.

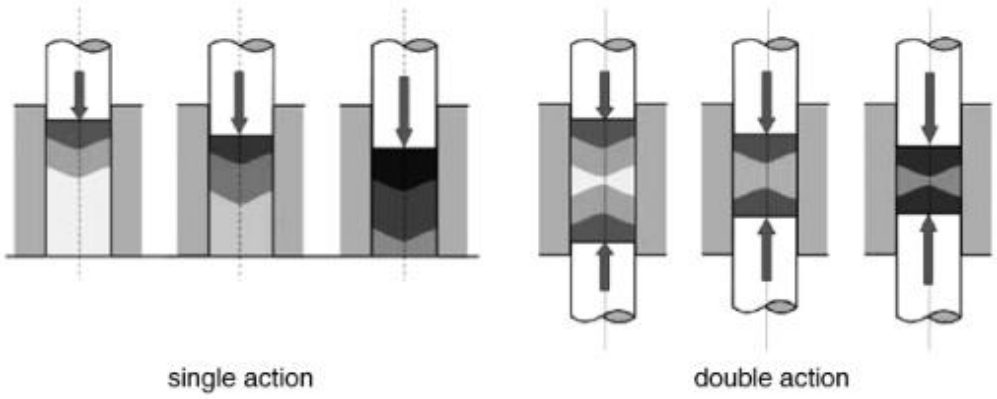

Figure 1: Single-action and double-action pressing techniques (Oberacker, 2012).

In single-action pressing the load is applied using the upper punch, while the die and lower punch do not move. In double-action pressing both punches move into a stationary die to apply the load to the powder. Green compacts produced by either single-action or double-action pressing have a non-uniform density distribution. Density decreases from top to bottom in green compacts produced by single-action pressing, whereas density is lower at mid-height in double-action pressing. Double-action pressing gives slightly better densification since the lowest density achieved by single-action pressing is always significantly lower than that achieved by double-action pressing (Upadhyaya, 2002; Selig, 2012). The non-uniform density distribution in green compacts produced by single-action and double-action pressing is shown in Figure 2.

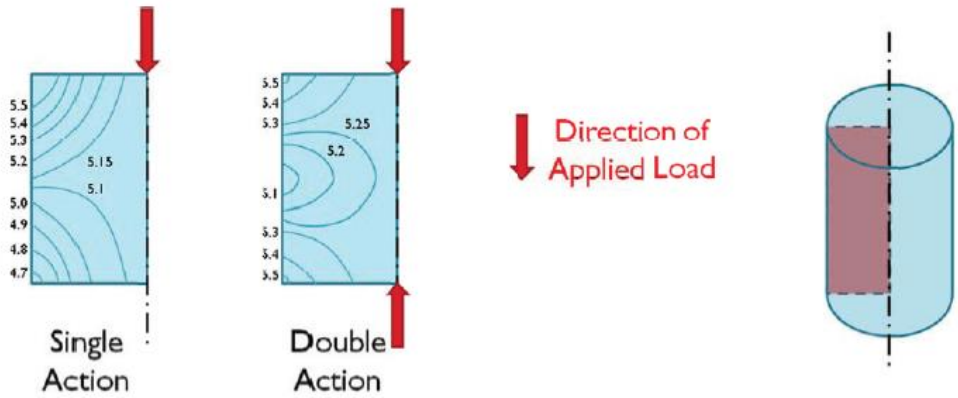

Figure 2: Non-uniform density distribution in green compacts produced by single-action and double-action pressing (German, 1994; redrawn by Selig (2012)).

Pressure gradients, caused by friction between the powder and the die walls, lead to non-uniform density distribution in green compacts (Glass & Ewsuk, 1995). The frictional

force opposes the applied force and decreases the amount of pressure transmitted to the powder for consolidation (Turenne *et al*., 1999).

The transmission of pressure in green compacts becomes poorer with an increase in height-to-diameter (H/D) ratio because of the adverse effect of friction on pressure transmission (Ozkan & Briscoe, 1997). Figure 3 shows how pressure varies across the length of green compacts with different H/D ratios.

Figure 3 shows that an H/D ratio of 0.42 gives a better pressure distribution across the length of the green compact than a ratio of 0.79 and an H/D ratio of 1.66 resulted in large variations in pressure across the length of the green compact. The pressure decreases from top to bottom as the applied pressure is opposed by the frictional force. The higher the H/D ratio, the more friction there is in the die to oppose the applied pressure. This explains why there is a more significant decrease in pressure from top to bottom in the green compact with a higher H/D ratio of 1.66 (Qangule, 2015; Ozkan & Briscoe, 1997).

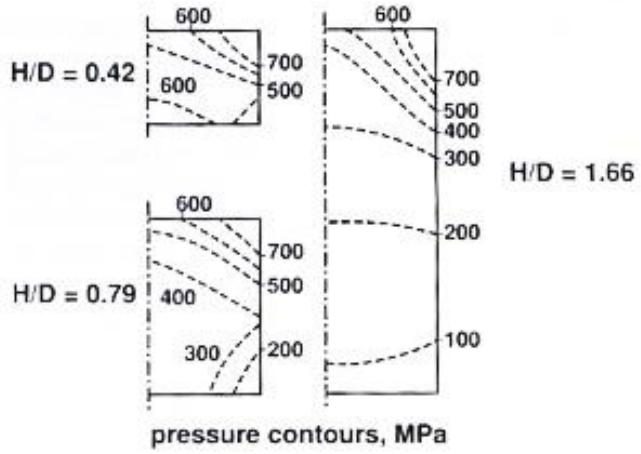

Figure 3: Pressure variations in green compacts with H/D ratios of 0.42, 0.79 and 1.66 (Qangule, 2015).

Lubricants are used to alleviate the adverse effects of friction during die compaction (Li *et al*., 2002). Interparticle friction (IPF) lowers the pressure transmitted to the powder for consolidation even further (Selig, 2012). Interparticle friction is influenced by powder characteristics such as particle size and shape (Hofmann & Bowen, 2011).

These powder characteristics can also influence compressibility. Compressibility can be defined as the extent to which a given pressure can increase the density of a powder (Heckel, 1961). Irregularly shaped particles and small particles are believed to have an adverse effect on compressibility because they increase interparticle friction and decrease

flowability (Klar & Samal, 2007). A powder with irregularly shaped particles has many interparticle contacts, *i.e.* a high co-ordination number, which increases friction. The voids between irregularly shaped particles are generally small and higher pressures are required to close these small voids. This issue is also experienced in powders with small particles because it is more difficult to collapse small pores. Spherical and larger particles have been reported to be easier to collapse due to lower interparticle friction and consequently lower compaction pressures are needed to consolidate the powders (Selig, 2012; Klar & Samal, 2007).

Particle size distribution also has an influence on the compressibility of powders. Powders with a mixture of different sized particles are said to result in better consolidation and higher green strength than mono-sized powders (Sundaresh, 2014). This can be attributed to the fact that better bonding is achieved, because smaller particles can fill the voids between coarser particles thus increasing the rate of densification. Porosity is also decreased significantly in powders with mixed particle sizes due to smaller particles filling voids and increasing the density of the powder.

The aim of compaction is to fabricate green compacts of high integrity. The integrity of green compacts is often compromised by defects such as cracks which can occur as the green compact is ejected from the die due to the release of stored elastic energy as well as breaking of weak interparticle bonds. The second stage of compaction results in elastic as well as plastic deformation. At the end of the compaction process the particles are predominantly plastically bonded but there are often still some elastic bonds (Campbell, 2013; Totten *et al*., 2002). Green compacts experience expansion (also referred to as springback) when the load is removed at the end of the compaction process due to the relief of elastic deformation. So during ejection of the green compact, cracking occurs when internal stresses are higher than the green strength (Totten *et al*., 2002).

Benbow (1983) stated that cracking can also be caused by ineffective die wall lubrication, die design and powder properties. Ineffective die wall lubrication increases friction which may lead to larger pressure gradients and non-uniform deformation. This creates weaker areas in compacts where interparticle bonds are weak, making these areas more susceptible to cracking (Benbow, 1983).

The reinforcement phase in MMCs or MMNCs makes consolidation more challenging (Long *et al*., 2014), as the reinforcing particles hinder movement of matrix particles.

During compaction, the stiffer reinforcement phase bears most of the pressure that is applied to the composite (Turner & Ashby, 1993). The composite therefore becomes difficult to consolidate because most of the applied pressure is supported by a stiff reinforcement phase that does not compact easily. This is known as the load transfer effect (Hesabi *et al*., 2007) which reduces plastic deformation in the matrix and lowers the achieved densification, since the rate of densification decreases.

Green compacts are then sintered to increase density and therefore the strength of compacts (Long *et al*., 2014).

2.2.3 Sintering

Sintering is a densification technique that normally follows cold compaction (Long *et al*., 2014). The sintering temperature is below the melting point of the matrix material (Borgonovo & Apelian, 2011). Sintering occurs in stages as shown in Figure 4 (De Jonghe & Rahaman, 2003).

During sintering the first process is neck formation (De Jonghe & Rahaman, 2003). Necks form faster if the interparticle distance in the compact is small, so sintering will be faster in compacts with particles that are closer to each other. Secondly, as sintering progresses, pore sizes are reduced due to continued growth of necks, and grain growth occurs by grain boundary diffusion (Angelo & Subramanian, 2009). During sintering, the strength of the compact increases due to a decrease in porosity (De Jonghe & Rahaman, 2003). The pores become more rounded as sintering progresses. Necks and grains continue to grow and the rate of densification finally slows down when most of the pores have collapsed. Very small pores which become difficult to close up often remain in the compact (Angelo & Subramanian, 2009).

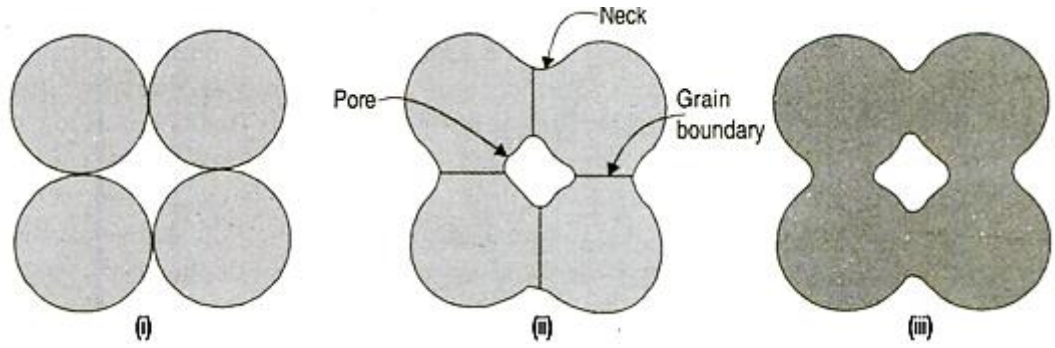

Figure 4: Stages of sintering: i) particle contact increases ii) formation of necks, grain boundary diffusion and reduction of pores iii) sintered part (Angelo & Subramanian, 2009).

Densification is achieved by decreasing the porosity, which may occur as a result of grain growth induced by diffusion of atoms. The relationship between sintering temperature and diffusion (Rahimian *et al*., 2009) is best described by Equation 1 (Butrymowicz *et al*., 1973):

$$D = D_o e^{(\frac{-Q}{RT})} \quad [1]$$

where: D is the diffusion coefficient,

D_o is the constant value (not influenced by temperature)

Q - Activation Energy required for diffusion to take place in kcal/mol

R- Gas constant in cal/K.mol

T- Temperature in K

In Equation 1 the diffusion coefficient is directly proportional to the sintering temperature which means that the densification improves as the sintering temperature is increased (Rahimian *et al*., 2009). As the temperature is raised the mobility of grains and grain boundaries improves, which ultimately leads to a decrease in porosity (Butrymowicz *et al*., 1973).

There are various studies which report that sintering has an effect on properties (*e.g.* density, hardness and strength) of composite materials. Zonta (2013) found that sintering had a positive effect on density, hardness and strength of Al/SiC composites. Al/SiC (5 or 10 wt. %) green compacts were sintered at 580°C and 620°C for 1 hr. It was found that there was an increase in density and hardness at both sintering temperatures. Bending strength improved by up to 80% when sintering temperature was increased from 580°C to 620°C (Zonta, 2013).

Guo *et al*. (1997) reinforced commercially pure (99.9%) aluminium powder with fly ash (5-20 wt. %), cold compacted the composite powder at 414 MPa and sintered at 600,625 and 645°C. The effect of sintering on density, hardness and compression strength was then evaluated. It was found that at 645°C the hardness of the composites was higher than that of the unreinforced aluminium. This increase in hardness was only observed between 0.5 and 2.5 hrs. It was thus concluded that at 645°C, sintering for longer than 2.5 hrs did not improve hardness. Guo *et al*. (1997) reported that volume fraction of fly ash in aluminium matrix also influenced the properties of the composites. The strength of composites

containing less than 10 wt. % of fly ash was low; even in the sintered condition (Guo *et al*., 1997).

The presence of reinforcing particles in the matrix affects sinterability of composite materials (Razavi-Tousi *et al*., 2011). Experiments were carried out where an Al with Al_2O_3 composite was sintered (Rahimian *et al*., 2009). The sintering temperature was between 500°C and 600°C and sintering time was set at a value between 30 and 90 minutes. It was observed that the densification and mechanical properties decreased with the size of reinforcing particles and an increase in sintering time reduced strength. Rahimian *et al*. (2009) showed that sinterability of the composite was not reduced at 550˚C even when sintering time was increased by 30 minutes. However, at 600˚C, the strength of the composite decreased and this worsened with an increase in sintering time. This result shows that to achieve the best quality in the final product, sintering time and temperature should be chosen carefully.

Sintered MMC and MMNC compacts may be extruded to produce products and improve distribution of reinforcing particles in the matrix (Hirianiah *et al*., 2012).

2.3 Extrusion of MMCs and MMNCs

Extrusion can be defined as a plastic deformation process where the cross-sectional area of a billet is reduced by applying a compressive force and forcing the billet to flow through a die hole with a smaller diameter. The extrusion process has been in existence for over a century and is a technique that is constantly evolving (Samanta, 1972). The different types of extrusion processes can be divided into two categories: *conventional* and *hydrostatic* extrusion. In conventional extrusion, the billet is pushed through the small die hole by applying a ram force directly to the billet, whereas in hydrostatic extrusion a fluid is used to apply pressure to the billet (Li *et al*., 2011). Hydrostatic extrusion is useful in the extrusion of brittle materials (Skiba *et al*., 2014).

The extrusion process can be performed at different temperatures. The *hot extrusion* process is carried out at high temperatures; approximately 50 - 75% of the matrix metal melting point in degrees Celsius (Hirianiah *et al.*, 2012). Extrusion is often performed at high temperatures due to the fact that there is more plastic flow at high temperatures thus more deformation is achieved (McQueen & Bourell, 1987). *Cold extrusion* is done at

temperatures between room temperature and 30% of the matrix metal melting point (in degrees Celsius) (Palumbo, 1998).

In *direct extrusion*, the applied force pushes the billet towards the die hole (Genders, 1954). The motion of the billet inside the container causes friction at the billet-container interface. The friction causes the material at the centre of the billet to flow through the die hole first because, unlike the material in contact with the sides of the container, its motion is not opposed by frictional forces. *Indirect extrusion* occurs when the billet and the container move simultaneously. Lower pressures are required in indirect extrusion due to the absence of friction forces (Sheppard *et al*., 1982). The extrusion process is often applied after primary processing to improve porosity, distribution of the reinforcing particles in the matrix material, bonding, mechanical and physical properties, as well as to refine the grain structure (Nair & Karamis, 2010).

The quality of the extruded part is influenced by many parameters which need to be understood and controlled, such as: temperature, speed, extrusion ratio and applied load (Saha, 2000). The extrusion temperature is an important parameter because it influences other process variables (Saha, 2000). When the extrusion temperature is increased, plastic flow in the billet is improved due to a decrease in flow stress, so the required load is lowered as deformation becomes easier. However, the integrity of extruded parts may be compromised if the extrusion temperature is too high. This is especially evident when extruding Metal Matrix Composites (MMCs) and Metal Matrix Nano Composites (Fard & Akhlaghi, 2007). Excessively high temperatures do not favour the required uniform particle distribution in the matrix, but cause accumulation of particles on the grain boundaries and banding. This phenomenon was observed by Fard & Akhlaghi (2007) when extruding a SiC reinforced aluminium alloy. The extrusion temperature was increased from 500°C to 550°C. At 550°C, the aluminium alloy began to partially melt at the grain boundaries and the SiC particles became suspended in the melted metal. The applied stress caused alignment of the SiC particles which then formed bands in the matrix material. This result suggests that increasing the extrusion temperature is advantageous only up to a certain critical temperature (Fard & Akhlaghi, 2007).

The extrusion temperature also affects the temperature distribution across the length of the billet. The thermodynamics in extrusion have to be understood because during the extrusion process heat is both generated and lost. The deformation and friction generate heat which is then lost to the container and surroundings. This heat may also be distributed

across the billet, thus causing heating of the billet. It is imperative that this heat generation is taken into account when the extrusion temperature is selected, otherwise the exit temperature of the billet may become too high (Saha, 2000). This may be detrimental to the die and tool life, causing the process costs to increase significantly if the equipment has to be replaced more frequently (Arif *et al*., 2003). Extremely high temperatures promote formation of defects such as surface cracks which may degrade the properties. Properties that may be affected include: hardness, tensile strength, ductility and fatigue resistance (Sheikh *et al*., 2002).

It is not enough to only understand the heat balance in the extrusion process but the process variables affecting the heat balance should also be identified and controlled, such as the extrusion ratio which is calculated using Equation 2 (Sellars, 1985):

$$r = \frac{A_0}{A_f} \qquad [2]$$

where: r is the extrusion ratio

A_o is the original area prior to extrusion in mm^2

A_f is the area after extrusion in mm^2

The extrusion ratio is used to give an indication of the reduction in area that will take place during an extrusion experiment (Dieter, 1986).When the extrusion ratio is large, the billet undergoes severe plastic deformation and more heat is generated due to deformation work. This means that the exit temperature may be increased by a large extrusion ratio (Saha, 2000). The extrusion speed also needs to be monitored. Productivity may be negatively affected by slow extrusion speeds (Dieter *et al*., 2003). The required load may be increased by slow extrusion speeds because the billet may cool down and become more difficult to deform due to poor plastic flow and an increase in flow stress. High speeds are also not recommended because they could cause the billet to overheat which may compromise the final properties of the extruded part due to surface defects. It can be inferred that there is a relationship between extrusion temperature, extrusion speed, extrusion ratio and applied load (Zhou *et al*., 2004). The extrusion process may be optimised if the relationships between these process parameters are understood.

The optimum extrusion conditions can be defined as the conditions that produce the best quality product in a given extrusion experiment. Experiments were carried out by Lieblich *et al*. (2006) where an aluminium alloy reinforced with 10 or 15 vol. % Al_2O_3 was extruded

using an extrusion ratio of 37:1. The extrusion speed was 0.3-12 $mm.s^{-1}$ at an extrusion temperature of 450°C. Lieblich *et al.* (2006) observed that the extruded parts contained blisters and this was attributed to lack of cleanliness of the Al_2O_3 particles. The mechanism by which the blisters formed was not adequately explained by the authors, thus work done by other researchers concerning the formation of blisters was consulted. It was found that blisters form as a result of entrapped air in the extruded part, mainly due to an uneven temperature distribution along the length of the billet (Perry *et al*., 1953). This result highlights the importance of temperature selection and control during extrusion.

Dasgupta *et al*. (2014) extruded an aluminium alloy reinforced with fine SiC particles between 300 and 350°C. The extruded billets were heated up to the selected extrusion temperature and then soaked. The soaking time was varied, the extrusion speed was monitored and an extrusion ratio of 10:1 was used. Dasgupta *et al*. (2014) determined the optimum extrusion temperature and speed as 350°C and 0.36 $mm.s^{-1}$ respectively. A soak time of 2 hours was optimum for this chosen condition (Dasgupta *et al*., 2014).

The final properties of the extruded part are highly influenced by the type of processing technique and the processing parameters used to fabricate the extruded material. This becomes apparent when the work done by Lieblich *et al*. (2006) is compared to that carried out by Pakdel *et al*. (2007) who used the same extrusion temperature as Lieblich *et al*. (2006) of 450°C. However, Pakdel *et al*. (2007) kept the extrusion speed constant at 1 $mm.s^{-1}$ while three extrusion ratios: 6:1, 12:1 and 18:1 were used (Lieblich *et al*. used 37:1). Pakdel *et al*. (2007) observed that all the extruded parts were of good quality and no blistering was detected on the surfaces of the extruded parts. The extrusion parameters improved the distribution of the reinforcement phase in the matrix, decreased the porosity and improved ductility. When comparing these two experiments, Pakdel *et al*. (2007) used lower extrusion ratios and speed which could have improved control of the process, explaining why blistering was averted, even though the same extrusion temperature was used. Common industrial practice is to operate at high extrusion ratios and speeds while keeping the temperature low (Torralba & Caruana, 1997). Production of high quality products via extrusion is highly dependent on finding a balance between extrusion temperature and speed (Dieter *et al*., 2003).

The application of a secondary process, such as extrusion, is advantageous since there is evidence of improved mechanical and physical properties such as hardness and porosity, particularly in the processing of MMCs and MMNCs (Hirianiah *et al*., 2012). Dasgupta *et*

al. (2010) and Ezatpour *et al*. (2013) performed extrusion of MMCs and in both cases an improvement in properties was observed. Table 1 shows process parameters used by Dasgupta *et al*. (2010) and Ezatpour *et al*. (2013).

Table 1: Process parameters used by Dasgupta *et al*. (2010)and Ezatpour *et al*. (2013) in extrusion experiments.

	Composite	
	Al with SiC Dasgupta *et al*. (2010)	Al with Al_2O_3 Ezatpour *et al*. (2013)
Vol. % of reinforcement in matrix material	10	5 or 7
Reinforcement particle size (μm)	10-20	~20
Extrusion temperature (°C)	350	500
Extrusion ratio	Not disclosed	1.56 or 1.77

The hardness of the Al + Al_2O_3 composite was 20% higher than that of the unreinforced aluminium alloy after extrusion (Ezatpour *et al*., 2013). Addition of SiC particles to the aluminium alloy increased hardness by 40% and extrusion improved the hardness of the Al with SiC MMC further by 10% (Dasgupta *et al*., 2010). A more uniform distribution of the reinforcement phase and a decrease in porosity was achieved in both cases. Ezatpour *et al*. (2013) found that a 50% reduction in porosity was attained in the Al composite with Al_2O_3 reinforcement. This decrease in porosity and increased interfacial bonding contributed to the increase in hardness. The improved distribution of the reinforcement phase in the matrix gave a more uniform distribution of hardness across the samples and also improved the yield and ultimate tensile strength in the Al with Al_2O_3 composite (Dasgupta *et al*., 2010; Ezatpour *et al*., 2013). There was a steady increase in yield strength with increase in volume fraction of Al_2O_3 in the Al with Al_2O_3 composite (Ezatpour *et al*., 2013). Uniformly dispersed reinforcing particles have a pinning effect on grain boundaries and impede dislocation movement. Plastic deformation is thus limited by the decreased mobility of grain boundaries and grains, the stress needed for deformation is increased and the yield strength increases (Zhang & Chen, 2006).

The damage caused by high temperature is avoided when cold extrusion is used. The main challenge encountered during cold extrusion is poor workability due to limited plastic flow as a result of high flow stress (Zhang & Chen, 2006). Workability was improved by performing cold extrusion in steps where the extruded materials were subjected to intermediate heat treatment processes (Jiang & Dodd, 1995). A 2124-Al with SiC MMC

was subjected to an overageing heat treatment to improve its ductility before extrusion. The extrusion process was carried out in three steps where the composite was subjected to a heat treatment process after the first and second extrusion steps to improve ductility and thus workability. It was concluded that it is possible to plastically deform MMCs at low temperatures (Jiang *et al*., 1995).

Several authors have reported an increase in mechanical properties such as hardness and an improvement in distribution of reinforcing particles in matrix due to extrusion. Designing extrusion experiments tends to be time consuming and costly, because the design phase encompasses experimental trials conducted in the laboratory and sometimes on an industrial scale (Wang *et al*., 2015). A thermomechanical simulator such as a Gleeble may assist with efficient and cost effective design of an extrusion process. A Gleeble can be used to understand the deformation behaviour of materials in bulk deformation processes and thus aid selection of process parameters such as temperature, strain, strain rate and load without having to carry out extensive or industrial scale experimental trials (Wang *et al*., 2015).

2.4 Thermomechanical simulation

Designing metal forming processes such as extrusion involves laboratory scale or commercial plant trials which are costly, disruptive and time consuming. These metal forming processes can be designed more economically with the aid of a thermomechanical simulator such as a Gleeble (Harris *et al*., 2004). The Gleeble can perform physical simulations of material behaviour under various loads, temperatures, strains and strain rates (Norris & Wilson, 1999).

Uniaxial compression tests performed on a Gleeble can be used to understand deformation behaviour of materials and thus assist in selecting suitable parameters to successfully deform materials (Dieter, 1986).

Zhang *et al*. (2010) studied the deformation behaviour and microstructures of an Al composite with 15% SiC by performing compression tests on a Gleeble 1500® between 440 and 500°C. Strain rate was varied between 0.001 and 1 s^{-1}. It was observed that temperature had a similar effect on flow stress at all strain rates where the flow stress decreased with an increase in temperature. All the stress-strain curves seemed to follow the same trend where the stress increased with an increase in strain up to a maximum value (shown by a peak) followed by a sharp decrease and then deformed at a constant, lower

stress as strain continued to increase. In this study it was also found that the flow stress was directly proportional to strain rate since it increased as strain rate increased. At a temperature of 440°C, the maximum true stress of the composite increased from approximately 11 MPa to 29 MPa when the strain rate increased from 0.001 to 0.01 s^{-1}. This maximum stress was found to be even higher (~78 MPa) at a strain rate of 1 s^{-1}. This result was attributed to increased work hardening at higher strain rates.

Dynamic recovery (DRV) and dynamic recrystallisation (DRX) are softening mechanisms that occur when metals and alloys are deformed at elevated temperatures (Reti, 1970). DRV occurs through the annihilation of dislocations while DRX involves the formation of new grains (Reti, 1970; Humphreys & Hatherly, 1995). These new grains nucleate predominantly from pre-existing grain boundaries (Hallberg *et al*., 2010). DRV and DRX cause a decrease in flow stress and counteract the work hardening which takes place during deformation (Dieter *et al*., 2003).

Figure 5 shows typical stress-strain curves obtained when materials have undergone strain hardening under cold deformation as well as dynamic recovery and dynamic recrystallisation during hot deformation. The curve illustrating behaviour during DRV shows that there is initially an increase in stress with an increase in strain until a maximum stress is reached and the stress then remains constant as strain continues to increase. The initial increase in stress is attributed to strain hardening and as deformation proceeds the dislocation density increases. In hot deformation processes the increase in dislocation density is counteracted by DRV and the point where stress is constant is indicative of strain hardening and DRV being at equilibrium (Guo-zheng, 2013). A higher softening rate during dynamic recrystallisation leads to a decrease in stress from a maximum value (Tisza, 2002). The decrease in stress is attributed to the fact that the work hardening rate loses its ability to counteract the softening due to DRX, thus softening by DRX dominates the deformation process (Tisza, 2002).

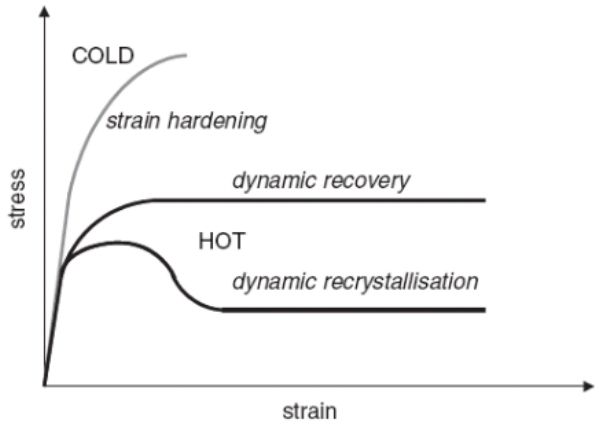

Figure 5: Typical stress-strain curves obtained during cold and hot deformation, showing different flow stress responses (Guo-zheng, 2013).

The increase of flow stress with an increase in strain rate is not a trend which is unique to Al with SiC composites since the same trend was identified by Yang *et al*. (2012) when they studied the deformation behaviour of an Al with Al_2O_3 composite. Uniaxial compression tests on a Gleeble 1500® were done at temperatures of 360 - 480°C and strain rates of 0.00 – 1 s^{-1} (Yang *et al*., 2012). The effect of strain rate on flow stress was similar to what was found by (Zhang *et al*., 2010), where flow stress increased with an increase in strain rate.

Stress-strain curves for an aluminium composite with 5% Al_2O_3 also suggested that dynamic recovery (DRV) occurred between 360 and 440°C within a strain rate range of 0.001- 0.01 s^{-1}. At a higher temperature of 480°C, microstructures revealed partial crystallisation in the composite. The term 'partial crystallisation' was used to highlight that only some of the grains recrystallised and this was attributed to the fact that the time that the composite was exposed to the deformation conditions was not enough to result in full recrystallisation. The stress-strain curves at 480°C showed a sharp decrease after peak stress was reached and this result was thought to be due to the inability of work hardening effects to balance the dynamic softening that was taking place. The sharp decrease after peak stress worsened with an increase in strain rate and at a strain rate of 0.001 s^{-1} the decrease was the least. Yang *et al*. (2012) concluded that the optimum temperature and strain rate were 480°C and 0.001 s^{-1} respectively (Yang *et al*., 2012). Figure 6 shows the stress-strain curves obtained by Yang *et al*. (2012) at 480°C.

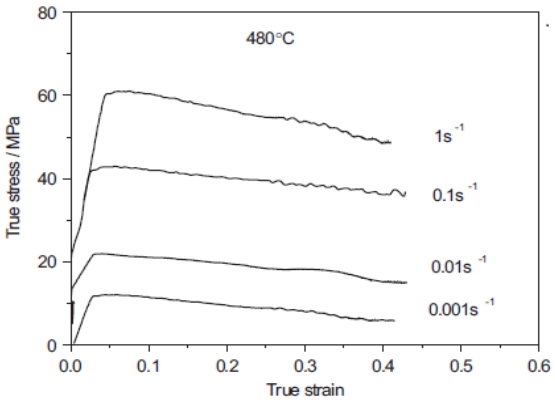

Figure 6: Deformation behaviour of an Al + 5% Al_2O_3 composite at 480°C (Yang *et al*., 2012).

Results obtained from uniaxial compression tests performed on a 2024-Al with 35% SiC composite using a Gleeble 1500D® thermomechanical simulator showed that flow stress was significantly affected by deformation temperature and strain rate. At a constant temperature, the flow stress increased with an increase in strain rate while an increase in deformation temperature decreased flow stress. Hao *et al*. (2014) noted this as 'typical behaviour of metals deformed in hot working conditions and since a similar trend was identified by Zhang *et al*. (2010 and Yang *et al*. (2012) in previous years this statement had some merit. Hao *et al*. (2014) also did a metallographic evaluation on the deformed samples and found defects on compacts deformed at 350°C and strain rate of 0.1 s^{-1}. These defects were in the form of voids due to debonding at particle-matrix interfaces as well as particle fracture (Figure 7). An increase in temperature worsened the defects because particle fracture and void formation were also observed at 450°C (Hao *et al*., 2014).

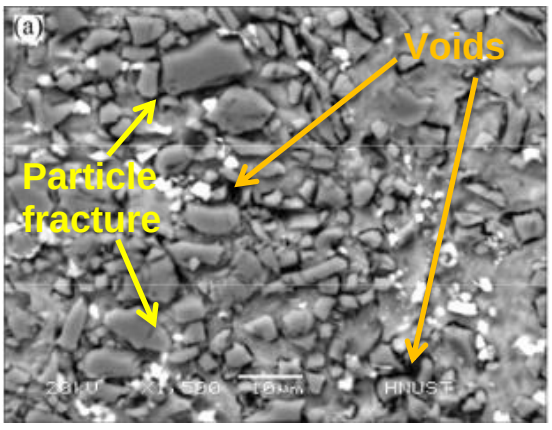

Figure 7: Particle fracture and void formation at 350°C, strain rate of 0.1 s^{-1} (Hao *et al*., 2014).

It was learned that a good combination of processing conditions had to be found in order to produce defect-free compacts and at 450°C and strain rate of 1 s^{-1} it was observed that the

compacts deformed without any particle fracture. The integrity of these compacts was further improved by increasing the temperature to 500°C (Hao *et al*., 2014).

It has been found that during deformation softening in materials can also occur by other mechanisms such as void nucleation, cracking, particle bonding and adiabatic heating (Fleck *et al*., 1989). These softening mechanisms, unlike DRV and DRX, are undesirable as they lead to microstructural damage which often causes failure *(*Prasad *et al.*, 2015). Void nucleation and cracking cause softening because they reduce the load bearing capacity of the deforming material; thus reducing flow stress (Zhang & Di, 2016). In composite materials void nucleation and cracking may occur during deformation, particularly at high strain rates, since the ductile matrix undergoes plastic deformation while the stiffer reinforcement phase does not (Ahamed & Senthilkumar, 2012). This may lead to debonding at the matrix-reinforcement interface; thus forming voids. In some instances, when the overall stress reaches a critical value, the reinforcement in the matrix may crack and these cracks create areas of weakness in the material; ultimately resulting in softening in the material (Shi *et al*., 2014). Adiabatic heating occurs when deformation is carried out at high strain rates because heat is generated due to deformation work and there is insufficient time for heat transfer to take place (Olson *et al*., 1982). This means that there is an increase in temperature in regions where plastic deformation has taken place. This temperature increase due to adiabatic heating leads to softening because it reduces resistance to deformation since dislocation movement become easier (Shi *et al*., 2014). All these softening mechanisms are potentially detrimental ,thus undesirable, because they result in microstructural damage and inhomogeneities; making the material susceptible to failure (Prasad *et al*., 2015).

According to Dieter (1986) the workability of a material can be described by showing relationships between the flow stress of a material and processing parameters such as strain rate, temperature and strain as well as studying the failure mechanisms and metallurgical transformations in the material (Dieter, 1986). Uniaxial compression tests performed on a Gleeble are suitable for designing deformation processes such as extrusion because the results obtained from these tests show how flow stress is influenced by parameters such as strain, strain rate and temperature. The microstructural evolution during deformation can also be evaluated by performing metallographic evaluations on the deformed samples. These uniaxial compression tests can give sufficient information on the workability of a material.

Chen *et al*. (1996) evaluated the effectiveness of using a Gleeble 1500® to design an extrusion process for MMCs. The MMCs were 6061-Al reinforced with 20 vol. % SiC (4µm) and 6082-Al containing 20 vol. % Al_2O_3 (30µm). The extrusion ratios used were 22:1 and 39:1. A homogenisation heat treatment was performed at 565°C for 2 hours before uniaxial compression-flow stress testing was done using a Gleeble. The test temperatures were in the range of 400 - 525°C and four strain rates were used: 0.05, 0.1, 1.0 and 10 s^{-1}. Interfacial friction and barrelling were minimised by placing a piece of graphite foil between the anvil and the specimen. This graphite foil also ensured that the temperature distribution in the specimen was uniform. A chromel-alumel thermocouple was used for temperature control and the true flow stress was acquired by dividing the applied force with the cross sectional area of the specimen. A slight temperature increase was observed at a higher strain rate of 10 s^{-1} and this was attributed to heat generated by deformation work (Chen *et al*., 1996).

The results obtained from the physical simulations performed using a Gleeble were used to design an extrusion process. Experimental extrusion trials, on a laboratory and industrial scale, were carried out. The presses for the laboratory and industrial scale extrusion trials had capacities of 100 and 3000 tons respectively. The billets for the laboratory trials had a diameter and length of 51 mm and 88 mm respectively while those for the industrial scale trial had a diameter of 184 mm and were 305 mm in length. In the laboratory trials, the billets were heated up to 467°C in a muffle furnace, transferred to an extrusion container which was heated up to 500°C and then extruded using an extrusion ratio of 30:1. Lower temperatures were used in the industrial trial: the billets were heated up to 429°C in a continuous gas-filled furnace and the extrusion container and die were heated up to 425°C and 336°C respectively. A slightly higher extrusion ratio of 33:1 was used (Chen *et al*., 1996).

A temperature increase due to the heat of deformation was observed in both cases. The temperature increase in the industrial scale trials was ~76°C and a lower increase of ~23°C was found in the laboratory scale trials. When the results obtained from the Gleeble and experimental trials were compared it was found that (Chen *et al*., 1996):

- The results were similar during the upsetting stage, however, a slight deviation of less than 10% was observed at higher loads in the experimental trials.

- The physical simulations showed that there was an increase in load at the end of the upsetting stage, which was confirmed by the experimental trials, but this load increase occurred much faster on the Gleeble.
- The Gleeble overestimated the billet temperature after the peak load was achieved, by 3%.
- Cracks were identified on the billets during the experimental trials and disappeared when the extrusion was done at higher speeds.
- Only half the capacity of the 3000 tonne press was used for the extrusion process.
- When the temperature increased from 470°C to 490°C at a strain rate of 14 s^{-1} the flow stress increased from 73 MPa to 82 MPa.

The work of Chen *et al*. (1996) showed that the Gleeble can be used to design an extrusion process. However, there are still some knowledge gaps that need to be filled since their work focused on hot (high temperature) extrusion and only one volume fraction of reinforcement in the matrix. It would be worthwhile to study the deformation behaviour of aluminium composites at lower temperatures since hot working seems to be the norm.

Overall this literature review shows that there is extensive knowledge on aluminium MMCs and MMNCs but there are still some knowledge gaps to be filled, especially concerning the deformation behaviour of 2000 series aluminium alloy MMCs and MMNCs at warm working temperatures.

3 Experimental Procedure

3.1 Overview

Experimental work was done to evaluate the warm temperature extrudability of aluminium Metal Matrix Composites (MMCs) and Metal Matrix Nano Composites (MMNCs) produced by powder metallurgy. The final properties of composite materials are influenced by the fabrication process (Park *et al*., 2001). The powder metallurgical process consisted of three steps: blending in a high energy ball mill, cold (*i.e.* ambient temperature) compaction and sintering.

Metallographic evaluations using optical and scanning electron microscopes (SEM) showed the microstructural evolution of the unreinforced 2124-Al alloy, SiC reinforced MMCs and Al_2O_3 reinforced MMNCs during each process step.

Challenges were encountered with cold compaction of both unreinforced 2124-Al alloy powder and blended, *i.e.* MMC and MMNC, powders. The green compacts fractured into thin, nearly horizontal slices during compaction. This fracturing was attributed to natural ageing of the powder due to long term storage. The unreinforced 2124-Al and blended powders were overaged at 350°C for 2 hours to reverse any natural ageing that may have occurred. Green compacts were successfully cold compacted from the heated treated powder, except those made from 2124-Al with 10% Al_2O_3. It was inferred that alternate consolidation techniques, such as spark plasma sintering (SPS), have to be explored for the 2124-Al with 10% Al_2O_3 powder. A Differential Scanning Calorimetry (DSC) study was done on the unreinforced 2124-Al and blended materials. It was found that the warm working temperature range for the unreinforced 2124-Al and the blended materials was between 168 and 336°C. The DSC results also assisted in selecting a sintering temperature, and the compacts were sintered at 490°C for 1 hour.

The deformation behaviour of unreinforced 2124-Al, MMCs and MMNC (*i.e.* 5 vol.% only) within the warm working temperature range, was studied by performing uniaxial compression tests (on green and sintered compacts) at temperatures of 170 - 280°C and strain rates of 0.01 and 5 s^{-1} using a Gleeble 3500®. Results from the uniaxial compression tests were used to simulate an extrusion process using Abaqus version 6.14 FEM (Finite Element Modelling) programme. Laboratory scale extrusion trials were then carried out using an Instron® press to validate results obtained from uniaxial compression and FEM.

3.2 Materials

The materials that were used in this work are 2124 aluminium (Al) alloy powder (45-90 µm), low micron sized (1-10 µm) SiC powder and nano-sized (40-70 nm) Al_2O_3 powder.

3.3 Research instruments

A Simoloyer CM-01® 2L horizontal high energy ball mill was used to blend the aluminium alloy (2124-Al) with reinforcing powders (Al_2O_3 or SiC). The grinding media was 5 mm steel balls in a 2l steel jar. The powders (as-received and blended) were stored in plastic containers and a spatula and small funnel were used to transfer the powders from the plastic containers to the milling jar. A balance was used to weigh the powders and steel balls for blending. After blending, the contents of the milling jar was emptied out into a laboratory test sieve with a pan placed underneath it to separate the steel balls. The powder was then transferred to a plastic container using a spatula.

A Leica DM15000M® optical microscope was used to examine the microstructures of green and sintered compacts. A Jeol-6510® scanning electron microscope (SEM) was used to characterise the as-received and blended powders as well as to analyse the deformed samples.

A Microtrac Bluewave® particle size and shape analyser, together with the SEM, was used to characterise the powders. An Enerpac VLP® 100 tonne hydraulic press and an 8 mm diameter die set made from high speed steel (HSS) were used to compact the unreinforced Al alloy and the blended powders to form green compacts. The limitation of the Enerpac press is that the powders can only be pressed at ambient temperature and the maximum applied pressure is dependent on die diameter. For example, the maximum allowable gauge meter reading for a die with an 8 mm diameter is 70 bars. A gauge meter reading of 70 bars means that a maximum pressure of 1989.44 MPa can be applied by the anvil on the powder during compaction. The results obtained from this press were still valuable in that the behaviour of 2124-Al alloy and blended powders during compaction could still be studied.

Thermal properties of unreinforced Al alloy and blended powders were studied using a Netzch STA 44F3 Jupiter® simultaneous thermal analyser and a muffle furnace was used to sinter some of the green compacts. Uniaxial compression tests were performed using a Gleeble 3500®. The compacts were mounted with black Bakelite powder using a mounting

press and an automatic polisher was used to prepare the samples for metallographic evaluation and hardness testing.

Hardness tests were performed after sintering, uniaxial compression and extrusion using a Future-Tech Vickers microhardness tester FM-700®. The extrusion laboratory experiments were performed using a die made out of W302 hot work steel and an Instron® press. The densities of the green compacts, sintered compacts, uniaxially compressed samples and extrusion products were measured with the aid of an Ohaus Explorer® density kit by applying Archimedes' principle.

3.4 Method

Figure 8 shows the experimental procedure that was followed.

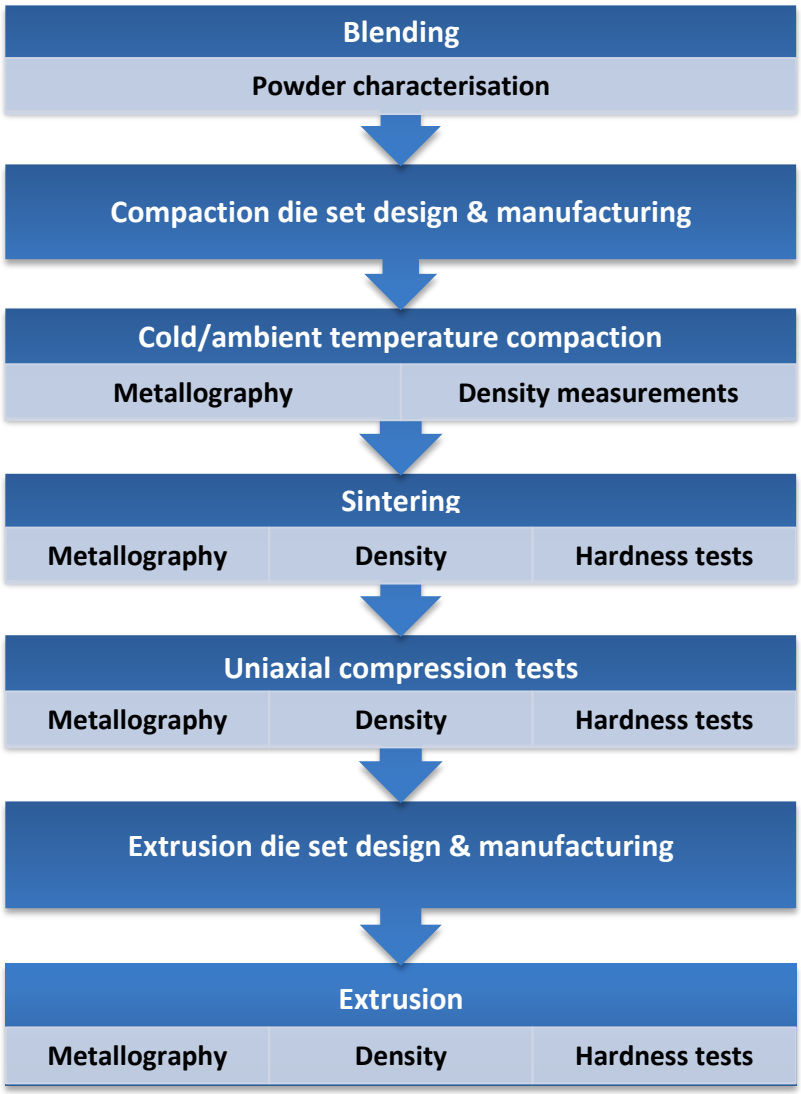

Figure 8: Experimental procedure.

3.4.1 Blending

A Simoloyer CM-01® 2L horizontal high energy ball mill was used to fabricate aluminium low micron Metal Matrix Composites (MMCs) and Metal Matrix Nano Composites (MMNCs). In both cases 2124-Al alloy (45-90 µm) powder was used as the matrix material. In the low micron MMCs the reinforcement was SiC (1-10 µm) while Al_2O_3 (40-70 nm) was used as the reinforcing material in the MMNCs. Three batches of powder consisting of 2124-Al alloy powder reinforced with Al_2O_3 or SiC powder were blended. Batch 1 was blended a few months before Batches 2 and 3 for preliminary work. This was focused on solid state forming of the aluminium MMCs and MMNCs. Table 2 lists the volume fractions of Al_2O_3 and SiC that were added to the aluminium alloy matrix.

Table 2: Amount of reinforcement phase in the matrix for MMCs and MMNCs (in vol. %).

Al_2O_3 (40-70nm)	**SiC (1-10µm)**
5	10
10	15

The volume fraction of micron-sized SiC in the aluminium alloy matrix was larger than that of the nano-sized Al_2O_3 for two reasons. Firstly, nano-sized particles produce a better hardening effect than micron-sized particles and as a result a smaller volume fraction of the nanoparticles is needed in the matrix (Razavi-Tousi *et al*., 2011). Secondly, when micron-sized particles are used their volume fraction in the matrix has to be high for good wear properties (Govindarajan & Aravas, 1994).

Once the required volume fractions of reinforcement in the matrix (Table 2) were chosen, the mass of matrix alloy powder and reinforcement powder needed for each powder blend was determined.

The 2124-Al alloy powder consists of mostly aluminium and typically contains eight other elements (Mason & Ritchie, 1997): chromium (Cr), copper (Cu), iron (Fe), magnesium (Mg), manganese (Mn), silicon (Si), titanium (Ti) and zinc (Zn). The typical elemental compositions of the major alloying elements are: 3.8 - 4.9%, Cu, 1.2 - 1.8% Mg and 0.30 - 0.90% Mn. These reported ranges were used to calculate average values for the elemental compositions of the alloy.

Equation 3 was used to calculate the density of the 2124-Al, and the proof for Equation 3 is shown in Appendix A:

$$\frac{1}{\rho_{mix}} = \frac{x_{Al}}{\rho_{Al}} + \frac{x_{Cr}}{\rho_{Cr}} + \frac{x_{Cu}}{\rho_{Cu}} + \frac{x_{Fe}}{\rho_{Fe}} + \frac{x_{Mg}}{\rho_{Mg}} + \frac{x_{Mn}}{\rho_{Mn}} + \frac{x_{Si}}{\rho_{Si}} + \frac{x_{Ti}}{\rho_{Ti}} + \frac{x_{Zn}}{\rho_{Zn}} \quad [3]$$

where: ρ_{mix} = density of the 2124 aluminium alloy (g.cm^{-3}), x_x = mass fraction of alloying element x in the 2124 aluminium alloy, ρ_x = density of alloy x (g.cm^{-3}).

Table 3 shows the elemental compositions and densities of elements in the 2124-Al alloy.

Table 3: Elemental compositions of alloying elements in 2124-Al alloy in wt %.

	Al	Cr	Cu	Fe	Mg	Mn	Si	Ti	Zn
Elemental compositions (wt %)	92.55	0.1	4.35	0.3	1.5	0.6	0.2	0.15	0.25
Mass fraction	0.9255	0.001	0.0435	0.003	0.0015	0.0060	0.002	0.0015	0.0025
ρ_{elem} (g.cm^{-3})	2.701	7.105	8.963	7.866	1.741	7.404	2.341	4.502	7.138

The calculated density of the 2124-Al alloy was 2.78 g.cm^{-3} which agrees with literature (Jung *et al*., 1999). The density of SiC was found to be 3.21 g.cm^{-3} (Jung *et al*., 1999) and according to the manufacturer's specifications the density of the Al_2O_3 used in this work is 3.60 g.cm^{-3}. For each powder blend, the mass of the 2124-Al alloy and reinforcement required was determined by calculations.

Mass and density were used to calculate the 2124-Al alloy volume. The required vol. % of 2124-Al alloy in each powder blend was known since the vol. % of reinforcing material was specified (Table 2). The volume fraction of 2124-Al alloy in the composites can be expressed as:

$$Volume\ fraction_{Al\ alloy} = \frac{V_{Al\ alloy}}{V_{composite}} \quad [4]$$

Equation 4 was used to determine the final volume of the composite. It was assumed that volumes are additive since the 2124-Al alloy and ceramic reinforcements (Al_2O_3 and SiC) do not react during blending. This implies that:

$$V_{composite} = V_{Al\ alloy} + V_{reinforcement} \quad [5]$$

Once volumes of 2124-Al alloy and composite had been calculated, the volume of the reinforcing material was determined by finding the difference between the two volumes

(*i.e.* V_{comp}-$V_{Al\ alloy}$). The mass of the reinforcing material was then calculated using Equation 6:

$$\rho = \frac{m}{v} \quad [6]$$

where: ρ is the density (g.cm^{-3})

m is the mass (g)

v is the volume (cm^3)

A powder-to-ball weight ratio of 1:10 was used.

Once the powders and steel balls were in the jar, the jar was closed and connected to the high energy ball mill. The high energy ball mill has to be connected to water pipes as water cooling prevents the ball mill from overheating. A thermocouple is connected to the jar as a safety measure designed to switch off the ball mill if the temperature exceeds 50°C. The powder was weighed after blending to calculate the yield by Equation 7. The yield gives an indication of how much powder was recovered after blending. This is important because powder may adhere to the grinding media or be lost as dust.

$$Yield = \frac{M_{powder\ after\ blending}}{M_{powder\ before\ blending}} x100 \quad [7]$$

3.4.2 Powder characterisation

The as-received and blended powders were characterised using a Microtrac Bluewave® particle size and shape analyser and scanning electron microscopy.

The dry or wet analysis methods can be used on the Microtrac particle size and shape analyser. The difference between these two methods is that the wet analysis method analyses the powder sample while it is suspended in a medium such as distilled water while with the dry method there is no medium. The wet analysis method is preferred as the sample can be circulated in the sample chamber and analysed multiple times, increasing the accuracy of the results obtained (Horiba Scientific, 2010). To analyse each powder a small amount of powder (less than 1 g) was poured into the sample chamber filled with distilled water and analysed three times before being drained from the sample chamber.

The data obtained from the particle size analysis was used to construct particle size distribution (PSD) curves. The particle size distribution data can be reported from three perspectives: volume, number and surface distribution, which all give particle size distribution results but differ in the way in which these results are recorded:

- Volume distribution - the volume of particles in each particle size class.
- Number distribution - the number of particles in each particle size class.
- Surface distribution - the surface area of particles in each particle size class.

When particle size results are reported, it is important to use different notation to stipulate which perspective was used, as the different perspectives yield slightly different results. For example, the particle size (in microns) where 50% of particles in the powder have particle sizes less than it is referred to as D50. To specify which perspective was used to record the data, D50 would be written as:

- D_v50 for a volume distribution
- D_n50 for a number distribution
- D_s50 for a surface distribution

The data was recorded as a volume distribution, as this is the preferred method in industry (Horiba Scientific, 2010).

The as-received and blended powders were analysed by SEM. To adhere powder particles and maintain conductive properties, carbon tape was attached to small brass rods. The powder was sprinkled onto the carbon tape and then blown with compressed air to remove any loose particles that did not adhere to the tape. The small brass rods were then placed into sample holders and one sample was analysed at a time. The ideal working distance between the beam and the surface is 10mm, so the protruding height was always taken into account. Secondary electron micrographs of each powder were taken at various magnifications and saved for further analysis.

3.4.3 Design and making of compaction die

The powder compaction equipment consists of a hydraulic press and a die. The latter is made up of a top punch, die, bottom punch, two punch holders, pressure plates and a spacer (Figure 9). The material of construction for the die and punches was high speed steel (HSS) with a Rockwell Hardness (HRC) value of 64. The pressure plates were manufactured from tool steel (1: 2379), AISI=D2, with an HRC value of 58.

Premeasured powder was fed into the die cavity and the top punch was placed into the cavity to seal off the powder. The assembled die was then placed into the hydraulic press and the powder was compacted under a calculated pressure to form a green compact. The top punch and spacer were removed after compaction, enabling the bottom punch to move so that the green compact could be ejected.

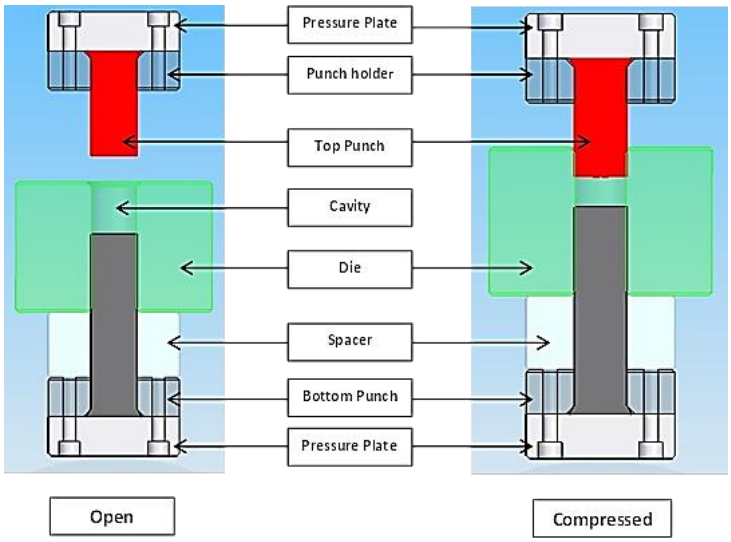

Figure 9: Mechanical components of the compaction die in the open and compressed positions.

3.4.4 Compaction

The unreinforced 2124-Al alloy powder and blended powders were cold compacted into cylindrical green compacts with a diameter and height of 8 mm and 12 mm respectively in preparation for the uniaxial compression tests on a Gleeble 3500®. These dimensions were selected according to the specifications of the Gleeble.

The Enerpac VLP® series 100 tonne hydraulic press that was used to compact the powders has limited maximum pressure that can be applied during compaction. The pressure that is applied on the powder by the anvil is determined by a gauge meter reading that is set prior to compaction. The maximum allowable gauge meter reading is governed by the diameter of the die that will be used to compact the powder. According to the press specifications, for a die with a diameter of 8 mm, the maximum allowable gauge meter reading is 70 bars.

To compact the powders into green compacts:

- The inside of the die was lubricated using a zinc stearate spray lubricant.
- 1.68 g of powder was weighed and then poured into the die cavity.
- The anvil was fitted into the die cavity and the die setup was placed in the hydraulic press.
- The desired gauge meter reading was set and the powder was compacted.

The unreinforced 2124-Al alloy powder was compacted first. After the first three green compacts were produced it was observed that there were surface cracks, which had

propagated all around the compact circumferences. The height-to-diameter (H/D) ratio of these fractured green compacts was 1.5, so it was thought that this ratio was too high and may have been contributing to the fracturing of the green compacts. The H/D ratio plays a significant role during the compaction process (Qangule, 2015). When this ratio is high, the pressure differential across the length of green compacts is also high which results in inhomogeneous properties across the length.

Extensive experimental work which involved pressing various masses of powder to investigate the effect of H/D ratio and the use of different dies (7 and 17 mm diameter) showed that the fracturing of green compacts was not due to a high H/D ratio or die malfunction. As the 2124-Al alloy powder used in this work was purchased in 2012, it was then speculated that the powder had naturally aged.

Ageing, also known as precipitation hardening, is a process which increases the hardness of metal alloys through uniform dispersion of precipitates (Fransson, 2009). Ageing is preceded by two processes: solution treatment and quenching (Meluch, 2009). During solution treatment the metal alloy is heated to a temperature above the solvus where some of the alloying elements are dissolved in the matrix (Jang *et al*., 2013). The matrix in this instance is the metal with the highest elemental composition in the metal alloy or the main metal in the alloy. Alloying elements have a certain solubility in the matrix which is often represented as the maximum amount (as wt %) of the alloying elements that can dissolve into the matrix. A decrease in temperature decreases the solubility of alloying elements in the matrix (Meluch, 2009). A supersaturated solid solution is formed when the maximum amount of alloying element dissolves into the matrix phase at high temperature and the solid solution is quenched rapidly (Rdzawski, 2010). The ageing process then occurs at ambient or elevated temperatures, when precipitates form and disperse in the matrix. Natural ageing occurs at ambient temperature while artificial ageing takes place at elevated temperatures (Sjolander & Seifeddine, 2010). The hardness of the metal alloy increases due to ageing because the precipitates that form impede dislocation movement (Mimica, 2015).

The 2124-Al alloy powder that was used in this work is an Al-Cu-Mg alloy made by TLS Technik Spezialpulver (Garcia, 2015). The powder was made using a gas atomisation process where the metal alloy was heated to liquid phase and then atomised using argon. The particles solidify rapidly in the atomisation tower and are collected in a powder container. It is possible that during heating some of the Cu and Mg could have dissolved

into the aluminium and were then in solid solution due to rapid solidification. Thus over time precipitates formed and the hardness of the powder increased due to natural ageing. One of the best descriptions of the precipitation sequence in Al-Cu-Mg alloys is given by Parel *et al.* (2010):

$$Supersaturated\ solid\ solution\ (SSS) \rightarrow CuMg\ co-clusters \rightarrow S''/GPB2 \rightarrow S(CuMgAl_2)$$

Cu-Mg co-clusters form at temperatures between 160 and 200°C during artificial ageing and may form within a few days in natural ageing (Parel *et al*., 2010; Khan *et al*., 2008). The co-clusters are believed to be responsible for approximately 60% of the total increase in hardness (Parel *et al*., 2010). These co-clusters are the main strengthening mechanisms during natural ageing (Shen *et al*., 2013). The S''/GPB2 phase is formed prior to reaching peak hardness. Literature states that the S'' phase is not formed during natural ageing and only has a significant influence on strengthening in Al-Cu-Mg alloys which contain less than 1 wt % Cu (Khan *et al*., 2008). The *S* phase is an equilibrium phase which results in peak strengthening (Parel *et al*., 2010).

Nazarenko *et al*. (2014) reviewed work done by several researchers on the effect of long term storage of aluminium powders on their characteristics. They reported that all the researchers found that aluminium powders are extremely susceptible to natural ageing and storage conditions such as slightly elevated temperature and humidity play a role in driving the ageing process (Nazarenko *et al*., 2014).

A material is overaged when it is exposed to ageing conditions for too long or to conditions more severe than the ageing conditions. The peak hardness is exceeded and the material begins to soften due to coarsening of precipitates (Daniel & Granholt, 2012).

Figure 10 illustrates that peak hardness was reached after 10 hours when ageing an Al-Cu-Mg alloy at 190°C. Thus, to overage this alloy it would have to remain at 190°C for more than 10 hours which would make the overageing process very energy intensive and therefore costly. Peak hardness can be reached faster when the ageing temperature is increased because the rate of precipitation is faster at higher temperatures, thus allowing for overageing to be done in a shorter period of time (Shen *et al*., 2013).

In this work, the unreinforced 2124-Al and blended powders were overaged at 350°C for 2 hours. These overageing conditions improved the compressibility of the powders and the green compacts made from the heat treated powders did not fracture. However, the overageing heat treatment did not improve the quality of the green compacts made from

2124-Al with 10vol. % Al_2O_3 powder. Sections from the surface and the core of these fractured compacts were taken for metallographic evaluation. Several green compacts were set aside for density measurements, metallographic evaluation, sintering, uniaxial compression tests on a Gleeble 3500® and laboratory scale extrusion experimental trials.

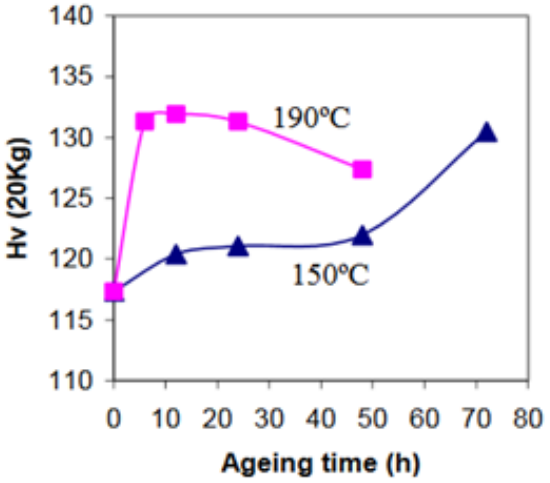

Figure 10: Hardness as a function of ageing time for an Al-Cu-Mg alloy (Shen *et al*., 2013).

3.4.5 Sample preparation of green compacts

One green compact was mounted at a time in black Bakelite powder using a hot mounting press.

The mounted samples were ground sequentially using 1000, 1200, 2400 and 4000 grit papers. An automatic polishing machine was used. For grinding, a force of 20 N and time of 3 minutes were used. The samples were then polished using 15 µm, 3 µm and 1 µm polycrystalline diamond paste using a force of 20 N for 5 minutes at each step. The samples were then polished with colloidal silica at 15 N for 15 minutes and water for 5 minutes.

After polishing the microstructures of the compacts were analysed using optical microscopy and SEM.

3.4.6 Sintering

A Netzsch STA 449F3 Jupiter® simultaneous thermal analyser was used to study the thermal behaviour of unreinforced 2124-Al and blended powders. The results from the Differential Scanning Calorimetric (DSC) study were used to identify a suitable sintering temperature for the materials. The DSC study was done using the following parameters:

- Temperature = sample heated up to 680°C
- Heating rate = 20.0 K/min
- Sample size = ~32.0 mg

Once the sintering temperature (490°C) and time (1 hr) had been determined, a muffle furnace was used to sinter the green compacts.

3.4.7 Uniaxial compression tests

Uniaxial compression tests were performed on a Gleeble 3500® (Figure 11) to study the deformation behaviour of unreinforced 2124-Al alloy, MMCs (2124-Al + 10 or 15 vol. % SiC) and MMNCs (2124-Al with 5vol. % Al_2O_3). Tests were done on green and sintered compacts at warm working temperatures in the range of 30 and 60% of the matrix phase melting point (Van Tyne, 2004). The green compacts had a diameter and height of 8 mm and 12 mm respectively. The DSC results showed that most of the 2124-Al alloy, MMCs and MMNCs started melting at ~560°C (solidus temperature). This meant that the warm working temperature range for the 2124-Al alloy was between 168 and 336°C.

Uniaxial compression tests were first carried out at ambient temperature and the Taguchi method (Unal & Dean, 1991) was used to create a test matrix for the uniaxial compression tests performed at higher temperatures. The two variables were temperature (°C) and strain rate (s^{-1}). Three temperatures of 170, 220 and 280°C within the warm working temperature range were chosen. Literature shows that strain rates used in compression tests for aluminium alloys and their composites can range from 0.01 to 10 s^{-1} (Prasad *et al.*, 2015). The lowest strain rate of 0.01 s^{-1} and an average of the lowest and highest value of 5 s^{-1} were chosen. A total strain of 0.3 was chosen. In previous work, cold extrusion at a total strain of 0.5 was unsuccessful (Gxowa *et al.*,2015) and it was speculated that this strain may have been too high. It was then decided that for this work a slightly lower total strain would be used. At ambient temperature a strain of 0.1 was used, this strain was later increased to 0.3 to improve deformation.

In initial testing at programmed temperatures, above ambient, electrical resistance heating of the green compacts did not occur, which was attributed to the high electrical conductivity and low resistance of the aluminium samples. High electrical conductivity resulted in poor heat generation because electrical (and heat) resistance in the samples was low (Ozturk *et al.*, 2016). It was presumed that the small sample size (d=8 mm, h=12 mm) also caused rapid heat loss. After further experimentation, the green compacts were heated

successfully by using glass fibre wool and a conductive foil wrapped around the samples as insulation in order to retain heat. A soaking time of 6 minutes was used at all conditions. At conditions which resulted in the best deformation, the soaking time was increased to 20 minutes to improve deformation even further.

Figure 11: Gleeble 3500® used for uniaxial compression testing.

The stress-strain data obtained from the uniaxial compression tests were used to construct engineering stress-strain curves to analyse the deformation behaviour of each material. The temperature and strain rate parameters that resulted in deformed samples with the best quality, *i.e.* deformed well with minimal surface cracking, together with finite element analysis (FEA) on Abaqus, were used to design a laboratory scale extrusion experiment.

3.4.8 Laboratory scale extrusion experiments

The extrusion experiments were used to validate the physical results obtained from the uniaxial compression tests and the FEA results; thus evaluating whether a thermomechanical simulator such as a Gleeble can be used to design an extrusion experiment.

An extrusion temperature of 280°C was used. Uniaxial compression tests showed that a strain rate of 5 s^{-1} produced uniaxially compressed samples with the best integrity. According to the FEA a strain rate of 5 s^{-1} is equivalent to an extrusion speed of 7 mms^{-1}, which was then used for the extrusion trials. An extrusion die was designed to reduce the diameter of the samples from 8 mm to ~5.6 mm, a 30% reduction, and the die set was manufactured from BOHLER W302 H13 hot work tool steel. An Instron® press was used for the extrusion experiments and a high temperature furnace was used to heat up the samples and the die.

For each extrusion test, a green or sintered compact was placed inside the extrusion die, which was then loaded onto the Instron® press. The induction furnace was then inserted around the die setup to heat the sample and die simultaneously. The die and furnace had small holes where the thermocouple was fitted to monitor the temperature. It took 3-4 hours for the sample and die setup to reach 280°C. Once the setup had stabilised at 280°C, it was allowed to soak at 280°C for 20 minutes before the load was applied to extrude the samples. Figure 12 is an image of the die, Instron® press and furnace setup for the extrusion experiments and Figure 13 gives a closer look at the setup.

The extruded parts were photographed and density measurements, metallographic evaluation and hardness tests were done.

Figure 12: Die, Instron® press and furnace setup for extrusion experiments.

Figure 13: Furnace and die for extrusion experiments.

3.4.9 Hardness testing

Microhardness tests with a 100 g load were done on the compacts after sintering, uniaxial compression tests and extrusion using a Future-Tech Vickers microhardness tester FM-700®. Fifteen indentations were made on each sample across the diameter of the compacts using a distance of 0.200 mm between indents. An average of the fifteen hardness values was calculated to determine hardness for each sample. Hardness tests were carried out according to ASTM standard E92 (ASTM E92-17, 2017).

3.4.10 Density measurements

Archimedes' principle was used to determine densities of green compacts, sintered compacts as well as uniaxially compressed and extruded parts (Lima, 2012). To calculate the density of any object the mass and volume of that object is needed. According to Archimedes' principle the volume of an object can be found by subtracting the mass of the object when it is immersed in liquid from its dry mass. Any object's apparent weight will decrease if it is immersed in a liquid. When the object is in the liquid it displaces some of the liquid and the weight loss is equal to the weight of the liquid that is displaced (Lima, 2012). Equation 8 was used to calculate density in $g.cm^{-3}$ according to the ASTM B962 standard (ASTM B962-17, 2017):

$$\frac{density\ of\ compact}{density\ of\ fluid} = \frac{M_{dry}}{M_{dry} - M_{immersed}} \quad [8]$$

4 Results and Discussion

4.1 Overview

Results from blending of 2124-Al with Al_2O_3 or SiC powder, cold (*i.e.* ambient) temperature compaction, differential scanning calorimetry (DSC), sintering, uniaxial compression using a Gleeble 3500®, finite element analysis (FEA) on Abaqus and laboratory scale extrusion experimental trials are presented, analysed and discussed in this chapter.

Characterisation of blended powders showed that a more uniform distribution of reinforcing particles on 2124-Al particle surfaces was achieved in Al_2O_3 reinforced MMNCs than SiC reinforced MMCs. A fairly uniform distribution of nano-sized Al_2O_3 on 2124-Al particle surfaces was maintained during blending even when the volume fraction of Al_2O_3 increased from 5 to 10 vol. %. Poorer blending in SiC reinforced MMCs was shown by loose SiC particles in SEM SEI micrographs and the bi-modal nature of the Particle Size Distribution (PSD) curves for SiC reinforced MMCs.

During cold compaction, the green compacts of the unreinforced and blended powders fractured into thin, nearly horizontal slices. This was attributed to the natural ageing of the 2124-Al alloy powder due to long term storage (Nazarenko *et al.*, 2014). The powders were then exposed to an overageing heat treatment at 350°C for 2 hours in order to reverse the effects of ageing. Green compacts were pressed successfully from overaged powder; except those from 10 vol. % Al_2O_3 powder. The 10 vol. % Al_2O_3 powder had poorer compressibility even in the overaged condition; indicating that alternate consolidation techniques, such as spark plasma sintering (SPS), should be explored in future work. Optical and SEM microscopy revealed that there was a density variation from the surface to the core of green compacts. This variation in density resulted in non-uniform densification and properties such as hardness.

Shallow exothermic peaks between 496 and 518°C were observed in the MMCs and MMNC during the DSC study. In literature no exothermic peaks were reported above 340°C. It was deduced that the shallow exothermic peaks were due to the addition of the

reinforcement phase (Al_2O_3 or SiC) and may have formed from interfacial reactions which occurred.

The temperature and strain rate that resulted in uniaxially compressed samples with the best integrity were 280°C and 5 s^{-1}, respectively. Combining sintering with an increase in soaking time (from 6 to 20 minutes) prior to uniaxial compression improved plastic flow in MMCs by improving mobility of dislocations, grains and grain boundaries. This enabled better deformation and improved ductility (*i.e.* shown by larger plastic region). Warm temperature uniaxial compression of SiC reinforced MMCs was successful and the best deformation (*i.e.* good ductility; shown by large plastic region and high flow stress) was achieved in the 2124-Al with 10% SiC MMC because it plastically deformed at the highest stress (~153 MPa) up to the maximum strain of 0.3.

Uniaxial compression tests and FEA showed that SiC reinforced MMCs can be deformed successfully at warm working temperatures but some minor surface cracks should be expected. Extrudability of unreinforced 2124-Al was good while the Al_2O_3 reinforced MMNC and SiC reinforced MMCs had poorer warm temperature extrudability, which was attributed to a lack of lubrication during extrusion. Distribution of SiC particles in 2124-Al with 10% SiC improved slightly due to uniaxial compression and extrusion showed potential to improve distribution of SiC reinforcing particles. However, higher deformation is required to optimise the SiC distribution.

4.2 Blending

The purpose of the blending process was to fabricate aluminium-based Metal Matrix Composites (MMCs) and Metal Matrix Nano Composites (MMNCs) using a powder metallurgical processing route.

4.2.1 As-received powders

The 2124-Al alloy powder was used as the matrix material while the Al_2O_3 and SiC powders were the reinforcing materials. SEM secondary electron images (SEI) in Figure 14 show the different morphologies and particle size distributions of the starting powders before blending.

Figure 14a shows that the particles of the 2124 Al alloy powder were spherical and of the same size. As Al_2O_3 powder had poor conductivity and the particles were not clear even at higher magnifications on the Jeol-6510® SEM, an ultra-high resolution ZEISS ΣIGMA®

SEM was used. Figure 14b shows that the size of the Al_2O_3 powder was ~100-500 nm and the particles were irregularly shaped. The SiC powder particles were irregularly shaped with sharp edges, with sizes ~5-10 µm (Figure 14c).

The Al alloy particles were significantly coarser than the Al_2O_3 and SiC reinforcements.

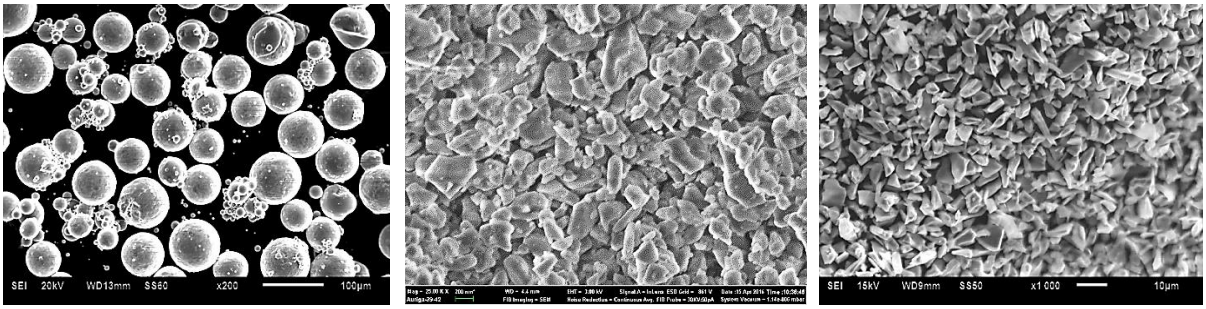

a b c

Figure 14: SEM SEI images of: a) 2124-Al alloy powder (scale bar=100 µm) b) Al_2O_3 powder (scale bar=200 nm) and c) SiC powder (scale bar=10 µm).

4.2.2 Blended powders

For good blending, the reinforcing particles should adhere to the Al alloy particles. Three batches of each powder were blended, which helped to assess if the properties that were obtained after blending were consistent. Micrographs of 2124-Al powders blended with Al_2O_3 (5 or 10 vol. %) or SiC (10 or 15 vol. %) are presented, analysed and discussed in this section.

<u>5% Al_2O_3</u>

Three batches of 5% Al_2O_3 MMNC powder, *i.e.* 3 x 100 g of 2124-Al blended with 5 vol. % Al_2O_3, were blended, as shown in Figure 15. It can be observed that there are light, fine Al_2O_3 particles on the surfaces of the coarse, spherical 2124-Al alloy powder particles. Visually, it appears that the three batches had a relatively uniform distribution of Al_2O_3 particles on the aluminium alloy particles. Figures 15a and 15b show that during blending some of the Al alloy particles changed shape due to plastic deformation and some fractured into smaller particles.

The larger, light particle indicated by an orange arrow in Figure 15e was confirmed to be an agglomeration of smaller Al_2O_3 particles by EDX analysis (Figure 16), as it contained 61.4 at.% O, 0.1 at.% Cu and 38.5 at.% Al and it was most likely formed during blending. The small amount of copper detected may have been an impurity in the Al_2O_3 powder. Agglomeration was only observed in Batch 3.

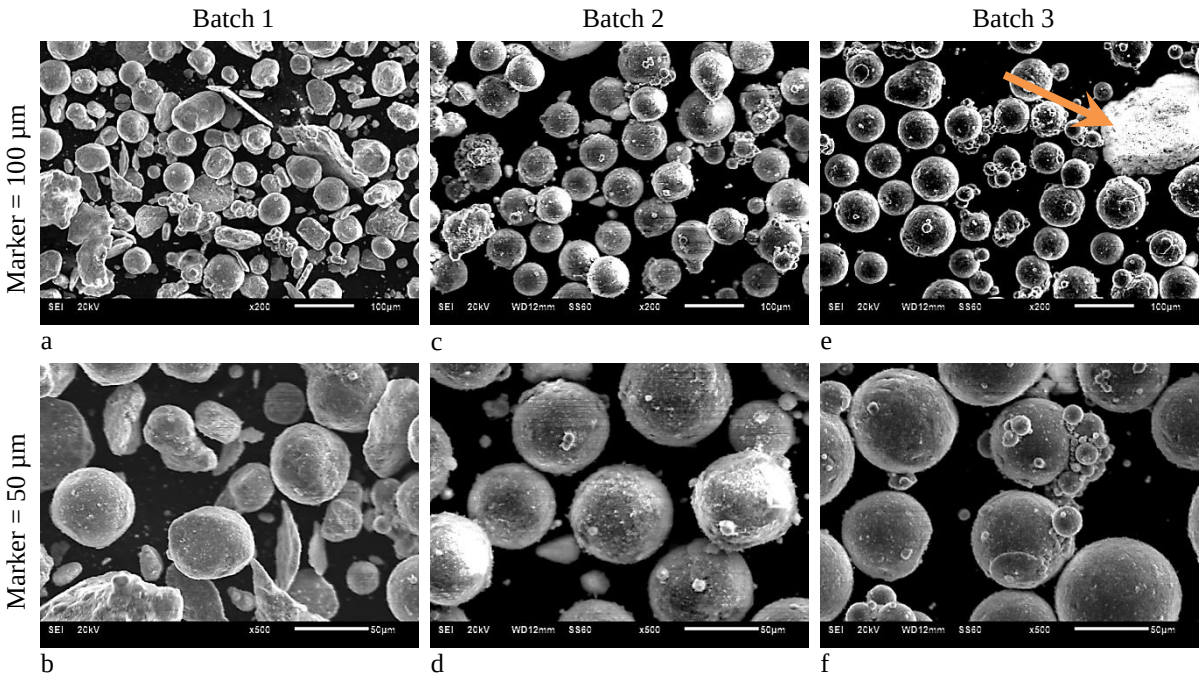

Figure 15: MMNC blended powders of Al alloy with 5 vol. % Al_2O_3.

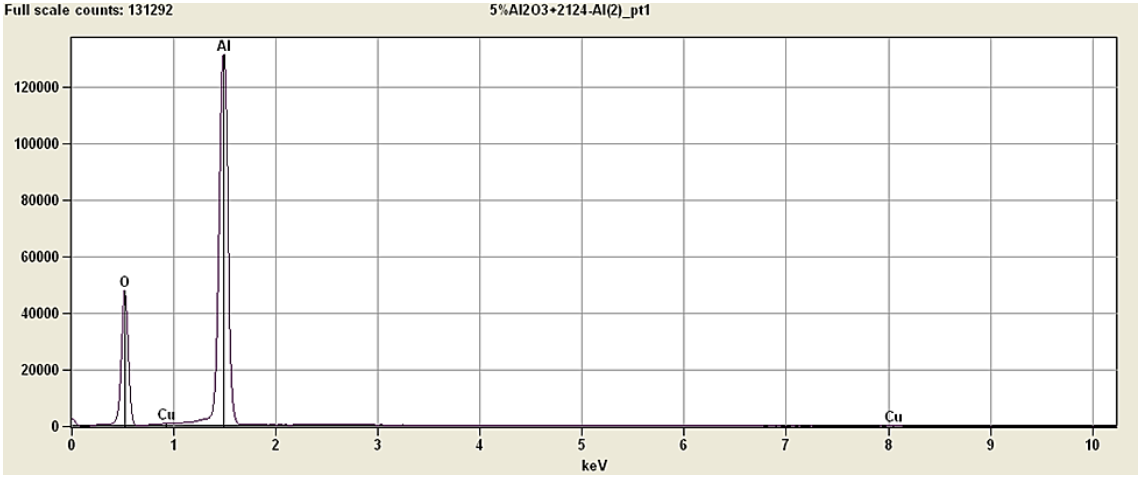

Figure 16: EDX spectrum showing the elemental analysis of the large Al_2O_3 particle (shown by orange arrow observed in Figure 15e).

10% Al_2O_3

Figure 17 shows a fairly uniform distribution of Al_2O_3 nano-sized particles on the 2124-Al powder particles, despite the increase from 5 to 10 vol. % Al_2O_3. This finding contradicts results found in liquid state processing (Borgonovo & Apelian, 2011), where the tendency of nanoparticles to form agglomerates increased as their volume fraction in the matrix increased. This uniform distribution can be attributed to good blending parameters, as any particle clusters that may have formed would have been broken up as the blending process progressed. The positive result in this work is an indication that the problems of agglomeration encountered in liquid state processes could be averted by using solid state techniques.

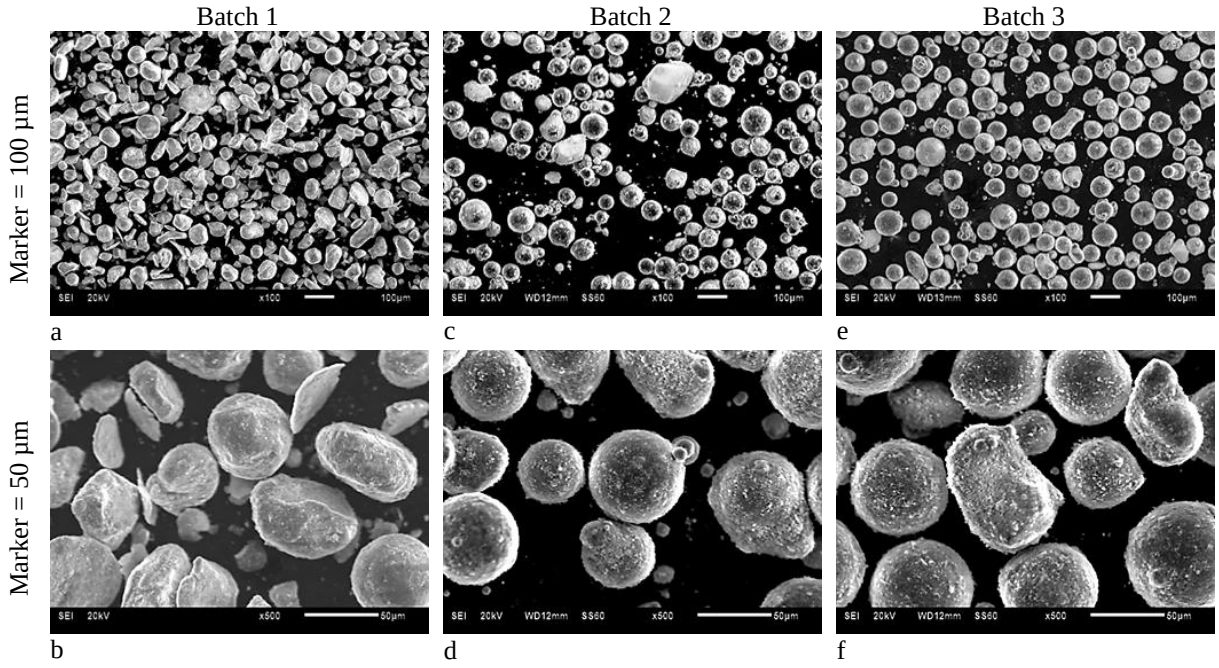

Figure 17: MMNC blended powders of Al alloy with 10 vol. % Al_2O_3.

10% and 15% SiC

The micrographs in Figures 18 and 19 show that all SiC batches contained spherical 2124-Al alloy particles surrounded by small, irregularly shaped SiC particles. As only a small amount of the SiC particles adhered to the 2124-Al alloy particles, and most of the SiC particles were loose, it can be inferred that the SiC powder did not blend adequately with the Al alloy powder. This inadequate blending could have been due to non-optimised blending procedure for SiC reinforced powders: milling time, speed, amount of powder in the jar (*i.e.* fullness) or ratio of balls to powder.

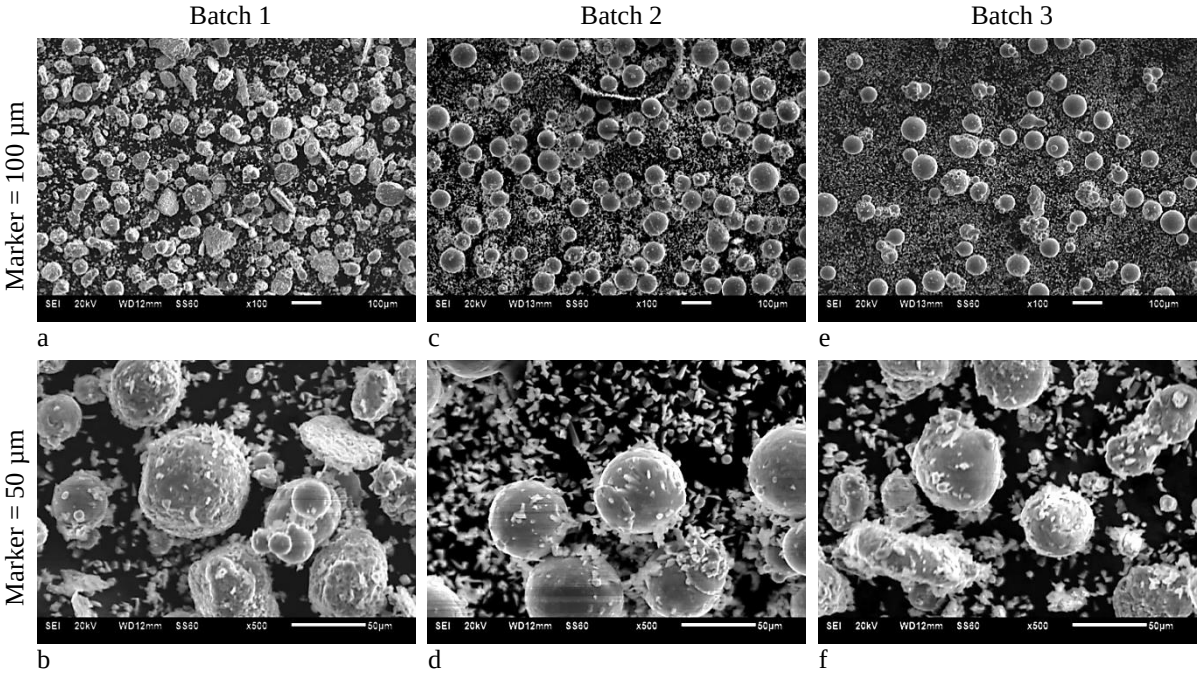

Figure 18: MMC blended powders of Al alloy with 10 vol. % SiC.

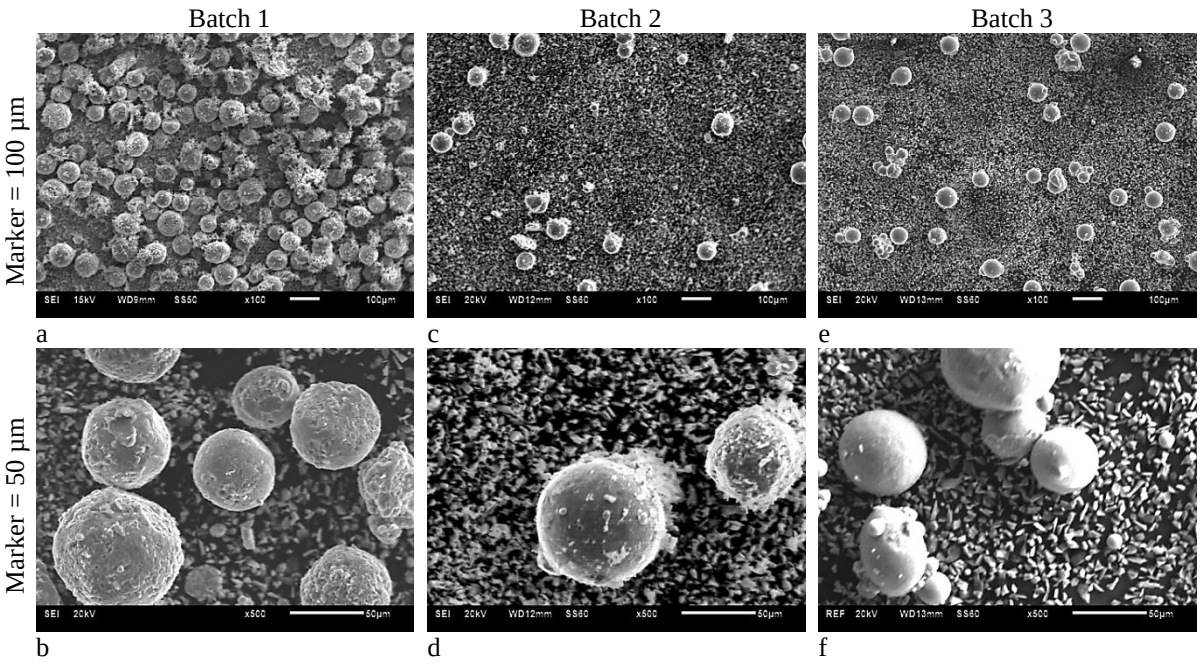

Figure 19: MMC blended powders of Al alloy with 15 vol. % SiC.

4.2.3 Yield

Yield gives an indication of how much powder is lost during blending, in the form of dust and powder particles adhering to grinding media. The yield was calculated separately for powders in each of the three batches of blended powder. Figure 20 shows that the yield calculated for each powder in all three batches was above 96%. As less than 4% of each powder was lost, it was inferred that the blending process was efficient in retaining powder. The highest yield of 98.87% was achieved in Batch 2, 5 % Al_2O_3 powder, while Batch 1, 15 % SiC powder, had the lowest yield of 96.54%.

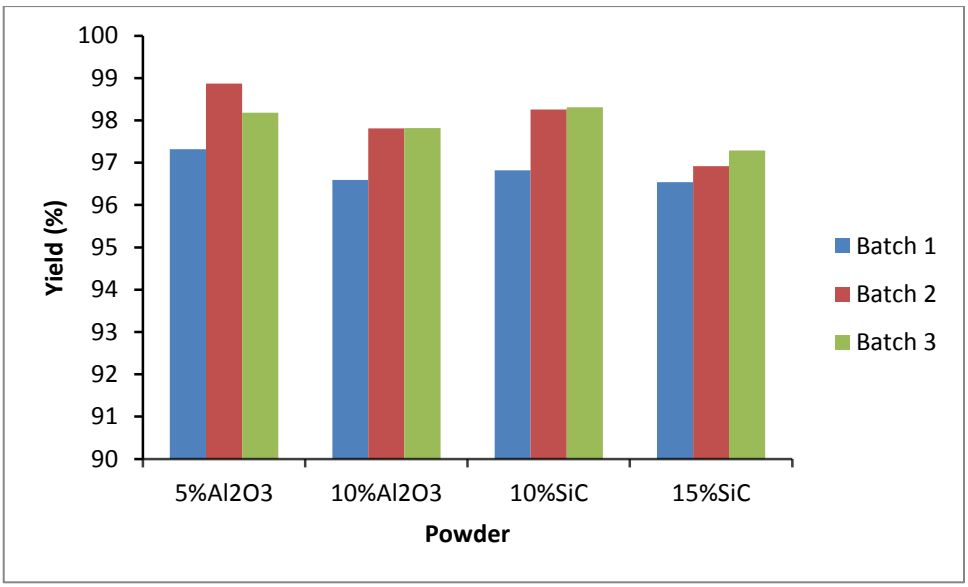

Figure 20: Powder yield calculated for each batch after blending.

4.3 Powder Characterisation

Powder characterisation is important because the morphology of particles and particle size distribution of the powder may have an influence on powder compressibility (Heckel, 1961) and ultimately final properties of a material (Chaubey *et al*., 2016).

The Particle Size Distribution (PSD) of the as-received and blended powders are presented, analysed and discussed in this section.

4.3.1 Characterisation of the as-received powders

Each supplied powder was characterised before blending the MMC and MMNC powders. The small area under the peak in Figure 21a shows that the PSD of the 2124-Al alloy powder was narrow (between 10 and 100 µm). Figure 21b shows that particle sizes for the Al_2O_3 powder were mostly in the ~0.1-10 µm range. The SiC powder had a bi-modal distribution shown by two peaks (Figure 22). The major peak shows that there were particles within the ~3-22 µm range as well as finer particles between ~0.8 and ~3 µm (minor peak). Table 4 shows that the 2124-Al powder had coarser particles than the reinforcing powders (Al_2O_3 or SiC) and the modes show that Al_2O_3 had the finest particles.

The closer the value for sphericity is to 1, the more spherical the particles in the powder are and consequently the further away the value is from 1 the more irregularly shaped the powder particles are (Mora & Kwan, 2000). The 2124-Al alloy powder had the most spherical particles since it had the highest value for sphericity (Table 4) and, with the lowest sphericity, SiC had the least spherical particles. These results agree with Figure 14, where micrographs show that 2124-Al powder had spherical particles while SiC particles were the most irregularly shaped and had sharp edges.

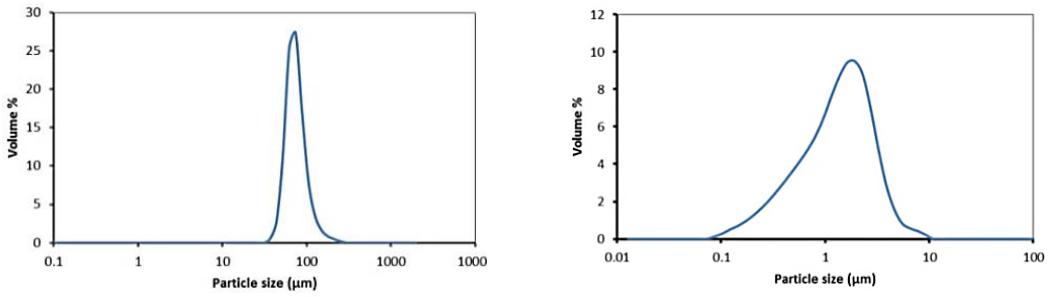

a b

Figure 21: PSD curves for a) 2124-Al b) Al_2O_3 powders before blending.

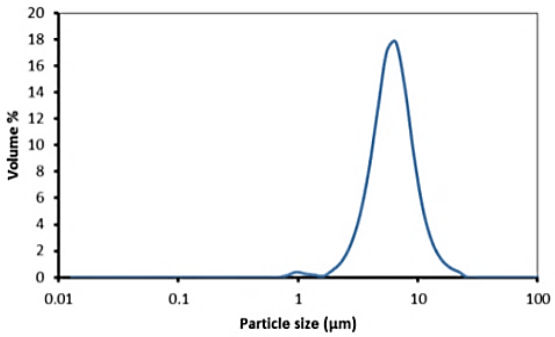

Figure 22: PSD curve for SiC powder before blending.

Table 4: PSD data for 2124-Al, Al_2O_3 and SiC powders before blending.

	2124-Al	Al_2O_3	SiC
D_v10 (µm)	49.59	0.34	3.27
D_v50 (µm)	66.03	1.27	5.61
D_v90 (µm)	96.66	2.85	9.39
Mode (µm)	74.00	1.95	6.54
Sphericity	0.91	0.85	0.81

4.3.2 Characterisation of blended powders

For each MMC and MMNC, the 3 batches of blended powder were characterised separately to assess the repeatability of the blending process.

The mode of the particle size distribution (PSD) for the unreinforced 2124-Al alloy powder was 74 µm. Figures 23a and 24a show that the addition of 5 vol. % Al_2O_3 to the 2124-Al powder caused no difference to the shape or mode of the PSD curves for Batches 2 and 3 (mode of 74 µm), but the mode of Batch 1 was 62.23 µm, indicating breakage of some 2124-Al particles. There was less scatter with 10 vol. % Al_2O_3 addition (Figures 23b and 24b), with PSD modes of Batches 2 and 3 between 62-74 µm, and the mode of Batch 1 at 62 µm.

The 2124-Al with SiC powder batches had distinct bi-modal size distributions (Figure 25), shown by two peaks on the PSD curves, with the major peaks close to that of the pure 2124-Al powder. The minor peaks at ~5.5 µm observed in Figure 25 and detailed in Figure 26 are due to loose SiC particles that did not adhere to the 2124-Al powder. However, there was no minor peak for 10% SiC Batch 1, as there was a gradual increase in size from ~2.75-37 µm, showing agglomeration of the SiC particles. All batches of 10% and 15% SiC added powders had major peak modes of 62-74 µm, showing slight attrition of the 2124-Al powder particles. The bi-modal nature of the SiC-added PSD curves show a

much lower adherence of SiC than Al_2O_3 to the 2124-Al particles (Figure 28), indicating poorer blending behaviour of SiC.

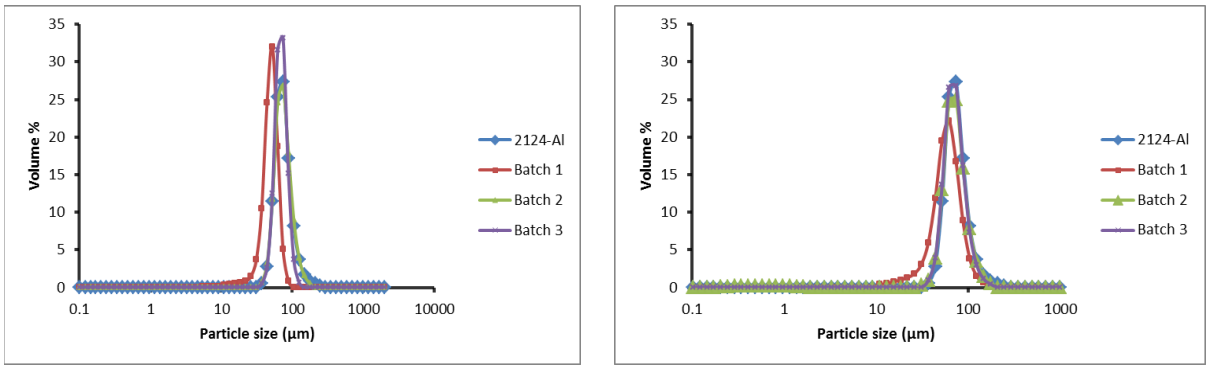

a b

Figure 23: PSD curves for 2124-Al with a) 5% Al_2O_3 and b) 10% Al_2O_3 powders.

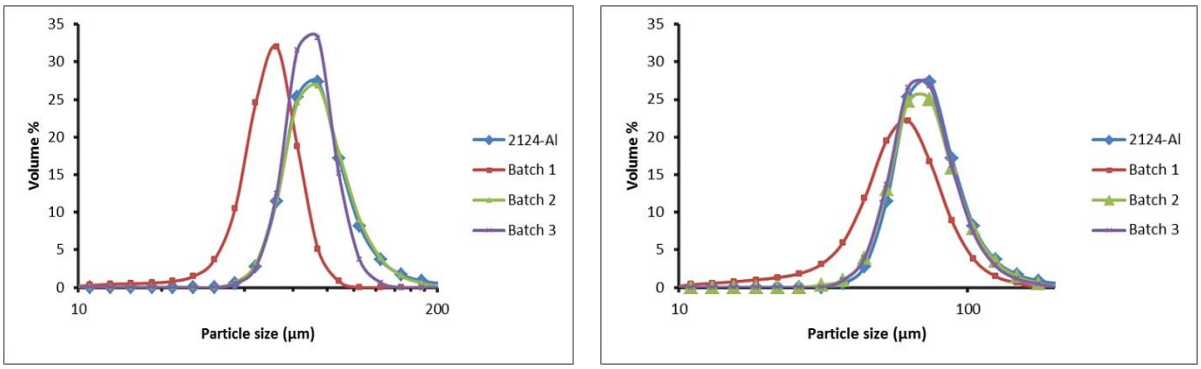

a b

Figure 24: Peaks shown in Figure 23 for PSD of 2124-Al with a) 5% Al_2O_3 and b) 10% Al_2O_3.

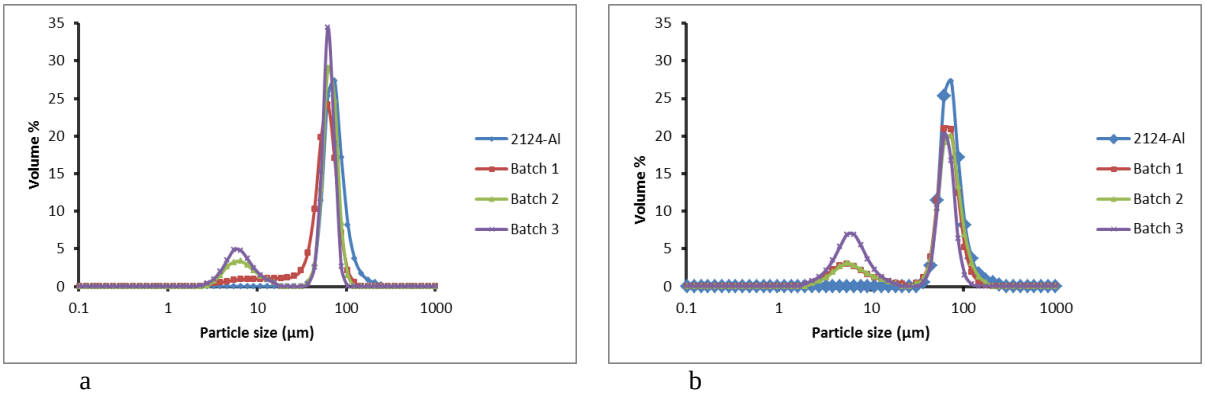

a b

Figure 25: PSD curves for 2124-Al with a) 10%SiC and b) 15%SiC powders.

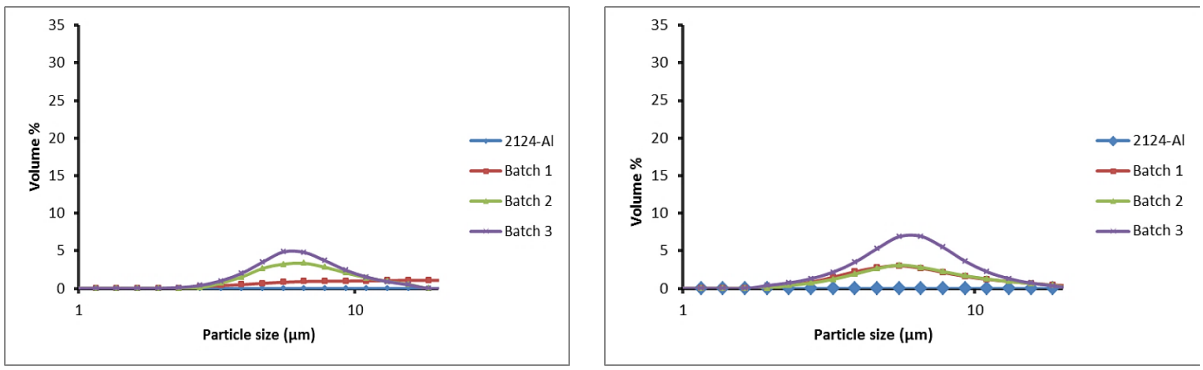

a b

Figure 26: Minor peaks shown in Figure 25 for 2124-Al with a) 10% SiC and b) 15% SiC.

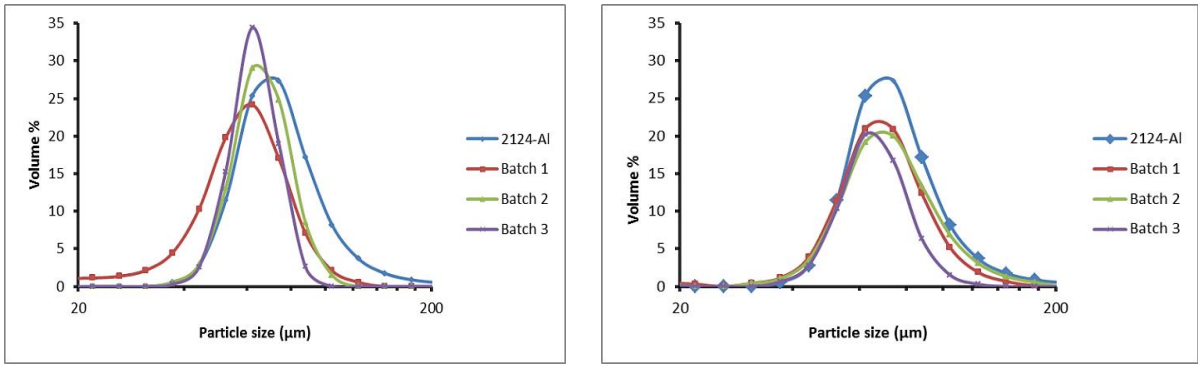

a b

Figure 27: Major peaks shown in Figure 25 for 2124-Al with a) 10% SiC and b) 15% SiC.

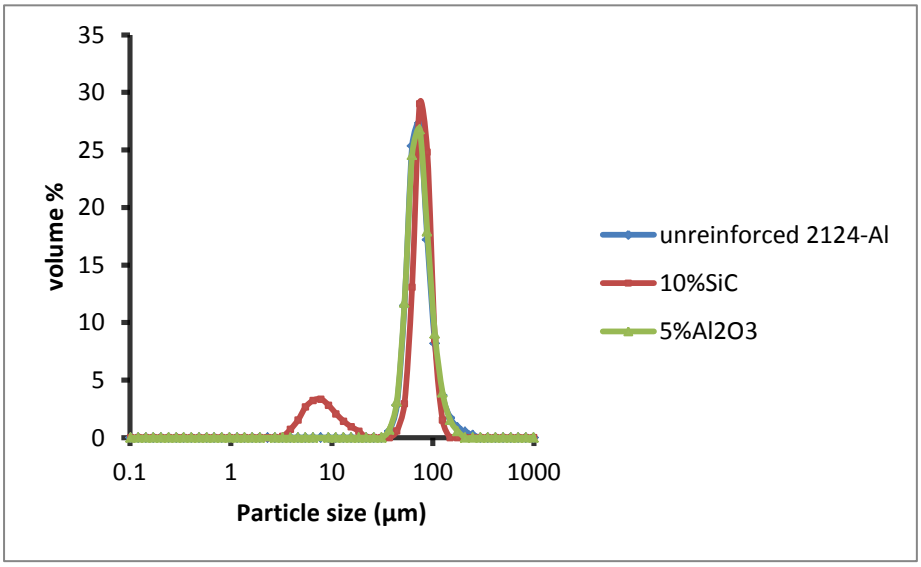

Figure 28: Poorer adherence of SiC to 2124-Al particles shown by bi-modal nature of PSD for 2124-Al with SiC powder.

4.4 Compaction

Fracturing of green compacts during compaction (Figure 29) led to an investigation into the influence of height-to-diameter (H/D) ratio on compaction.

It has been reported by Qangule (2015) that H/D ratio plays a significant role during the compaction process. The pressure differential across the length of green compacts increases as the H/D ratio increases. This results in inhomogeneous properties across the length of green compacts. The height and diameter of the fractured green compacts were 12 mm and 8 mm respectively, *i.e.* an H/D ratio of 1.5. The influence of H/D ratio on the integrity of green compacts was investigated by compacting different masses of powder; keeping D the same and varying H (Table 5). Figure 30a shows a green compact with an H/D ratio of 2.68 after compaction and Figure 30b shows the fractured green compacts, with H/D ratios of 1.79, 1.53, 1.34 and 0.89 after compaction.

The highest H/D ratio (2.68) resulted in green compacts with the best integrity. This was unexpected since, according to Glass & Ewsuk (1995), compacts with higher H/D ratios experience greater pressure differentials across their lengths; making their integrity inferior to green compacts with lower H/D ratios. The green compact with H/D ratio of 2.68 (Figure 30a) had surface cracks, which also caused it to fracture. It was deduced that the integrity of green compacts did not differ much with H/D ratio, indicating that H/D ratio had very little influence on fracturing.

Figure 29: Fractured 2124-Al green compact after cold compaction.

Table 5: Height-to-diameter (H/D) ratios corresponding to different compacted powder masses.

Mass (g)	Diameter (mm)	Height (mm)	H/D
3.00	8	21.43	2.68
2.00	8	14.29	1.79
1.68	8	12.21	1.53
1.50	8	10.71	1.34
1.00	8	7.14	0.89

a b

Figure 30: a) Green compact with an H/D ratio of 2.68 and b) Typical fractured green compact.

Green compacts were sectioned at mid-height and samples from the surface and core were taken so that the consolidation at the two positions could be studied for each green compact.

Figure 31 shows that the 2124-Al alloy particles underwent plastic deformation under the compressive load and showed some consolidation. However, the consolidation was not consistent as there were large voids (shown by darker areas on micrographs) where particles had not consolidated. Higher consolidation was achieved at the surface (Figure 31a) than the core (Figure 31b) of the green compact. Pressure gradients, caused by the friction between the powder and the die walls, lead to non-uniform density distribution in green compacts (Glass & Ewsuk, 1995; German, 1994). The frictional force opposes the applied force and decreases the amount of pressure transmitted to the powder for consolidation (Turenne *et al.*, 1999). The surface of the green compact is exposed to a higher pressure due to lower friction at the surface (Tiwari *et al.*, 2012). Thus the lower densification observed at the core of the sample (Figure 31b) is an indication of a non-uniform density distribution in the sample, where density decreased from surface to core of the green compact.

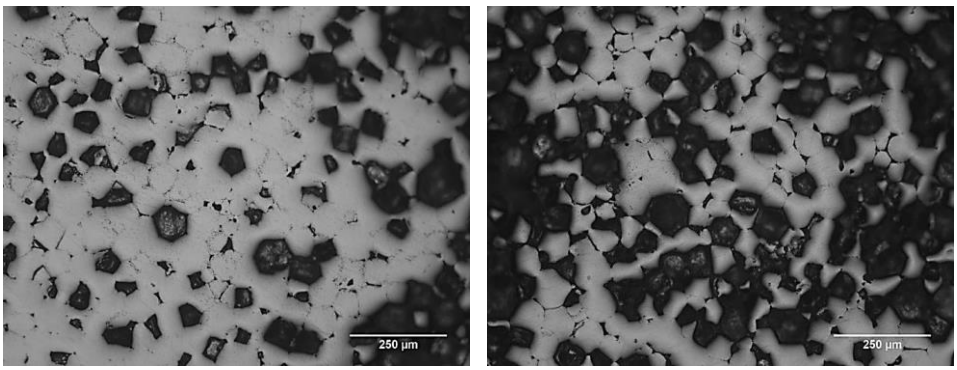

a b

Figure 31: Consolidation at the a) surface and b) core of a fractured green compact with an H/D ratio of 2.68 (scale bar = 250 µm).

The polished surfaces of the severely fractured green compacts with H/D ratios lower than 2.68 appeared dark when examined using an optical microscope due to the large number of voids in these green compacts. The depth of focus range of the optical microscope is small, and therefore unable to focus simultaneously on both the polished surface and the unpolished Al alloy particles lower than the surface, as shown in Figure 31b. SEM in secondary electron mode was more effective in examining the microstructures of the fractured green compacts because it has a better depth of focus when compared to the optical microscope. Figure 32 and Figure 33 show the SEM-SEI surface and core microstructures of the green compacts with H/D ratios of 1.53 and 1.34 respectively.

Figure 32a shows that just more than half of the particles on the surface plastically deformed and consolidated under the applied load, leaving large pores. The particles situated in the layer below the surface retained their spherical shape and did not deform during compaction. These particles had moved closer together as they are all touching but no particle bonding seems to have taken place. Figure 32b shows that the particles at the core of the sample did not bond with one another at all and are just touching. It can be inferred that the pressure exerted on the particles at the core was too low to induce plastic deformation and bonding. It was deduced from this that poor bonding caused fracturing in the green compacts.

Figures 33a and 33b show that there was poor consolidation between the Al alloy particles at the surface and the core. These micrographs are similar to those shown in Figure 32 which indicates that these two green compacts behaved in a similar manner during compaction even though their H/D ratios were different.

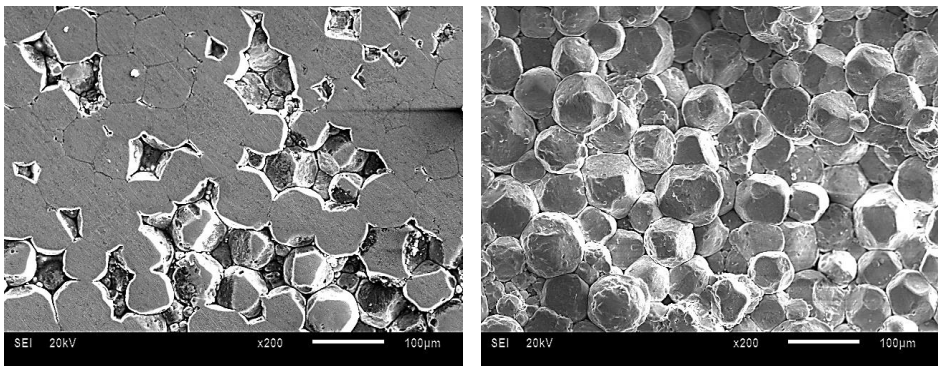

a b

Figure 32: SEM SEI micrographs showing consolidation at the a) surface and b) core of a green compact with an H/D ratio of 1.53 (scale bar= 100 µm).

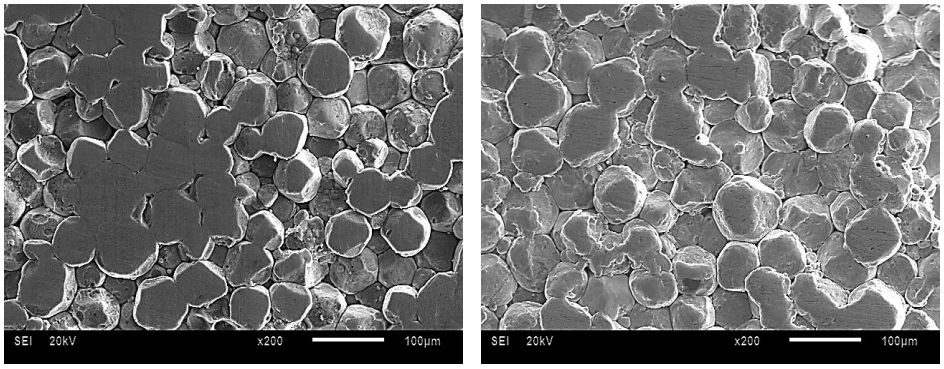

a b

Figure 33: SEM-SEI micrographs showing consolidation at the a) surface and b) core of a green compact with an H/D ratio of 1.34 (scale bar = 100 µm).

When comparing the micrographs in Figures 31, 32 and 33, it can be observed that:

- For all three samples slightly higher consolidation was achieved at the surface than the core.
- Green compacts with H/D ratios lower than 2.68 were affected in a similar manner by cold compaction.
- All the green compacts fractured in the same manner by breaking up into thin lateral slices.

The fact that all the green compacts fractured in a similar manner indicates that factors other than the H/D ratio, such as hardness, surface properties or particle size distribution, influenced the behaviour of the powders during compaction. The functionality of the 8 mm diameter die was tested by compacting the powder with a die which had a diameter of 17 mm.

Figure 34 shows that the two green compacts fractured in the same manner even though their H/D ratios were different. There is a possibility that characteristics of the powder such as surface properties and hardness changed over time since this powder had been compacted successfully with this same 17 mm diameter die by Gxowa *et al*. (2015) in 2014. Figure 35 shows the surface and core microstructures of the green compact from Figure 34a.

These micrographs show that extremely poor consolidation was achieved with the 17 mm diameter die at both the surface and the core. The particles had moved closer together under the applied load but only a few particles had plastically deformed and bonded. This shows similar behaviour to compaction with the 8 mm diameter die. From this result it was inferred that the integrity of the green compacts was influenced more by powder characteristics such as hardness, surface properties and particle size distribution than H/D ratio or type of die used.

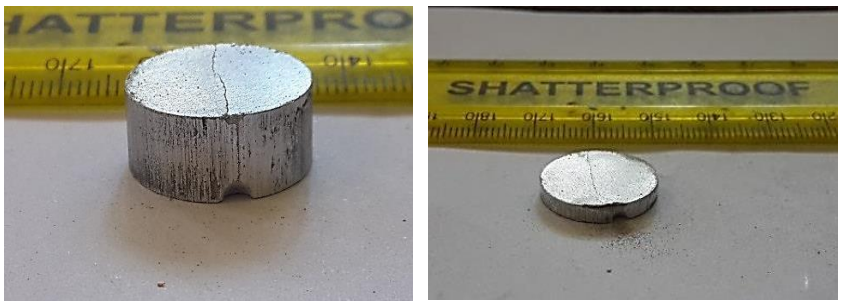

a b

Figure 34: Green compacts made with 17 mm diameter die a) H/D = 0.76, b) H/D = 0.23.

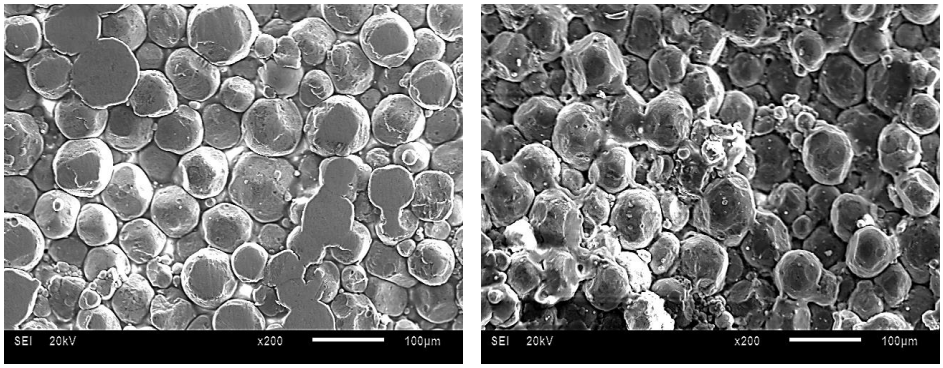

a b

Figure 35: SEM -SEI micrographs showing consolidation at the a) surface and b) core of a green compact from Fig. 30a (scale bar= 100 µm).

The poor consolidation observed in the green compacts was attributed to the possible presence of an oxide layer around the Al alloy particles and natural ageing of the powder due to long term storage. In an attempt to remove the oxide layer, 2124-Al alloy powder

was etched using 5 vol. % Hydrofluoric Acid (HF). These green compacts also fractured into slices after compaction. However, the bonds between the powder particles appeared stronger than those in green compacts made from unetched powder (Figures 32-35) since the slices did not disintegrate into powder when handled. Low magnification optical micrographs show improved surface and core consolidation (Figure 36).

The Al alloy particles plastically deformed and consolidated at both the surface and core (Figure 36). This result can be attributed to the removal or reduction in thickness of the oxide layer by HF, as the oxide layer was a thick barrier preventing consolidation between the Al alloy particles. In the absence of the oxide layer, the Al alloy particles moved closer together under the applied load and also bonded as they plastically deformed. This approach showed some potential but after careful consideration it was decided that this idea would not be explored any further as it would not be suitable to use on the Al alloy reinforced with Al_2O_3. HF would possibly remove the reinforcing Al_2O_3 particles from the Al alloy particle surfaces. HF is highly toxic and environmentally unfriendly.

The fact that green compacts made from etched powder still fractured into slices highlighted that there was poor load transfer across the length of the green compacts, possibly due to the Al alloy particles having higher hardness. It was suspected that the hardness of the Al alloy powder had increased due natural ageing, where precipitates form and disperse in the matrix over time impeding dislocation movement (Fransson, 2009). Green compacts were subjected to an overageing heat treatment to reverse any natural ageing that had occurred; thereby decreasing hardness and making the powder easier to compact. Various overageing conditions were explored (Section 3.4.4) and it was found that most of the green compacts made from powder overaged at 350°C for 2 hours had higher integrity because they did not fracture (Figure 37).

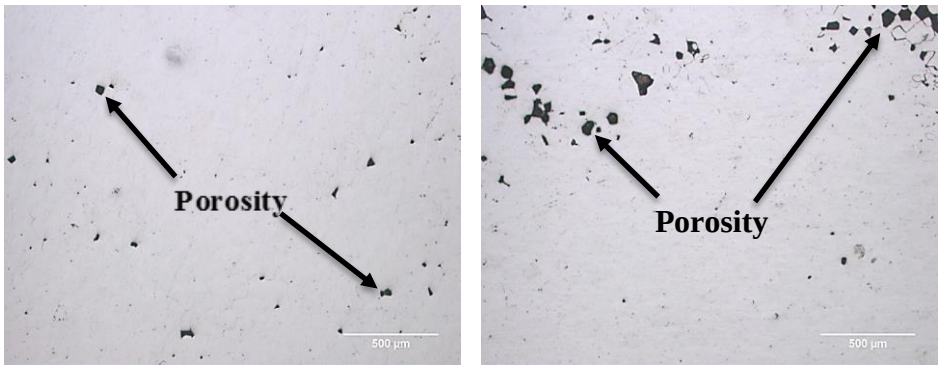

a b

Figure 36: Consolidation at the a) surface and b) core of a green compact made from etched powder (scale bar = 500 µm).

The improved integrity of the green compacts was attributed to improved plastic flow, deformation and bonding of the Al alloy particles due to a decrease in hardness. The surface still had a higher density than the core and this was due to the density variation which exists in green compacts (Figure 38).

However, green compacts made from the overaged 10 vol. % Al_2O_3 powder still fractured (Figure 39) and showed poor compressibility, poor consolidation and very little plastic deformation or bonding. This limited bonding could have been due to the higher density of Al_2O_3 particles on the surface of the 2124-Al powder, as shown in the polished section in Figure 40. There are sub-micron-sized Al_2O_3 particles on the Al alloy grain boundaries, which may have limited plastic deformation and bonding.

a b

Figure 37: Green compacts successfully produced from overaged powders: a) unreinforced 2124-Al, b) 2124-Al with SiC powder.

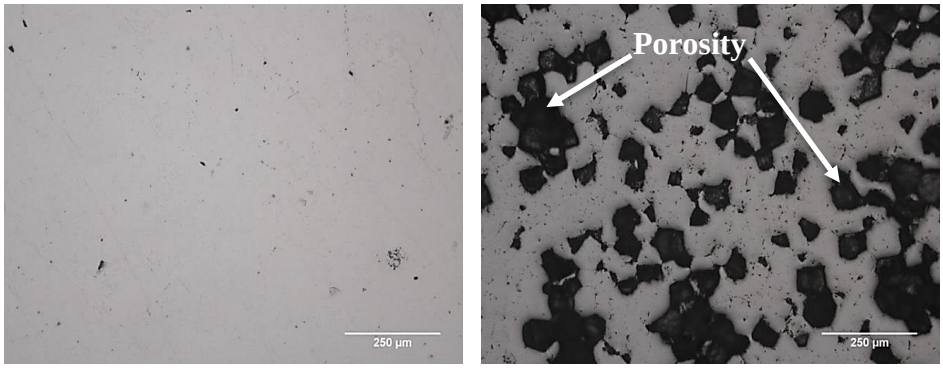

a b

Figure 38: Optical micrographs showing difference in consolidation at a) surface and b) core of a green compact made with unreinforced 2124-Al alloy overaged powder.

Figure 39: Fractured green compact fabricated from overaged 2124-Al with 10% Al_2O_3 powder.

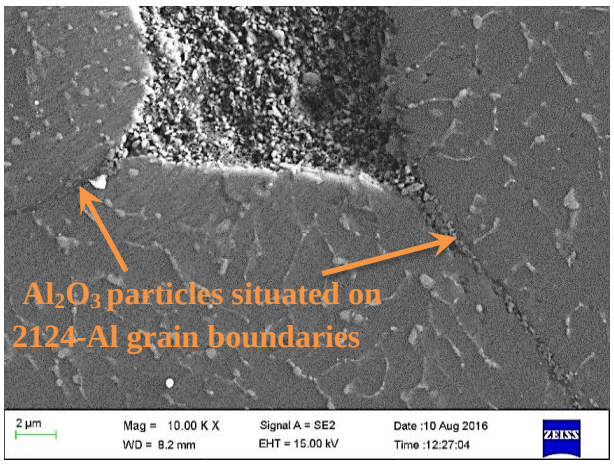

Figure 40: FEG-SEM SEI micrograph showing polished section of MMNC green compact with 10 vol. % Al_2O_3.

Through metallographic evaluation it was observed that in the Al_2O_3 MMNC and SiC MMC green compacts, consolidation was achieved by localised deformation at small contact points on the grain boundaries where there were few or no reinforcing particles (Figures 40 and 41).

The agglomeration of reinforcing particles at Al alloy grain boundaries observed in the MMC and MMNC green compacts (Figures 40 & 41) was attributed to limited plastic flow during cold compaction (Syu & Ghosh, 1993). So, during cold compaction, there is no mechanism for reinforcing particles at grain boundaries to migrate into the grains. It was thus deduced that, due to the nature of the cold compaction process, agglomeration of reinforcing particles at grain boundaries may occur even if a uniform distribution of reinforcing particles was achieved in the blending step.

Figure 41 shows that the distribution of the reinforcing particles was poor in the SiC MMC green compacts since virtually all the reinforcing particles agglomerated on the 2124-Al grain boundaries. This was expected, as there was poor blending and adhesion in the SiC reinforced powders, with a large amount of loose SiC particles situated between the 2124-Al alloy particles (Section 4.2.2: Figures 18 and 19).

The white phase (indicated by orange arrows in Figure 41) inside the Al alloy grains represents the eutectic (Yamaoglu & Olevsky, 2015).

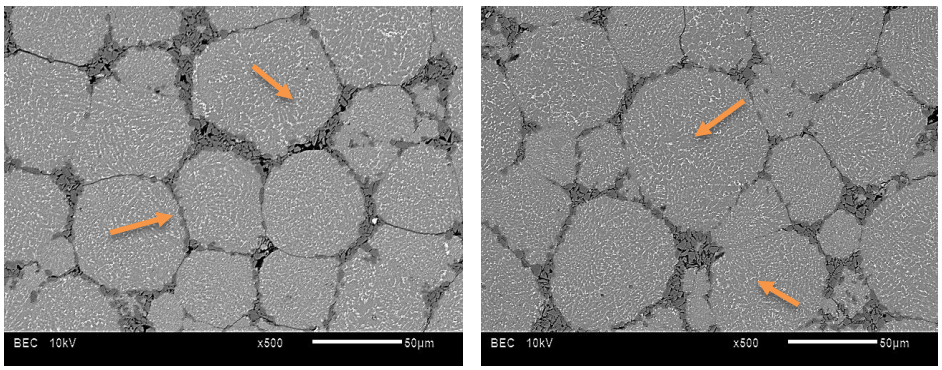

a b

Figure 41: SEM BSE micrographs showing consolidation at a) surface b) core of 2124-Al with 10%SiC green compacts. Arrows indicate the white eutectic phase.

4.5 Sintering

4.5.1 Selecting the sintering temperature

The heating curve for the unreinforced 2124-Al alloy in Figure 42 (green curve) shows that there is a small endothermic peak with an onset temperature of ~500°C. The eutectic, which normally consists of Al, Al_2Cu, Al_2CuMg and Al_8Mg_5 + Al_6CuMg_4 (Kaygısız & Maraşlı, 2015), starts melting at ~510°C so the smaller endothermic peak was attributed to eutectic melting (Wang & Starink, 2007). Figure 41 shows that the eutectic is clearly visible inside the 2124-Al grains. The larger endothermic peak represents the melting temperature range of the Al alloy where it starts melting at ~560°C (solidus temperature).

The heating curves for the SiC reinforced MMCs (Figure 42, blue and black curves) and Al_2O_3 reinforced MMNC (Figure 42, red curve) appear to indicate three peaks; a very small exothermic peak between 496 and 518°C, a small endothermic peak with onset temperature of ~518°C and a larger endothermic peak between 560 and 670°C. Several literature studies on DSC analysis of Al-Cu-Mg alloys were consulted and none of the studies reported the presence of exothermic peaks between 496 and 518°C (Wang & Starink, 2007; Paul, 2014). In fact, no exothermic peaks were reported at temperatures above 340°C. It was deduced that the shallow exothermic peaks were due to the addition of the reinforcement phase. The exothermic peaks have small peak areas, indicating that the amount of material involved in the reaction was small. It was presumed that the exothermic peaks could be representing temperature ranges where small amounts of metal-ceramic compounds were formed as a result of interfacial reactions which took place. An in-depth analysis on these exothermic peaks will be done in future work. It can also be observed

that the presence of reinforcing particles increased the onset temperature for eutectic melting from 490 to 512°C.

The DSC study showed that the unreinforced 2124-Al, SiC reinforced MMCs and Al_2O_3 reinforced MMNC start melting at ~560°C (solidus temperature). Thus, the warm working temperature range for the unreinforced 2124-Al, MMCs and MMNC is between 168 and 336°C ($0.3\text{-}0.6T_{solidus}$). Thus, to investigate deformation behaviour of unreinforced 2124-Al, MMCs and MMNC, within the warm working temperature range, uniaxial compression testing was done at 170-280°C.

Sintering is a densification technique that normally follows cold compaction (Long *et al*., 2014). The sintering temperature is often set to a temperature between 60 and 90% of the temperature where the matrix material starts melting (Meluch, 2009). For this work, the sintering temperature was set at 490°C.

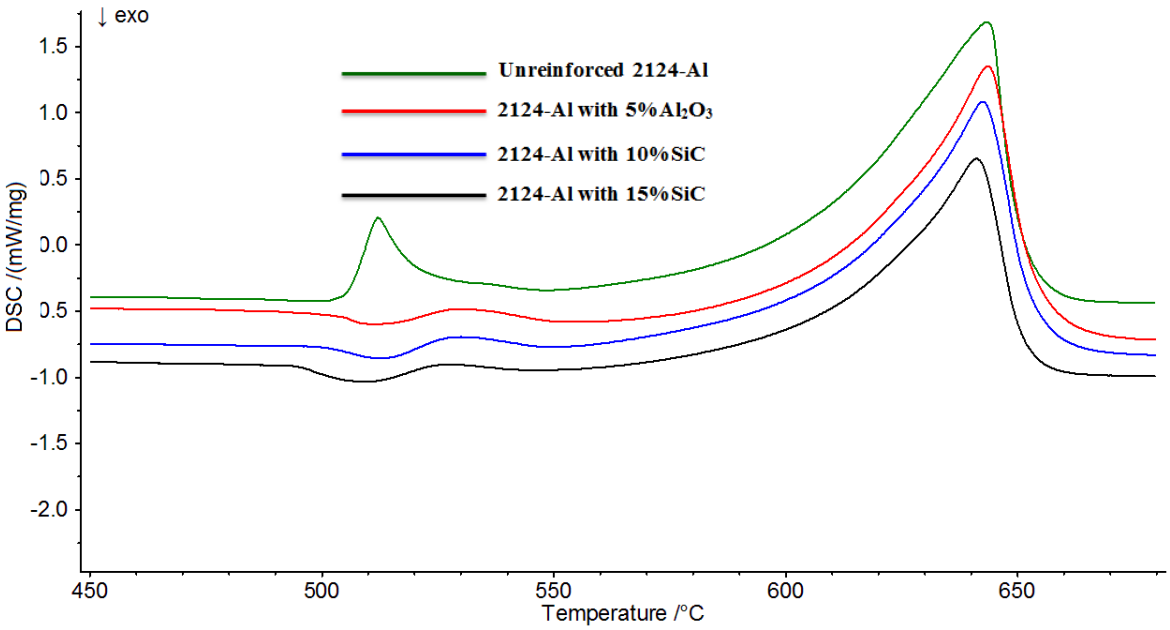

Figure 42: Graph showing DSC behaviour on heating of unreinforced 2124-Al alloy, and 2124-Al with: 5% Al_2O_3, 10% SiC and 15% SiC.

4.5.2 Metallographic evaluation of sintered compacts

Figure 43 shows that some 2124-Al particles bonded together due to sintering but there are still unbonded (dark) areas at the particle interfaces. Reinforcing particles are concentrated on the grain boundaries in the MMCs and MMNCs (Figures 44-48). This result is not unexpected since it was shown in Section 4.4 that after compaction the reinforcing particles were concentrated on the Al-alloy grain boundaries.

It can also be observed that the white eutectic phase spheroidised during sintering (Figures 43-50). X-ray mapping results show that the spheroidised eutectic particles consisted mainly of Cu (Figures 48-50) with small amounts of Si. Spheroidisation of the eutectic was attributed to incomplete eutectic dissolution during sintering, as the eutectic dissolution temperature is ~500°C. Also, spheroidisation minimises surface energy of the system, since fine lamellar eutectic phase particles have a larger surface energy than the spheroids (Zolotorevsky *et al*., 2007). Falticeanu *et al*. (2006) sintered an Al-Cu-Mg-Si alloy at 475°C and noticed that the microstructure consisted of undissolved Cu particles which appeared as bright, white particles. X-ray mapping analysis also showed that there were Si- and Mg- rich areas. The result obtained in this work is therefore quite similar to that of Falticeanu *et al*. (2006).

The implication of this incomplete eutectic dissolution is that there would be fewer precipitates formed if the materials were subjected to an ageing heat treatment, so the hardness in the aged condition would remain similar to the unaged alloy (Fransson, 2009).

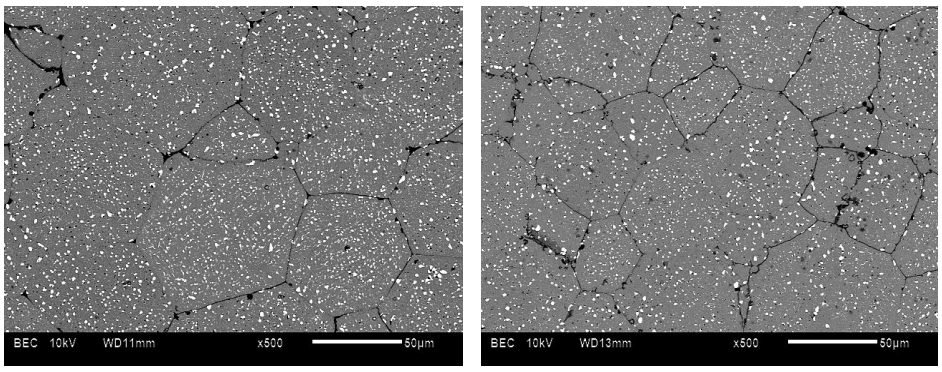

a b

Figure 43: SEM BSE micrographs showing consolidation at a) surface and b) core of sintered unreinforced 2124-Al compacts.

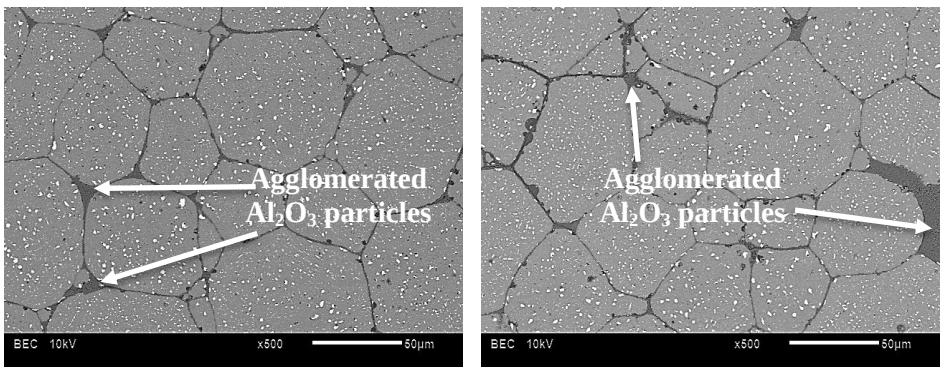

a b

Figure 44: SEM BSE micrographs showing consolidation at a) surface and b) core of sintered 2124-Al with 5% Al_2O_3 compacts.

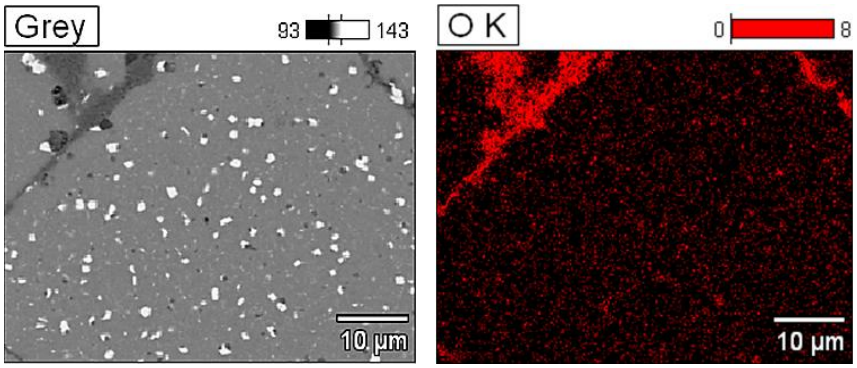

a b

Figure 45: X-ray mapping showing presence of nano-sized Al_2O_3 particles inside 2124-Al grains after sintering.

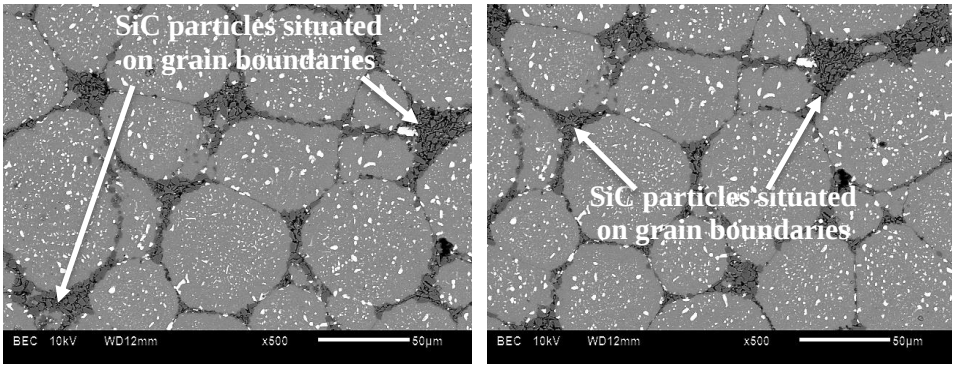

a b

Figure 46: SEM BSE micrographs showing consolidation at a) surface and b) core of sintered 2124-Al with 10% SiC compacts.

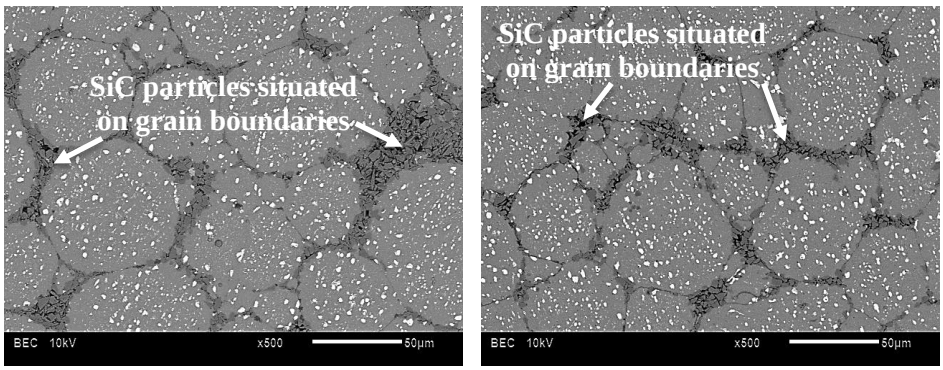

a b

Figure 47: SEM BSE micrographs showing consolidation at a) surface and b) core of sintered 2124-Al with 15% SiC compacts.

During sintering, increasing densification is achieved by decreasing porosity. Figure 51 shows that the relative densities of all the green compacts increased due to sintering, however full densification (a relative density of 100%) was not achieved. In the unreinforced 2124-Al alloy, this shows that the sintering conditions did not remove all the pores. In the composite materials, the reinforcing particles may have had a pinning effect on dislocations, grains and grain boundaries thus slowing down consolidation mechanisms during sintering (Dash *et al*., 2013). All the materials (unreinforced 2124-Al, Al_2O_3

MMNC and SiC MMCs) had relative densities above 90% prior to sintering which illustrates that the consolidation achieved by cold compaction was relatively good (Sridhar & Fleck, 2000).

The addition of reinforcing particles (Al_2O_3 or SiC) decreased the compressibility of the 2124-Al alloy, as the MMNCs and MMCs had lower relative densities than the unreinforced 2124-Al after compaction. The 15% SiC green compact had the lowest relative density after compaction (92.92%), which shows that compressibility decreased as reinforcement volume fraction increased. This confirms results of Long *et al*. (2014) and Casati & Vedani (2014), who found that consolidation of reinforced powders was poorer when compared to unreinforced powders due to the stiffer reinforcement phase reducing the plastic flow. Thus, composite powders are more difficult to compact because most of the applied pressure is supported by a stiffer reinforcement phase that does not compact easily (Hesabi *et al*., 2007).

The 10% SiC compact had the highest relative density (98.05%) after sintering which shows that better densification was achieved in this compact during sintering. The relative densities of the 5% Al_2O_3 MMNC (97.16%) and 15% SiC MMC (97.30%) were similar after sintering. So it can be inferred that 5 vol. % nano-sized Al_2O_3 particles had a similar effect on sinterability of 2124-Al alloy as 15 vol. % micron-sized SiC particles.

The 2124-Al with 5% Al_2O_3 composite had the lowest relative density, only increasing by 0.62% from 96.54 to 97.16%. A low increase in density due to sintering indicates a minimal amount of densification due to sintering. This was attributed to the fairly uniform distribution of the nano-sized Al_2O_3 particles inside the Al-alloy grains (Figure 45). The uniformly dispersed Al_2O_3 particles could have limited consolidation during sintering by pinning dislocations. Al_2O_3 particles concentrated at grain boundaries could have prevented interaction between Al alloy particles, thus hindering bonding and therefore densification (Rahimian *et al*., 2009). Thus the presence of nano-sized Al_2O_3 reinforcing particles lowered sinterability.

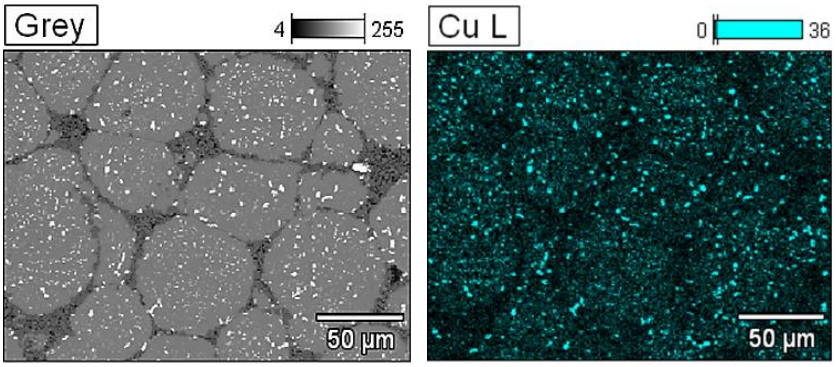

a b

Figure 48: X-ray mapping on sintered 2124-Al with 10% SiC compact.

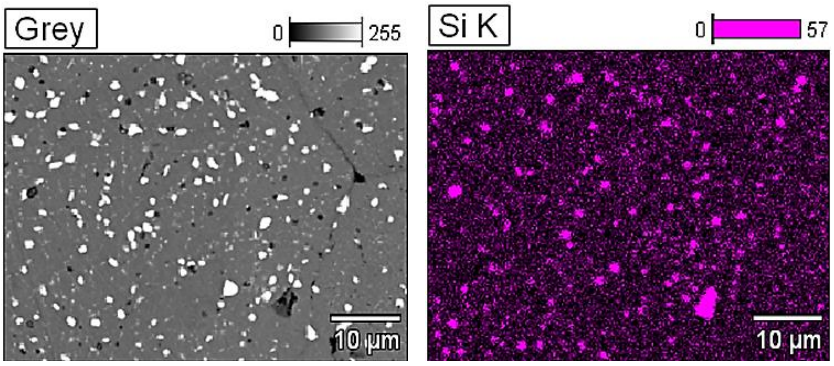

a b

Figure 49: X-ray mapping on sintered unreinforced 2124-Al alloy compact.

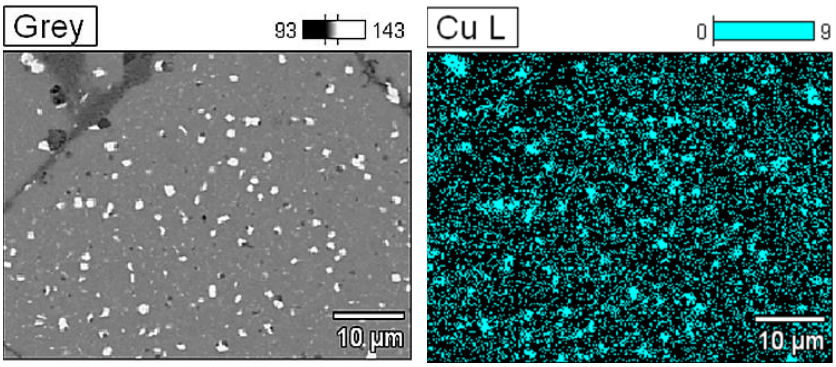

a b

Figure 50: X-ray mapping on sintered Al_2O_3 MMNC.

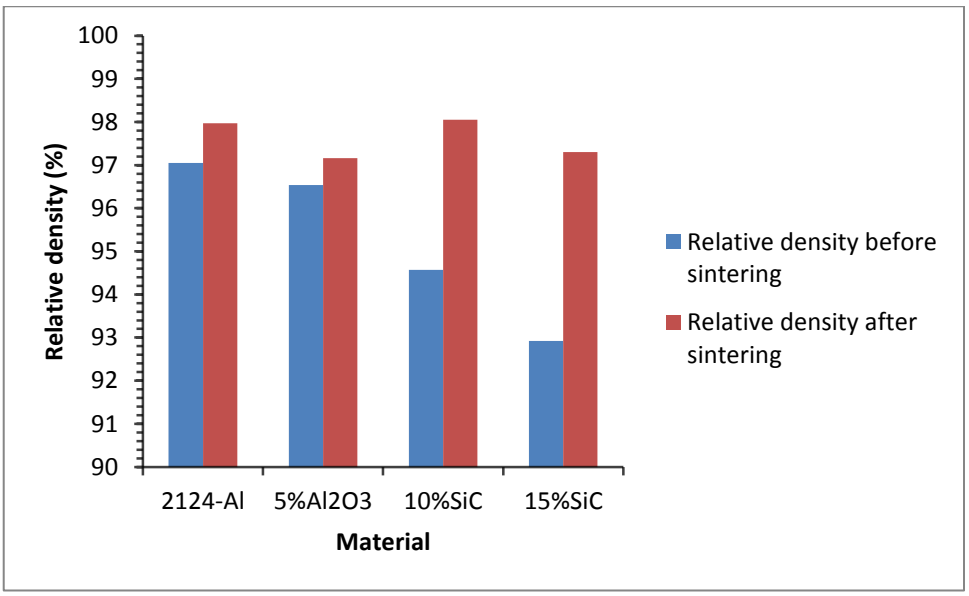

Figure 51: Relative densities before and after sintering.

4.6 Hardness of sintered compacts

Figure 52 shows that the hardness of the 2124-Al alloy was increased by the addition of Al_2O_3 or SiC reinforcement phases. Higher hardness was achieved at the core of the sintered compacts, except in the compact with 15% SiC. It was inferred that higher hardness was achieved at the core of the samples due to higher densification from sintering.

The difference in hardness from the surface to the core of the sintered compacts further supports the concept of non-uniform densification in compacted parts, which was discussed in Section 4.4. This variation in densification, and therefore hardness, means that the resistance to an applied load or permanent deformation is not uniform. This may compromise the load-bearing capacity of the compact since the regions with lower hardness will have lower resistance to applied load and deformation (Lim *et al.*, 2003). The hardness variation in the materials may lead to premature failure. For optimal performance of these materials in the sintered condition, this variation in hardness has to be taken into account in the design phase, where it may be beneficial to use the lowest hardness values. This also highlights the fact that surface hardness measurements do not give a true reflection of the hardness of a component made by compaction and sintering.

The core of the 2124-Al with 10% SiC sintered compact had the highest hardness of 93.80 $HV_{0.1}$ due to the high relative density after sintering (Figure 51). It can be deduced

that the micron-sized SiC particles had a better hardening effect than the nano-sized Al_2O_3 particles. This is contrary to Razavi-Tousi *et al*. (2011) who found that nano-sized reinforcing particles had a better hardening effect than micron-sized particles. Higher densification also increases hardness of the component (Suresh *et al*., 2015).

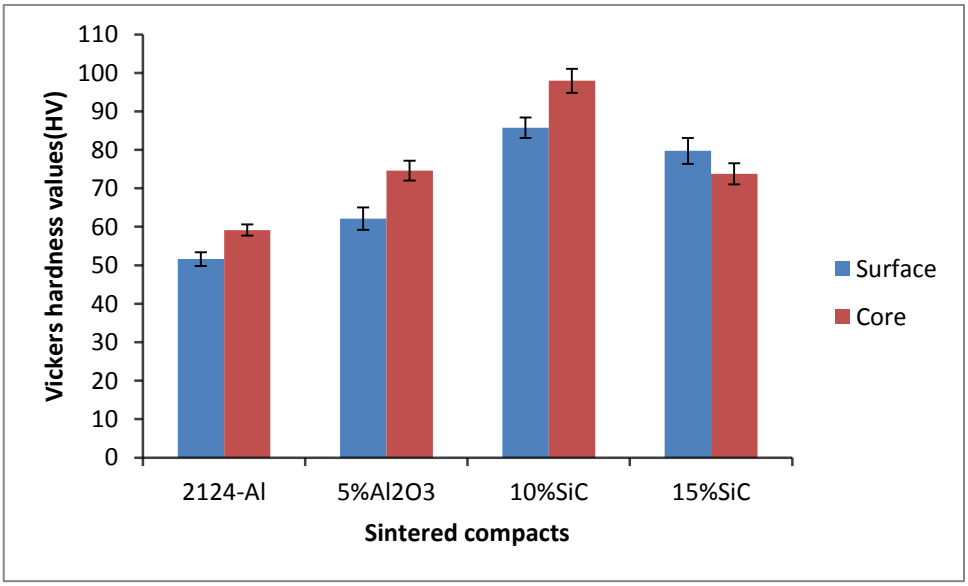

Figure 52: Average surface and core hardness of sintered compacts.

4.7 Uniaxial compression tests

4.7.1 Uniaxial compression of green compacts at ambient temperature

As expected, the green compacts fractured rapidly under the compressive load, during uniaxial compression tests, applied by the Gleeble 3500® at ambient temperature (Figure 53).

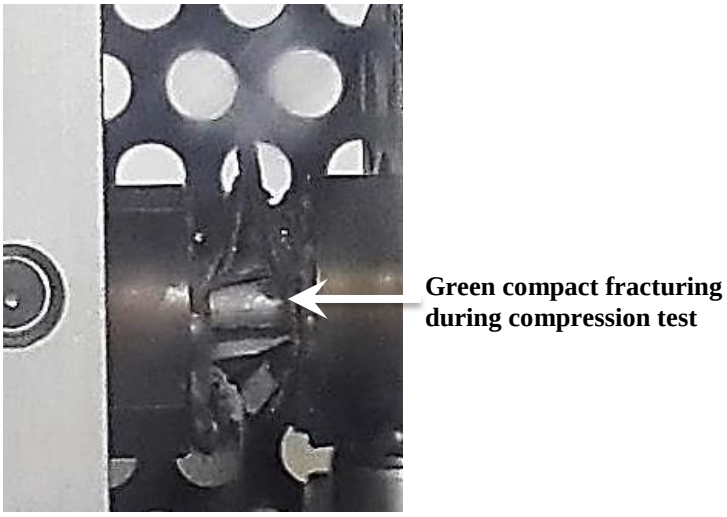

Figure 53: Compression test of a green compact at ambient temperature.

The compressive engineering stress-strain behaviour of the unreinforced 2124-Al, MMCs and MMNC was similar (Figure 54), and the compressive fracture stresses were similar at ~170 MPa.

The peculiar shape of the stress-strain curves in Figure 54 shows that the green compacts initially compressed and elastically deformed to a stress of ~170 MPa, and then started to fracture as the plastic region was approached, leading to a sharp decrease in stress due to a decrease in load bearing capacity as fracturing occurred (Orbulov & Ginsztler, 2012). The strains corresponding to ~170 MPa are 0.011 and ~0.02 for the unreinforced Al alloy and composites respectively. The poor workability of the unreinforced 2124-Al alloy, and alloys reinforced with 5% Al_2O_3 and 10% SiC was attributed to poor ductility at ambient temperature. At ambient temperature, ductility is poor because the dislocations and grains do not have enough energy to move, plastic flow is limited thus the bonds formed in the green compacts are weak which explains the severe fracturing in the materials (Syu & Ghosh, 1993).

There are two possible reasons for the major peaks in the stress-strain curves shown in Figure 54. Firstly, the sudden increase in stress may be due to a decrease in original diameter of the green compact caused as outer pieces spalled off during compression. Engineering stress-strain is based on the original diameter so a decrease in part diameter leads to an increase in stress since: $stress = \frac{Force}{Area}$ (Faridmehr *et al.*, 2014). Secondly, there could have been some strain hardening which led to an increase in stress (Brush Wellman Inc., 2010).

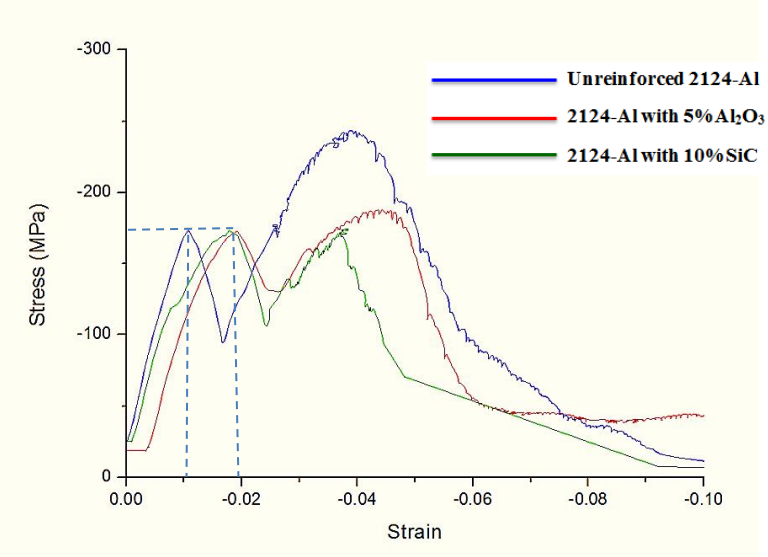

Figure 54: Compression behaviour of unreinforced 2124-Al alloy, 2124-Al with 5% Al_2O_3 or 10% SiC green compacts at ambient temperature, soak time = 6 min. and ε = 0.1 and $\dot{\varepsilon}$ = 0.01 s^{-1}.

4.7.2 Uniaxial compression of green compacts at 170°C

It was observed that at 170°C, similar to at ambient temperature, all the green compacts fragmented and this was attributed to limited ductility in the materials.

At a strain rate of 0.01 s^{-1} the SiC reinforcing particles had a better strengthening effect than the Al_2O_3 particles since reinforcing 2124-Al with SiC increased flow stress while the addition of Al_2O_3 led to a decrease in flow stress (Figure 55a). An increase in strain rate from 0.01 s^{-1} to 5 s^{-1} resulted in an increase in flow stress for the unreinforced 2124-Al alloy (90 to 98 MPa), a decrease in flow stress for 5% Al_2O_3 (52 to 40 MPa) and 15% SiC (95 to 84 MPa) while the flow stress of the 10% SiC compact increased by 1 MPa. An increase in strain rate may lead to heat generation due to an increase in deformation work and friction (Rajamuthamilselvan & Ramanathan, 2012). The generated heat, which is excess heat, increases the deformation temperature and may improve plastic flow by giving more atoms energy to move (Osakada, 1997). The decrease in flow stress of the MMCs and MMNC with an increase in strain rate could be due to an increase in temperature promoting softening due to improved dislocation climb and movement.

Nano-sized reinforcing particles are reported to have a better strengthening effect than micron-sized particles (Razavi-Tousi *et al.*, 2011). However, from Figure 55 it can be observed that the Al_2O_3 reinforced MMNC had a lower flow stress when compared to the SiC reinforced MMCs. This was attributed to agglomerated Al_2O_3 particles situated at grain boundaries (Figure 40, Section 4.4). Figure 41 shows that although there were agglomerated particles in the MMCs as well, there were also many areas at grain boundaries where there were no reinforcing particles and grains adjacent to one another could bond. These Al_2O_3 agglomerates situated at grain boundaries may have made the MMNCs susceptible to fracture during compression. Fracturing reduces the load bearing capacity of a material, resulting in a decrease in flow stress.

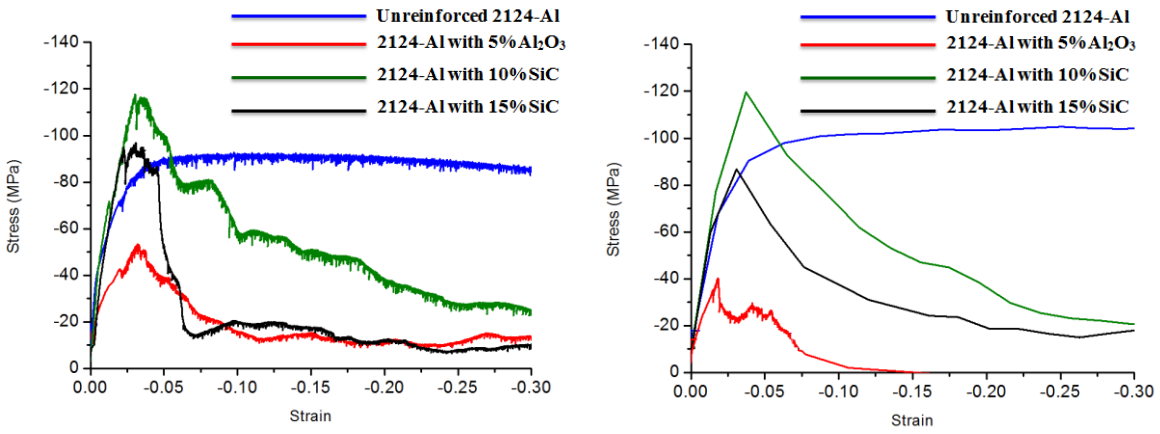

Figure 55: Compression behaviour of green compacts at 170°C, ε = 0.3, $\dot{\varepsilon}$ of a) 0.01 s^{-1}, b) 5 s^{-1}.
[Unreinforced 2124-Al alloy (blue curves), 5% Al_2O_3 (red), 10% SiC (green) and 15% SiC (black)]

4.7.3 Uniaxial compression of green compacts at 220°C

When Figures 56a and 56b are compared it can be observed that higher flow stresses were achieved at the lower strain rate of 0.01 s^{-1}. This can be attributed to the more pronounced effect of strain hardening at lower strain rates. The decrease in flow stress with an increase strain rate observed in Figure 56 could also be as a result of softening due cracking, void nucleation or particle debonding that may have become more pronounced at the higher strain rate (Fleck *et al*., 1989).

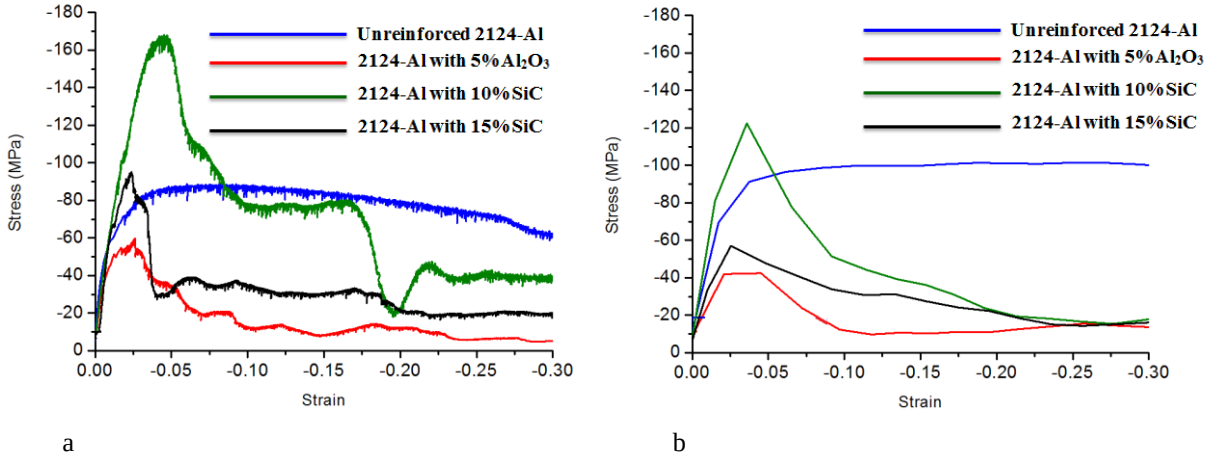

Figure 56: Compression behaviour of green compacts at 220°C, ε = 0.3, $\dot{\varepsilon}$ of a) 0.01 s^{-1}, b) 5 s^{-1}.
[Unreinforced 2124-Al alloy (blue curves), 5% Al_2O_3 (red), 10% SiC (green) and 15% SiC (black)]

4.7.4 Uniaxial compression of green compacts at 280°C

The deformation behaviour of the compacts at 170, 220 and 280°C is similar (Figures 55-57). The deformation behaviour of the 2124-Al alloy is substantially altered by the addition of Al_2O_3 or SiC reinforcing particles. The deformation behaviour of the 15% SiC MMC was the most affected by an increase in strain rate from 0.01 to 5 s^{-1} at 280°C since its flow stress increased from ~30 to 105 MPa (black curves in Figure 57). It is possible that the higher strain rate improved plastic flow due to improved mobility of dislocations, grains and grain boundaries (Osakada, 1997) in this compact which led to strain hardening and ultimately an increase in flow stress.

At 280°C and strain rate of 5s^{-1} the flow stress of the 15% SiC MMC and the 10% SiC MMC were the same. Under these conditions, 10 and 15 vol. % SiC had the same effect on flow stress therefore it is more efficient to add 10 vol. % SiC to the 2124-Al alloy to improve flow stress.

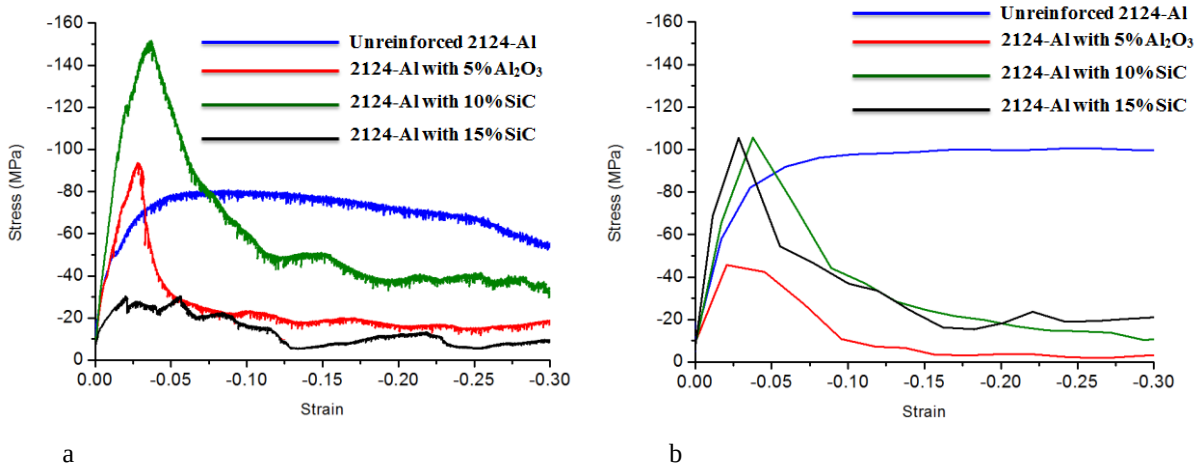

Figure 57: Compression behaviour of green compacts at 280C, ε = 0.3, $\dot{\varepsilon}$ of a) 0.01s^{-1}, b) 5 s^{-1}.
[Unreinforced 2124-Al alloy (blue curves), 5% Al_2O_3 (red), 10% SiC (green) and 15% SiC (black)]

Figures 55, 56 and 57 show the deformation behaviour of unreinforced 2124-Al alloy, 2124-Al with 5% Al_2O_3, 2124-Al with 10% SiC and 2124-Al with 15% SiC green compacts at 170, 220 and 280°C and strain rates of 0.01 and 5 s^{-1}. The results show that the unreinforced 2124-Al alloy deformed at a constant stress as strain increased. In the Al_2O_3 and SiC reinforced composites stress increased up to a certain point, decreased slightly and then steadily deformed at a lower stress as strain increased. At all temperatures (170, 220 and 280°C) and both strain rates (0.01 and 5 s^{-1}) the softening mechanism in the unreinforced 2124-Al alloy seems to be dynamic recovery (DRV) while engineering stress-strain curves for MMCs and the MMNC suggest that other softening mechanisms,

e.g. dynamic recrystallisation (DRX), cracking, void nucleation, particle debonding and adiabatic heating, decreased the flow stress. The curves showing deformation behaviour of the MMCs and MMNC (red, green and black curves) have a different shape to the blue curve of the unreinforced 2124-Al alloy. DRX in MMCs and MMNC can be attributed to an increase in stored strain energy due to an increase in dislocation density. The increase in dislocation density may be due to a coefficient of thermal expansion (CTE) and elastic modulus (EM) mismatch between the matrix and reinforcement as well as dislocation pile up near the stiffer reinforcing particles (Selvan & Ramanathan, 2013). The driving force for DRX is stored strain energy and there is a critical amount of stored strain energy that has to be reached for DRX to occur in a material (Llorca, 2002). So, an increase in dislocation density caused by the addition of reinforcing particles to the Al alloy matrix increased stored strain energy and promoted DRX (Ko *et al*., 1999). It can be observed that the shapes of some of the stress-strain curves for MMCs and MMNCs are not completely consistent with a typical curve indicating occurrence of DRX. It is indeed also likely that the softening observed in the stress-strain curves for MMCs and MMNCs was due to void nucleation, particle debonding and cracking (Fleck *et al*., 1989).

Dislocation climb and cross-slip occur easily in aluminium and its alloys due to high stacking fault energy. For this reason, stored strain energy in aluminium and its alloys is low thus DRV is the softening mechanism (Chu-ming *et al*., 2005). It can be deduced that the softening mechanism in the unreinforced 2124-Al alloy remained DRV at all conditions because of its high stacking fault energy. So the stored strain energy in the unreinforced 2124-Al alloy was not enough to induce DRX (Shao *et al.*, 2010).

According to Li *et al*. (2014), grain coarsening is expected to occur during DRV due to grain boundary migration. DRX is confirmed by recrystallised grains in the deformed microstructure (Doherty *et al*., 1997). It may be beneficial in future work to confirm the presence of DRV and DRX by transmission electron microscopy (TEM) analysis of the deformed microstructures, since fine (nucleated) grains, dislocation networks within grains and dislocation density in a material can be observed (Yadav & Bauri, 2012; Babu *et al*., 2016).

4.7.5 Integrity of the as-deformed green compacts

Visual inspection of the deformed samples showed that samples compressed at 280°C and 5 s^{-1} had the best integrity (Figures 58 and 59). The samples deformed and remained intact

(except the 5% Al_2O_3 sample) but the 2124-Al with SiC deformed samples showed surface cracks. The surface cracking was worsened by an increase in SiC volume fraction (from 10 to 15 vol. % SiC) in the Al alloy matrix. This was attributed to the embrittling effect of SiC reinforcing particles situated on Al alloy grain boundaries (Figures 46 and 47), poor bonding in the SiC reinforced composites as well as possibility of non-uniform deformation due to an inhomogeneous distribution of SiC particles in some areas of the Al alloy matrix. Non-uniform deformation is shown by the bulging of the deformed samples (Totten *et al*., 2002).

Overall, the uniaxial compression tests performed on the Gleeble 3500® illustrated that it is possible to deform unreinforced 2124-Al and SiC reinforced MMC green compacts at 280°C which is within the warm working temperature range.

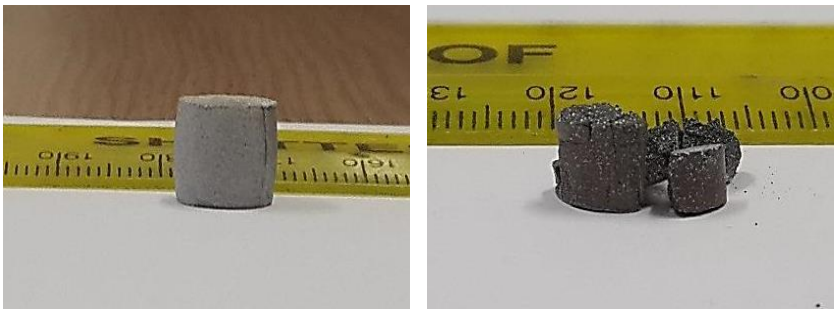

a b

Figure 58: Compacts after uniaxial compression at 280°C, strain rate of 5 s^{-1} and total strain of 0.3
a) unreinforced 2124-Al and b) 2124-Al with 5%Al_2O_3.

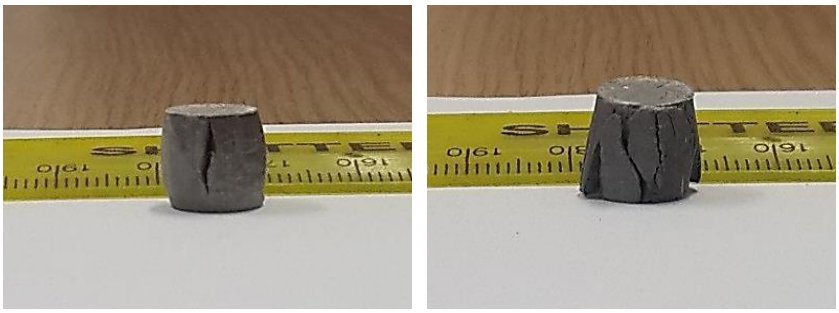

a b

Figure 59: Compacts after uniaxial compression at 280°C, strain rate of 5 s^{-1} and strain of 0.3
a) 2124-Al with 10%SiC and b) 2124-Al with 15%SiC.

4.7.6 Effect of sintering on deformation behaviour

The temperature and strain rate which provided the best warm compression behaviour were 280°C and 5 s^{-1} respectively. The green compacts were sintered at 490°C for 1 hour. The

deformation behaviour of these sintered compacts was then evaluated at 280°C, 5 s^{-1}, total strain of 0.3 and soaking time of 6 minutes.

When the results in Figures 60 and 61 are analysed, it can be seen that sintering affected the deformation behaviour of each material differently.

Unreinforced 2124-Al (Figure 60a): the stress increased with an increase in strain until the maximum strain of 0.3 was reached. The maximum stress of the unreinforced Al alloy was unchanged by sintering since it was ~100 MPa in both the unsintered and sintered condition.

The flow stress of the 2124-Al with 5% Al_2O_3 sample (Figure 60b) increased significantly due to sintering (45 to 99 MPa). During sintering, mobility of atoms, dislocations, grains and grain boundaries may be increased because keeping a sample at an elevated temperature for an increased period of time leads to more atoms gaining energy thus the flow of particles in the material is improved (Osakada, 1997). In the sintered condition, 2124-Al with 5% Al_2O_3 was therefore able to deform better and improve bonding in the material which led to an increase in flow stress. There seems to be a delay in the onset of DRX in the sintered condition, as the onset strain for DRX in the 2124-Al with 5% Al_2O_3 was 0.06 while in the unsintered condition DRX started at a lower strain of 0.04.

Sintering resulted in an increase in flow stress in the 10% SiC sample (Figure 61a) where the flow stress increased from 105 MPa (black curve, Figure 61a) to ~135 MPa (green curve, Figure 61a). In the 10% SiC the onset strain for dynamic recrystallisation (DRX) increased due to sintering from a strain of 0.04 (unsintered) to 0.15 (sintered), shown by the green curve in Figure 61a. The flow stress of the 15% SiC sample decreased significantly due to sintering: 105 MPa in the unsintered condition and ~56 MPa after sintering (Figure 61b). The onset strain for DRX increased from 0.025 to 0.05 after sintering in the 15% SiC sample.

The delay in DRX onset due to sintering was presumed to occur because sintering improved plastic flow, which meant that movement of dislocations and dislocation climb was easier thus delaying dislocation pile up (Morse, 2011). This slowed down the rate at which dislocation density increased which meant that it took longer to reach the critical stored strain energy for DRX to commence. The delay of the onset for DRX caused by sintering seems to be a positive effect because it allowed for the materials to be deformed at higher stresses over slightly larger strain ranges when compared to the unsintered condition.

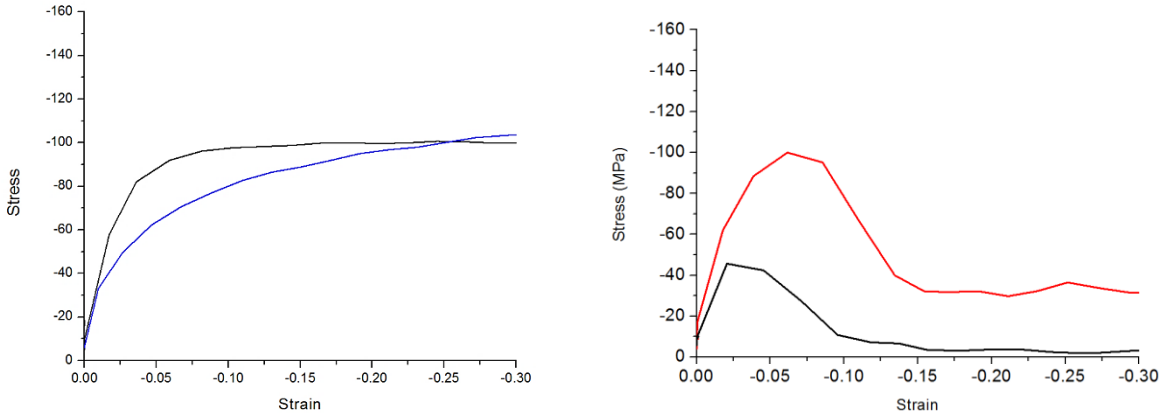

a b

Figure 60: Compression behaviour of sintered compacts at 280°C, strain rate of 5 s^{-1} and total strain of 0.3. a) unsintered (black curve) and sintered (blue curve) 2124-Al and b) unsintered (black curve) and sintered (red curve) 5% Al_2O_3.

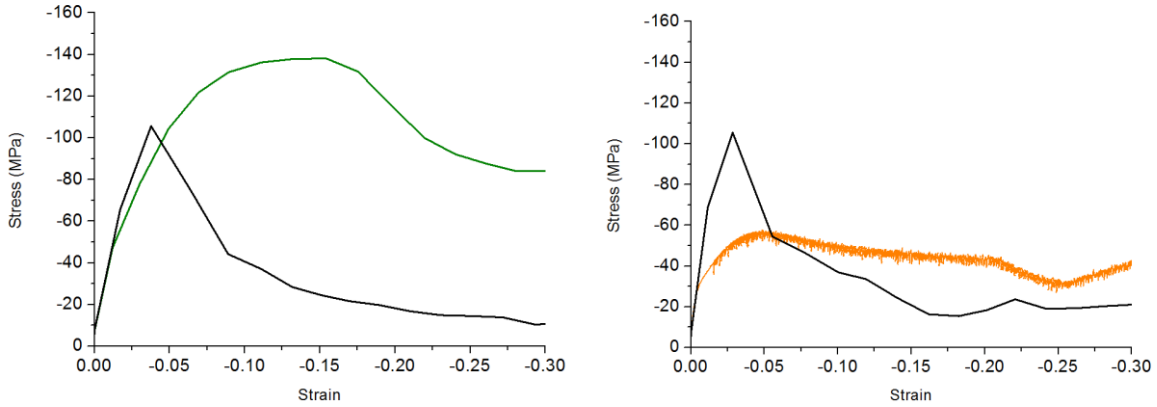

a b

Figure 61: Compression behaviour of sintered compacts at 280°C, strain rate of 5 s^{-1}, total strain of 0.3. a) unsintered (black curve) and sintered (green curve) 10% SiC and b) unsintered (black curve) and sintered (orange curve) 15% SiC.

4.7.7 Effect of increasing the soaking time from 6 to 20 min. on deformation behaviour

Unreinforced 2124-Al

Figure 62a shows that, with an increase in soaking time from 6 – 20 minutes (black vs. blue curves), stress increased with an increase in strain until the maximum strain of 0.3 was reached. It can be observed that a maximum stress of ~100 MPa was reached. This result is similar to that obtained after sintering (Figure 60a). The increase in stress with strain can be attributed to an increase in dislocation density and strain hardening as deformation occurred (Roylance, 2001). It can be seen that sintering at 490°C for 1 hour and increasing soaking time from 6 – 20 minutes at 280°C had a similar effect on

deformation behaviour of the unreinforced 2124-Al (green curve, Figure 62a). This result is positive because it can result in cost savings since it has been learned that for the unreinforced 2124-Al the sintering step can be eliminated. So, the unreinforced 2124-Al green compact can be soaked for 14 minutes longer at 280°C instead of sintering at 490°C for 1 hr prior to compression. The green curve in Figure 62a shows that sintering the unreinforced 2124-Al and then soaking it at 280°C for longer (*i.e.* 20 minutes) prior to uniaxial compression yielded a slightly lower flow stress of ~95 MPa.

5%Al_2O_3

The flow stress of the 5% Al_2O_3 compact decreased from ~45 MPa to 21 MPa when it was soaked at 280°C for a longer period of time (*i.e.* 20minutes) prior to uniaxial compression (black vs. blue curve, Figure 62b). This was attributed to the 2124-Al with 5% Al_2O_3 being easier to deform due to an improved mobility of dislocations, grains and grain boundaries (Robbins, 2012). It can be observed that sintering produced a higher flow stress than an increased soaking time because the flow stress of the 2124-Al with 5% Al_2O_3 was ~45 MPa and increased to 99 MPa after sintering. Sintering may have resulted in better plastic flow in the 2124-Al with 5%Al_2O_3 and dislocation density and strain hardening increased as deformation progressed. It can be observed that when the 2124-Al with 5% Al_2O_3 is sintered and then a longer soaking time of 20 minutes is used prior to uniaxial compression it experiences softening at a higher strain (green curve, Figure 62b). This is advantageous because it is able to withstand higher stresses over a larger strain range. It was thus inferred that for the 2124-Al with 5% Al_2O_3, it is beneficial to sinter and then use a higher soaking time of 20 minutes prior to uniaxial compression.

10%SiC

The flow stress of the 2124-Al with 10 %SiC green compact was positively affected by an increase in soaking time (black vs. blue curve, Figure 63a) as the flow stress of 2124-Al with 10% SiC increased from 105 MPa to 128 MPa. It can also be observed that sintering increased the flow stress of 2124-Al with 10% SiC more than an increase in soaking time (green curve, Figure 61a vs. blue curve, Figure 63a). The flow stress of the 2124-Al with 10% SiC was 134 MPa after sintering (green curve, Figure 61a). It was deduced that sintering had a better effect on flow stress and deformation behaviour of the 10% SiC compact. In the sintered condition (green curve, Figure 61a), the 2124-Al with 10% SiC only started to experience softening at a higher strain of ~0.15. The blue curve in Figure 63a shows that when a longer soaking time of 20 minutes was used, softening

occurred at a lower strain of 0.045. Combining sintering with an increase in soaking time prior to uniaxial compression had a very positive effect on the deformation behaviour of the 10 %SiC compact (green curve, Figure 63a). The green curve in Figure 63a shows that the flow stress of the 10% SiC was ~153 MPa as a result of sintering and increasing soaking time prior to uniaxial compression. It can also be observed that the 2124-Al with 10% SiC experienced no decrease in stress with an increase in strain. This means that it was able to deform at a flow stress of ~153 MPa until the maximum total strain of 0.3 was reached. The shape of the green curve in Figure 63a suggests that the softening mechanism in the 2124-Al with 10% SiC was changed from DRX to DRV by sintering at 490°C for 1 hr and then using a longer soaking time of 20 minutes prior to uniaxial compression at 280°C and strain rate of 5 s^{-1}.

The best deformation (*i.e.* good ductility; shown by large plastic region and high flow stress) was achieved in the 2124-Al with 10% SiC MMC because it plastically deformed at the highest stress (~153 MPa) up to the maximum total strain of 0.3. The deformed 2124-Al with 10% SiC sample was visually inspected and it was found that it deformed well with only a few minor surface cracks (Figure 64).

<u>15%SiC</u>

Increasing soaking time for the 15% SiC compact decreased flow stress from 105 MPa to 69 MPa (black vs. blue curve, Figure 63b). This could be due to the fact that mobility of dislocations, grains and grain boundaries improved and the sample became easier to deform thus requiring less pressure for deformation (Robbins, 2012). When Figures 61b and 63b are compared it can be seen that increasing soaking time had a better effect on flow stress than sintering. Sintering resulted in a lower flow stress of 54 MPa. This result makes sense because during sintering, the 15% SiC compact was exposed to a higher temperature (490°C *vs.* 280°C) for a longer period of time (1 hour vs. 20 minutes). This means that more atoms gained energy to move thus mobility of dislocations and grains improved. The 15% SiC compact was therefore much easier to deform in the sintered condition, which explains the lower flow stress (Robbins, 2012). The higher temperature probably also allowed for annihilation and easier slip of dislocations and this competed with strain hardening, which would explain the more steady decrease in stress depicted by the orange curve in Figure 61b as compared to the blue curve in Figure 63b (Morse, 2011).

The flow stress of the 15% SiC increased to 138 MPa (green curve, Figure 63b) when it was sintered at 490°C for 1 hour prior to testing, and soaked at 280°C for 20 minutes in the Gleeble before uniaxial compression. When the green curve in Figure 63b was analysed it was noted that the deformation behaviour of the 15% SiC sample also improved since: the transition from the elastic to the plastic region is much smoother, it plastically deformed at a higher stress over a larger strain range and only started experiencing softening at a higher strain of 0.175. It was inferred that the onset for DRX was delayed by this process of sintering and then increasing soaking time prior to uniaxial compression. This is possibly due to a delay in the accumulation of critical stored strain energy for DRX as a result of easier dislocation movement and overall improvement in plastic flow (Llorca, 2002). For 15% SiC, it seems to have been more beneficial to sinter and then increase soaking time from 6 to 20 minutes prior to uniaxial compression.

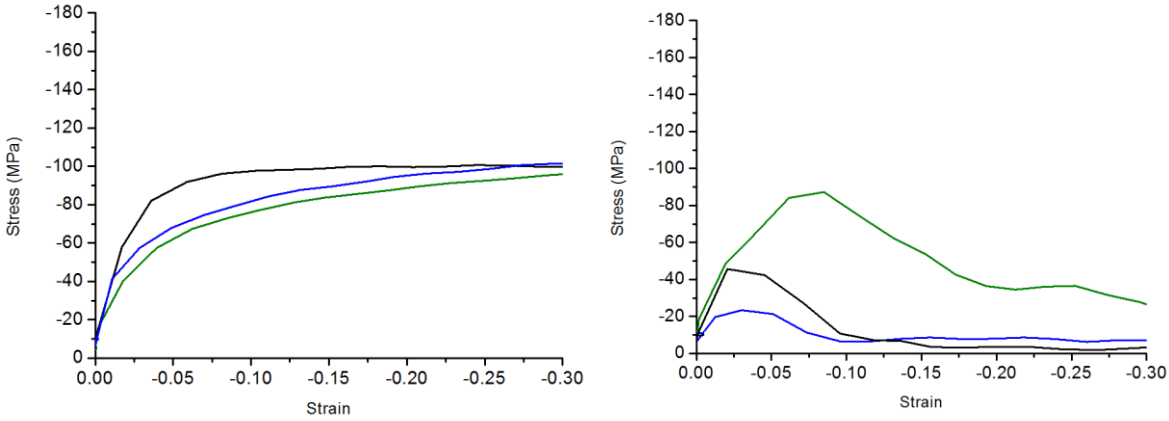

a b

Figure 62: Compressive behaviour of a) 2124-Al and b) 5%Al_2O_3 at 280°C, 5 s^{-1}, strain of 0.3 using a soaking time of 6 minutes (black curve), 20 minutes (blue curve) and sintering at 490°C for 1 hr prior to compression + using 20 minutes soaking time (green curve).

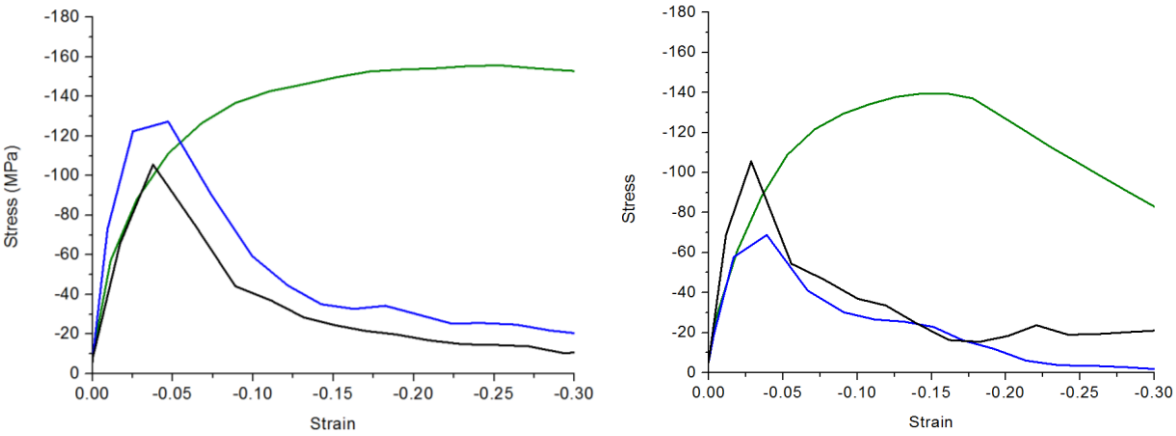

a b

Figure 63: Compressive behaviour of a) 10% SiC and b) 15% SiC at 280°C, 5 s^{-1}, strain of 0.3 using a soaking time of 6 minutes (black curve), 20 minutes (blue curve) and sintering at 490°C for 1 hr prior compression + using 20 minutes soaking time (green curve).

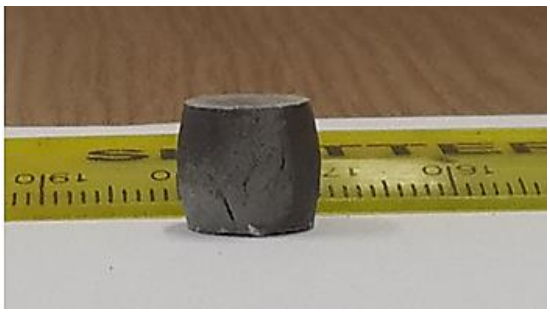

Figure 64: 2124-Al with 10% SiC sample which was sintered at 490°C for 1 hr, soaked at 280°C for 20 minutes and uniaxially compressed at 280°C and strain rate of 5 s^{-1} up to a total strain of 0.3.

4.7.8 Metallographic evaluation of uniaxially compressed samples

Unreinforced 2124-Al

In the unreinforced 2124-Al alloy sample deformation and bonding occurred due to uniaxial compression (Figure 65). There seems to be a lot of porosity (shown by smaller, darker spots). The pores found along the grain boundaries may be due to debonding. When comparing sintered unreinforced 2124-Al (Figure 66) and uniaxially compressed unreinforced 2124-Al (Figure 65) it can be seen that there is a slight change in the shape of the grains after uniaxial compression; indicating deformation. This change in shape is shown by the fact that the 2124-Al grains are more irregular in shape, with some slightly elongated, after uniaxial compression (Figure 65).

Engineering stress-strain curves for the uniaxially compressed unreinforced 2124-Al alloy suggested that it experienced dynamic recovery (DRV) during uniaxial compression. According to Li *et al*. (2014), grain coarsening is expected to occur during DRV due to grain boundary migration. The linear intercept method was used to measure grain size of sintered and uniaxially compressed unreinforced 2124-Al alloy. The average grain size increased from 39.42 µm to ~46.86 µm when sintered 2124-Al alloy samples were uniaxially compressed. This result confirms the occurrence of DRV in the unreinforced 2124-Al alloy since there was an increase in grain size. However, Standard Deviation (STDEV) values showed that this was not a significant increase since the STDEVs were close to each other. The STDEV for grain size measurement data was found to be 14.01 and 10.15 for sintered and uniaxially compressed samples respectively.

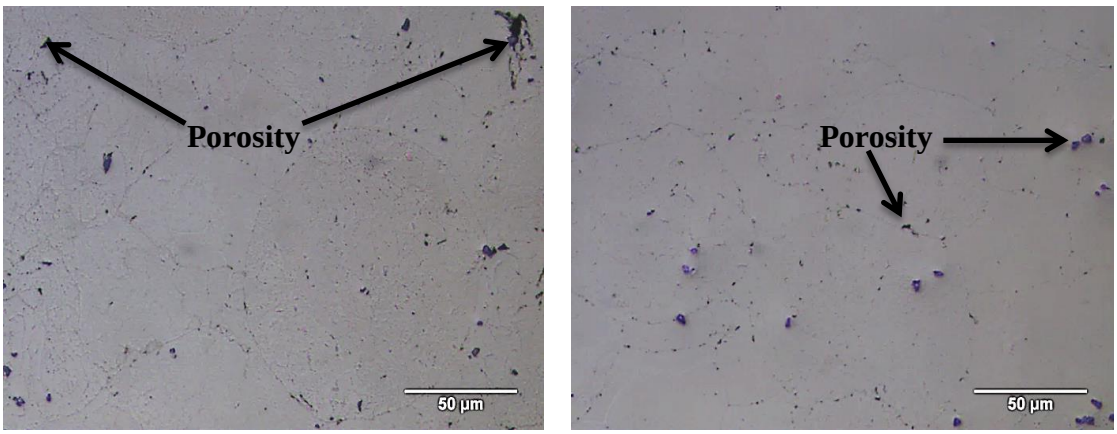

a b

Figure 65: Optical micrographs showing consolidation at the a) surface and b) core of unreinforced 2124-Al compact after uniaxial compression at 280°C and strain rate of 5 s^{-1} (scale bar= 50 µm).

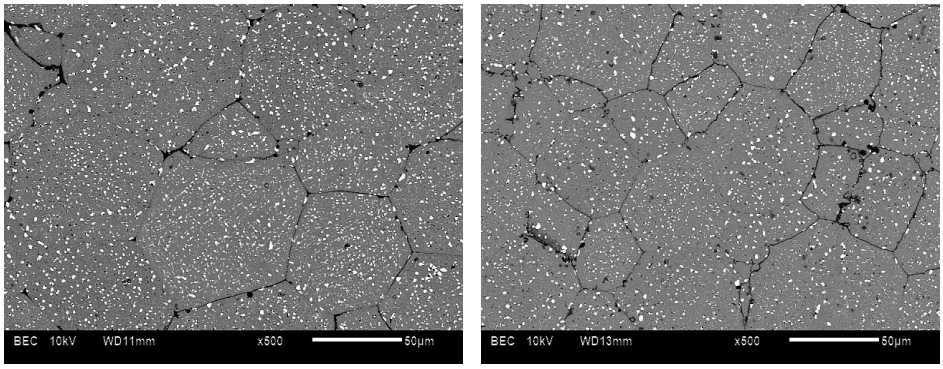

a b

Figure 66: SEM BSE micrographs showing consolidation at a) surface and b) core of sintered unreinforced 2124-Al compacts (scale bar = 50 µm).

5% Al_2O_3

Figure 67 shows that there were still nano-sized Al_2O_3 particles situated on Al alloy grain boundaries (shown by orange arrows) after uniaxial compression of 5% Al_2O_3 sample. These Al_2O_3 particles may have contributed to fragmentation in the alloy since they may have made grain boundaries brittle and thus susceptible to fracture. There are smaller grains that seem to have nucleated from the grain boundaries (shown by green arrows in Figure 67). These grains were thought to be recrystallised grains which may have formed as a result of dynamic recrystallisation (DRX) (Doherty *et al*., 1997). The number of recrystallised grains increases with deformation (Tian *et al*., 2004). It is possible that deformation was limited by fragmentation, which may explain why only a few recrystallised grains were seen. The spheroidised eutectic was still visible inside the 2124-Al grains as small, brighter particles.

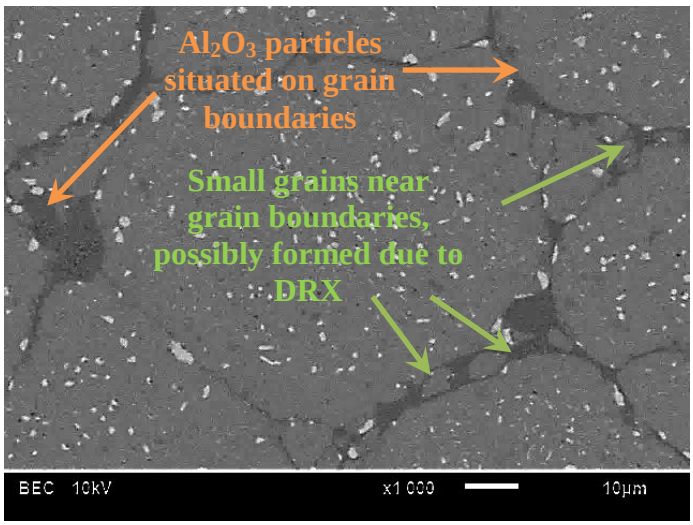

Figure 67: SEM BSE micrograph showing consolidation in the 2124-Al with 5% Al_2O_3 sample after uniaxial compression at 280°C, 5 s^{-1} and strain of 0.3 (scale bar=10 µm).

10%SiC

Figures 68 and 69 show that, in the 10% SiC uniaxially compressed sample, the shape of the Al alloy grains changed slightly (due to deformation) and bonding between grains also took place. There are SiC particles that are dispersed inside deformed Al alloy grains. There is a possibility that some of these particles could have broken away from agglomerates at grain boundaries, and then be forced into the grains during grinding and polishing. However, Figure 68 shows that SiC reinforcing particles can be moved inside the matrix grains by matrix flow during deformation, since there are SiC particles which seem embedded in the matrix. This highlights the importance of careful selection of grinding and polishing parameters (*e.g.* force and time) and sequence. Lower forces may not remove loose reinforcing particles from grain boundary clusters and forces that are too high may cause particle pull-out. Point 1 (red arrow in Figure 68) shows a particle that seems to be pulling out of the matrix, which may have occurred during grinding or polishing due to too much force being applied on the samples. Point 2 (orange arrows in Fig. 68) shows what was assumed to be residue of SiC particles that were possibly ground or polished away.

From Figure 69 it can be observed that in the 10%SiC sample, SiC particles dispersed inside slightly deformed 2124-Al grains; implying that deformation influenced distribution of SiC particles. This is likely because microstructures of 2124-Al with 10 %SiC compacts prior to uniaxial compression (Figure 70) showed no evidence of SiC particles which were dispersed inside Al alloy grains.

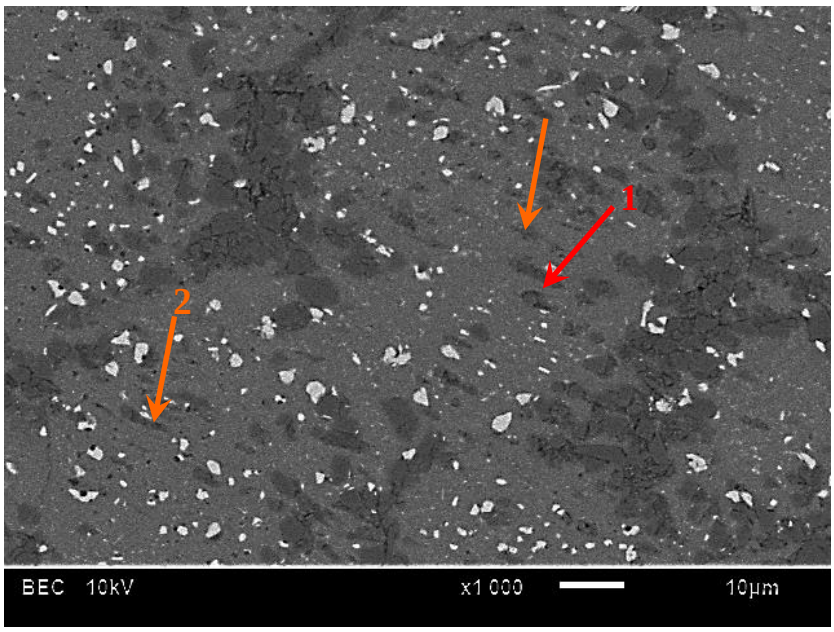

Figure 68: SEM BSE micrograph of uniaxially compressed 2124-Al with 10% SiC sample showing 1) particle which appears to be pulling out of the matrix 2) residue of SiC particles that seem to have been ground away.

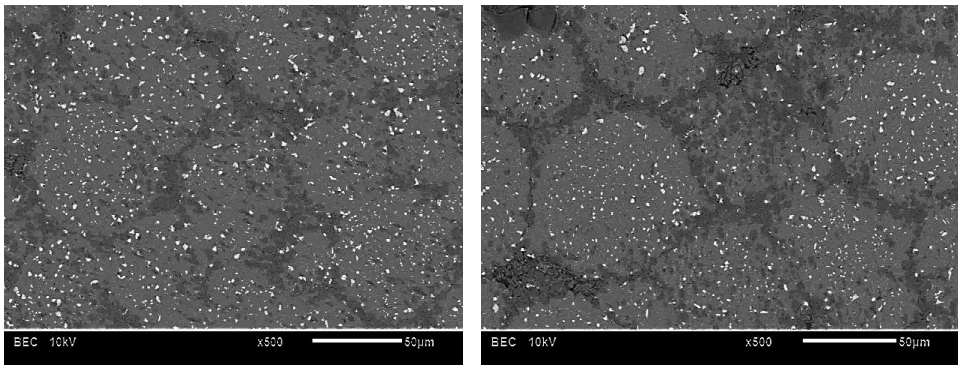

a b

Figure 69: SEM BSE micrographs showing deformation of uniaxially compressed 2124-Al with 10% SiC at the a) surface and b) core (scale bar = 50 µm).

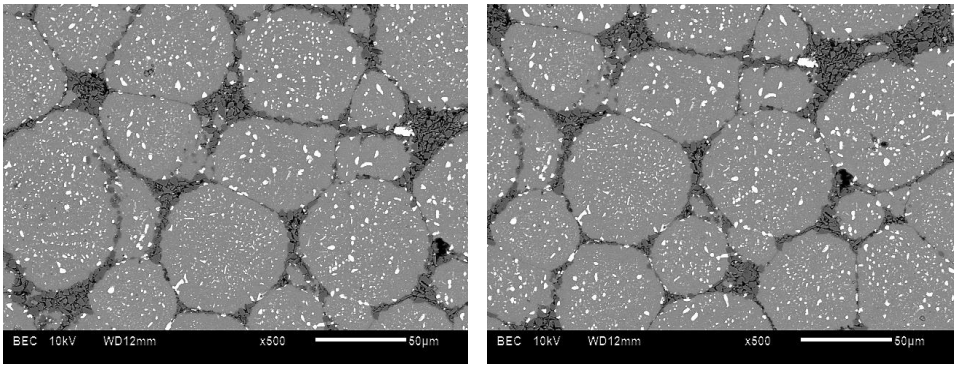

a b

Figure 70: SEM BSE micrographs showing consolidation at a) surface and b) core of sintered 2124-Al with 10% SiC compacts (scale bar = 50 µm).

15%SiC

The surface of the uniaxially compressed 15%SiC sample experienced a significant amount of deformation (Figure 71) where most of the grains elongated due to deformation. However, deformation seems to have had very little effect on the distribution of SiC particles. It was thought that the higher volume fraction of SiC resulted in larger SiC clusters at grain boundaries which were more difficult to disperse. Figure 71b shows an area where two Al alloy grains bonded and a few SiC particles are inside the grain (shown by green circle in Figure 71b). It was deduced that in the 15% SiC sample higher forces are required for deformation to have an effect on the distribution of SiC particles.

There seems to have been poorer load transfer in the 15% SiC uniaxially compressed sample since the surface deformed extensively (Figure 71) while very little deformation seems to have occurred at the core (Figure 72). This can be seen by the significantly smaller amount of grains whose shape was altered by uniaxial compression in the core of the sample. This suggests that deformation at the core was limited. The higher vol. % of SiC (*i.e.* 15%) resulted in poorer load transfer because there was a larger amount of harder and stiffer SiC particles to carry the applied load at the surface. More deformation is expected to occur with higher loads than lower loads. The considerably higher deformation at the surface supports this notion. When the 10% SiC (Figure 69) and 15% SiC (Figures 71 &72) uniaxially compressed samples are compared it can be deduced that a better distribution of SiC particles was achieved in the 10% SiC than 15%SiC sample after uniaxial compression.

An increase in soaking time from 6 to 20 minutes and sintering prior to uniaxial compression improved deformation behaviour of composite materials at 280°C significantly (Figures 62b and 63), especially that of the 10% SiC uniaxially compressed sample (green curve, Figure 63a and Figure 64). A comparison between Figures 69 and 73 shows that the distribution of SiC particles achieved was similar. It was therefore inferred that although an increase in soaking time resulted in a significant improvement in deformation behaviour, higher strains (due to more deformation) may be required to further improve distribution of SiC particles in the Al alloy matrix.

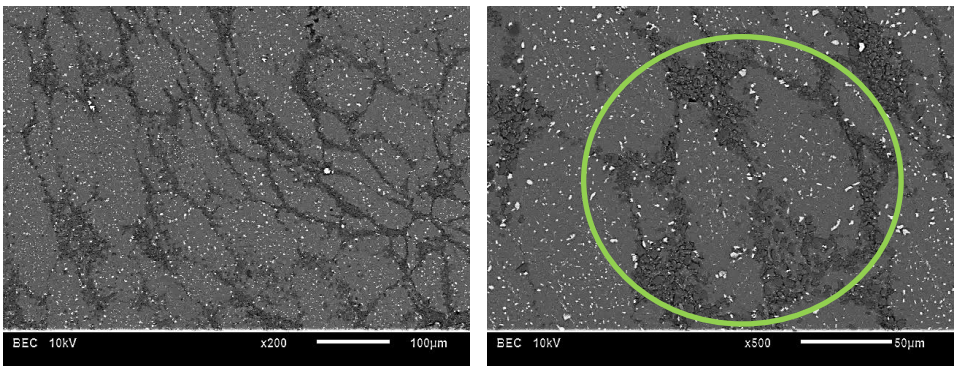

a b

Figure 71: SEM BSE images showing deformation at surface of uniaxially compressed 2124-Al with 15%SiC at a) scale bar =100µm and b) scale bar =50 µm.

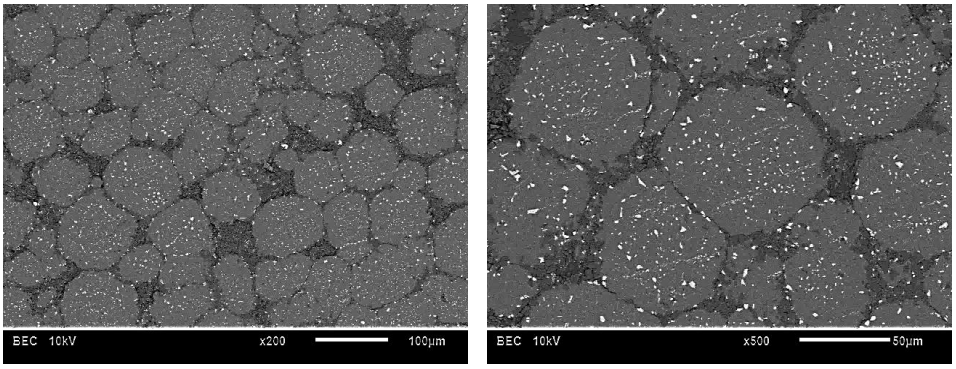

a b

Figure 72: SEM BSE images showing deformation at core of uniaxially compressed 2124-Al with 15%SiC sample at a) scale bar = 100µm and b) scale bar = 50 µm.

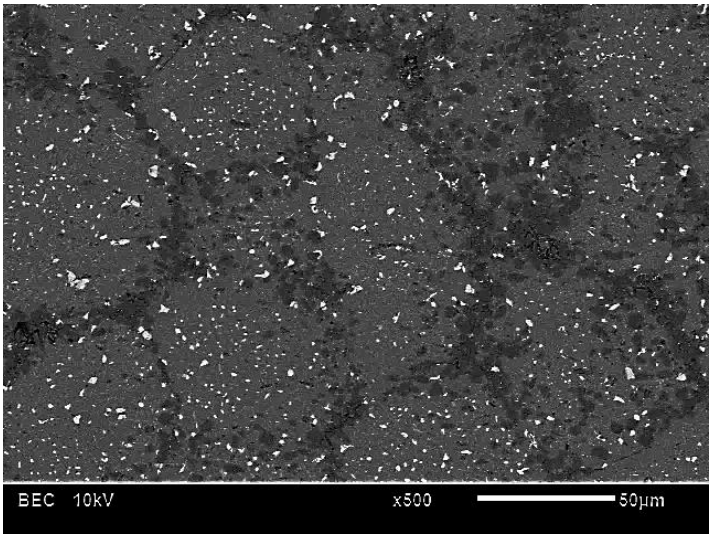

Figure 73: SEM BSE images showing deformation of a 2124-Al with 10%SiC uniaxially compressed sample when soaking time was increased from 6-20 minutes at 280°C.

Evidence supporting the occurrence of DRX was not found in the microstructures of the SiC reinforced MMCs. It may be beneficial in future work to do an analysis of the

microstructures using transmission electron microscopy (TEM) which can show fine, nucleated grains, dislocation networks within grains as well as give an indication of dislocation density in a material (Yadav & Bauri, 2012; Babu *et al*., 2016).

4.7.9 Effect of uniaxial compression on density

Figure 74 shows that the densities of the unreinforced 2124-Al and 2124-Al with 15% SiC decreased due to uniaxial compression while the densities of the 2124-Al with 5% Al_2O_3 and 2124-Al with 10% SiC increased. The decrease in relative density in the unreinforced 2124-Al was attributed to porosity since the microstructure of the unreinforced 2124-Al after uniaxial compression (Figure 65) shows small voids. Microstructures of the 2124-Al with 15% SiC (Figures 71 and 72) show no evidence of voids, however the decrease in relative density could have been caused by a decrease in strength of bonds in the composite as a result of poor bonding during deformation. A small increase in relative density of 0.213% (from 97.16 to 97.373%) was achieved in the 5% Al_2O_3 sample. This increase, although small, was unexpected because this composite fractured during uniaxial compression and it was assumed that consolidation due to uniaxial compression was poor. The microstructure of the 2124-Al with 5% Al_2O_3 after uniaxial compression (Figure 67) shows that bonding between Al alloy grains occurred in areas where there were no Al_2O_3 particles or agglomerates. It can thus be inferred that Al alloy grains in the 2124-Al with 5% Al_2O_3 composite bonded by localised bonding. This bonding seems to have been sufficient to result in a slight increase in relative density even though this composite fractured. The 2124-Al with 10% SiC experienced the highest increase in density from 98.05 to 99.43% (1.38%) after uniaxial compression. This result makes sense since visual inspection of the 2124-Al with 10%SiC deformed sample (Figure 64) together with stress-strain curve (Figure 63a) showed that the best deformation was achieved in this composite. When microstructures of the SiC reinforced (10 or 15 vol. %) MMCs are compared (Figure 69 vs. Figures 71 and 72), it can be observed that the size of the agglomerates in the 2124-Al with 10%SiC were smaller. This may have contributed to better consolidation, minimal cracking and ultimately higher increase in relative density.

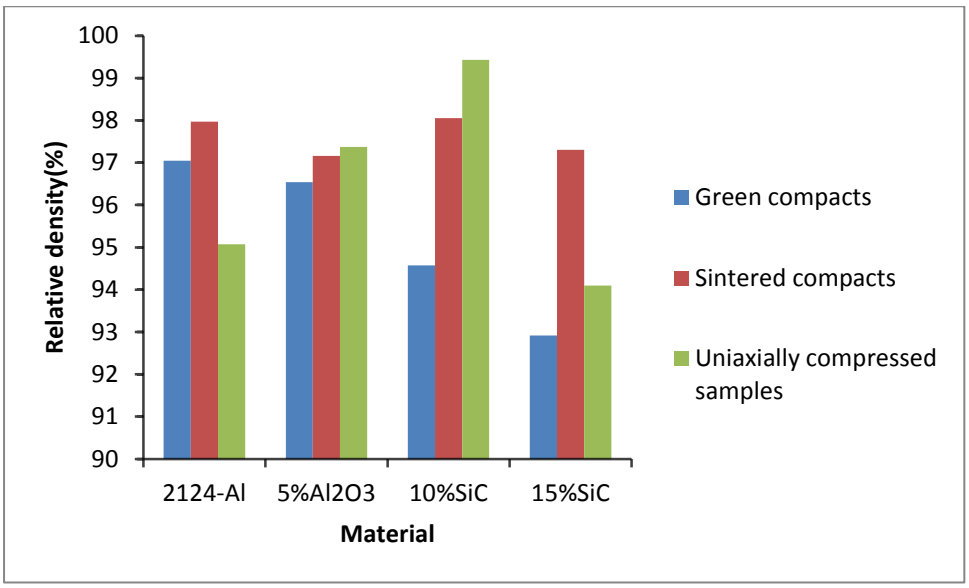

Figure 74: Relative densities of green compacts, sintered compacts and uniaxially compressed samples.

4.7.10 Hardness of uniaxially compressed samples

It can be observed that, much like the sintered compacts (Figure 52), the reinforced materials had higher hardness values than the unreinforced 2124-Al after uniaxial compression (Figure 75). The higher hardness in the composites was attributed to the presence of reinforcing particles. Reinforcing particles are believed to improve mechanical properties, such as hardness, of materials by improving load bearing capacity through the load transfer effect. The load transfer effect explains why composite materials are able to bear larger loads than the unreinforced materials. According to the load transfer effect, any load that is applied to composite materials is shared between the matrix material and the reinforcement. The reinforcement is stiffer and stronger and is able to bear larger loads than the matrix material. This therefore explains why composite materials have higher hardness values when compared to the unreinforced material (McWilliams *et al.*, 2012).

It can be observed that after uniaxial compression, there is still a hardness variation from the surface to the core of the samples. Higher hardness values were found for the core of the unreinforced 2124-Al, 5 %Al_2O_3 and 10 %SiC samples. It was inferred that higher hardness at the core was as a result of better plastic flow and densification at the core during uniaxial compression.

An improvement in hardness was considered to occur when the hardness increased in both the surface and the core of a sample. There seems to be a relationship between relative density and hardness. Density measurements done after uniaxial compression (Figure 74)

showed that the 10% SiC sample had the highest relative density of 99.43% and this sample had the highest hardness (surface=85.73 $HV_{0.1}$, core=97.96 $HV_{0.1}$) after uniaxial compression. Relative densities of the unreinforced 2124-Al and 15%SiC decreased due to uniaxial compression while only a slight increase in relative density (0.213%) was observed in the 5% Al_2O_3 sample. It was observed that after uniaxial compression, hardness of the unreinforced 2124-Al was lower at both the surface and core, hardness of 5% Al_2O_3 only increased at the core and hardness of 15% SiC only improved at the surface due to uniaxial compression. A metallographic evaluation done on the unreinforced 2124-Al sample after uniaxial compression (Figure 65) showed that there was significant porosity at both the surface and core of the unreinforced 2124-Al. This porosity was confirmed by the decrease in relative density of the unreinforced 2124-Al after uniaxial compression (Figure 74). Pores create areas of weakness in materials because they decrease load bearing capacity of materials (Millard, 2002). It was thus deduced that the decrease in hardness in the uniaxially compressed unreinforced 2124-Al sample was due to porosity. There seems to be a relationship between densification achieved and hardness. Hardness results for the 2124-Al with 15% SiC uniaxially compressed sample deviated from the trend observed in Figure 75 (*i.e.* higher hardness at core than surface). In the 15%SiC sample a higher hardness was found at the surface than the core. Figures 71 and 72 showed that there was more deformation at the surface than the core in the 15% SiC sample. It was thus inferred that the higher hardness at the surface was due to better densification at the surface of the 15% SiC than at the core.

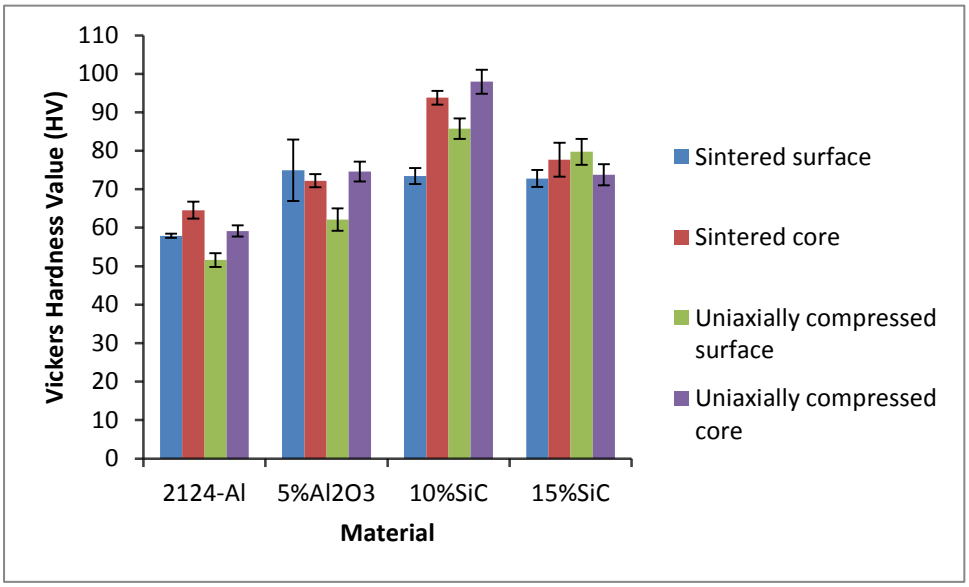

Figure 75: Hardness of surface and core of uniaxially compressed samples.

4.8 Simulation of extrusion process using Abaqus version 6.14

The uniaxial compression tests performed in the Gleeble 3500® showed that the temperature and strain rate that produced deformed samples with the best quality (*i.e.* deformation without fragmenting and few or no surface cracks) were 280°C and 5 s^{-1} respectively. It was decided that a temperature of 280°C would be used for extrusion. The data obtained from the uniaxial compression tests were then used to simulate the extrusion process using the Abaqus FEM software.

There are two reasons for simulating the extrusion process:

1. To analyse how the materials would behave in an extrusion environment. This would assist with better design of the extrusion process and possible minimisation of processing costs, since the results from the simulation will give an indication of what to expect during extrusion. The number of extrusion experimental trials could thus be minimised.
2. To see if the data obtained from the Gleeble could be used to design an extrusion process using Abaqus.

The direct extrusion of a cylindrical billet was analysed. The billet diameter was reduced by 30% from the initial diameter of 8 mm. The results of the billet made from 2124-Al with 5% Al_2O_3 are not included because the simulations failed at extrusion speeds larger than 2 $mm.s^{-1}$ so only three billet materials - unreinforced 2124-Al, 2124-Al with 10% SiC and 2124-Al with 15% SiC - were investigated.

The maximum pressure that the die can withstand is 1500 MPa (Böhler Steel Africa, 2011).

4.8.1 Method

The billet is shown in Figure 76 and the die assembly with the dimensions of the die applicable to the analysis are shown in Figure 77.

A two dimensional, axisymmetric analysis of the extrusion process was simulated. The meshed billet and die assembly are shown in Figure 78. The billet and die were meshed with 4-node bilinear axisymmetric thermally coupled quadrilateral (CAX4T) elements.

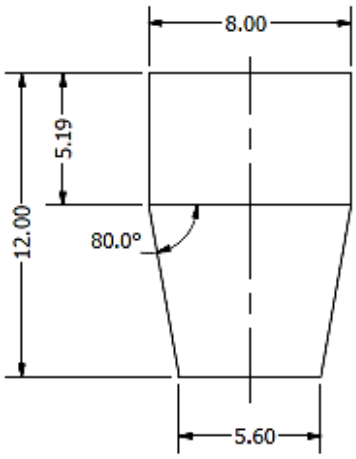

Figure 76: Sketch of the billet

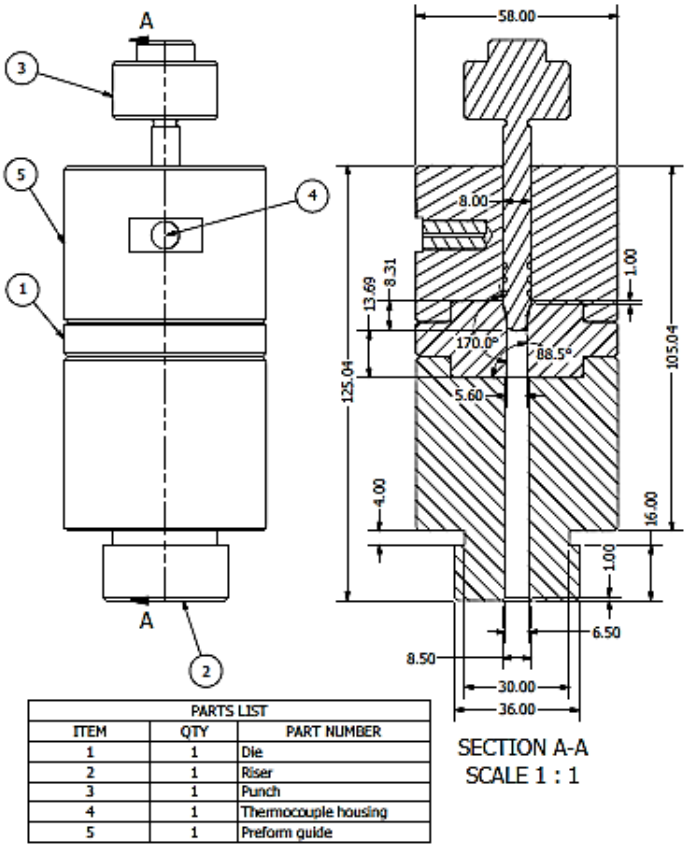

PARTS LIST		
ITEM	QTY	PART NUMBER
1	1	Die
2	1	Riser
3	1	Punch
4	1	Thermocouple housing
5	1	Preform guide

Figure 77: Die assembly

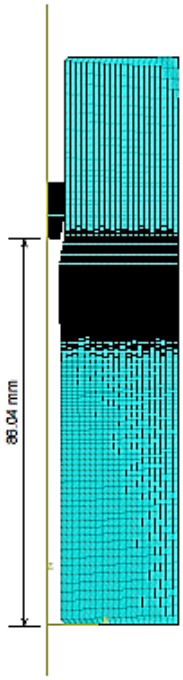

Figure 78: Meshed billet and die assembly.

Table 6 shows properties of the materials under investigation at 280°C. The stress-strain data at 0.01 and 5 s^{-1} for the three billet materials investigated are shown in Figures 79 and 80, respectively. The compression tests were conducted at 280°C. The initial sample diameter was 8 mm and the initial sample length was 12 mm. The unreinforced 2124-Al sample had the largest plastic deformation region in comparison to the other billet materials, as shown in Figures 79 and 80. There was a lot of noise in the data which is shown by oscillations on the stress-strain curves.

Table 6: Material properties of the 3 materials under investigation (Boyer & Gall, 1985).

Material property	**Unreinforced 2124-Al**	**2124-Al with 10 vol.% SiC**	**2124-Al with 15 vol.% SiC**
Density [$kg.m^{-3}$]	2780	2823	2844.5
Thermal conductivity [$W.m^{-1}.K^{-1}$]	193	214.09	245.60
Inelastic heat fraction	0.9	0.9	0.9
Specific heat [$J.kg^{-1}.K^{-1}$]	882	860.8	850.2
Young's Modulus [Pa]	$1.77x10^{9}$	$1.951x10^{9}$	$2.164x10^{9}$
Poisson's ratio	0.33	0.31	0.30
Coefficient of expansion [K^{-1}]	$24.7x10^{-6}$	$22.74x10^{-6}$	$21.76x10^{-6}$

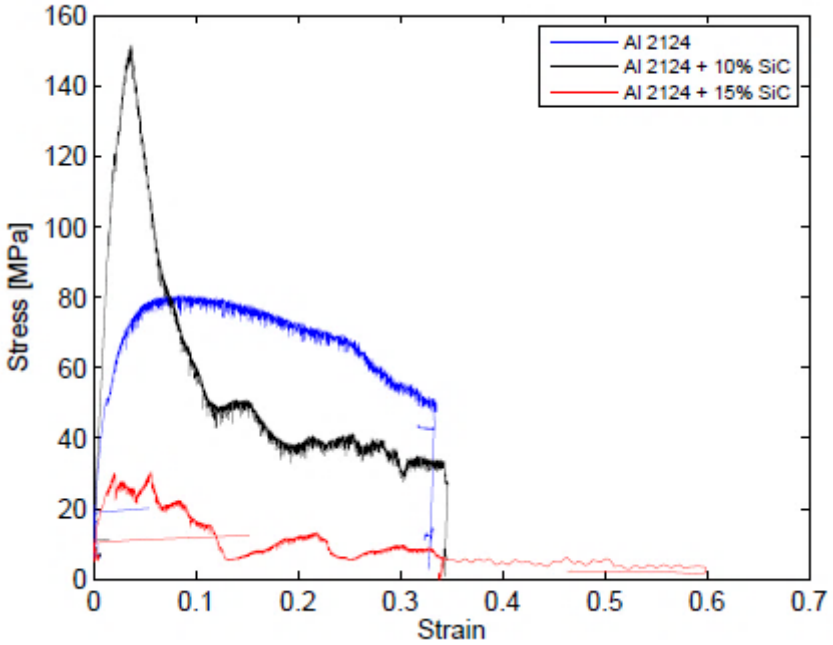

Figure 79: Engineering stress-strain data at 0.01 s^{-1} generated by Gleeble compression at 280°C for unreinforced 2124-Al (blue curve), 2124-Al with 10% SiC (black curve) and 2124-Al with 15% SiC (red curve).

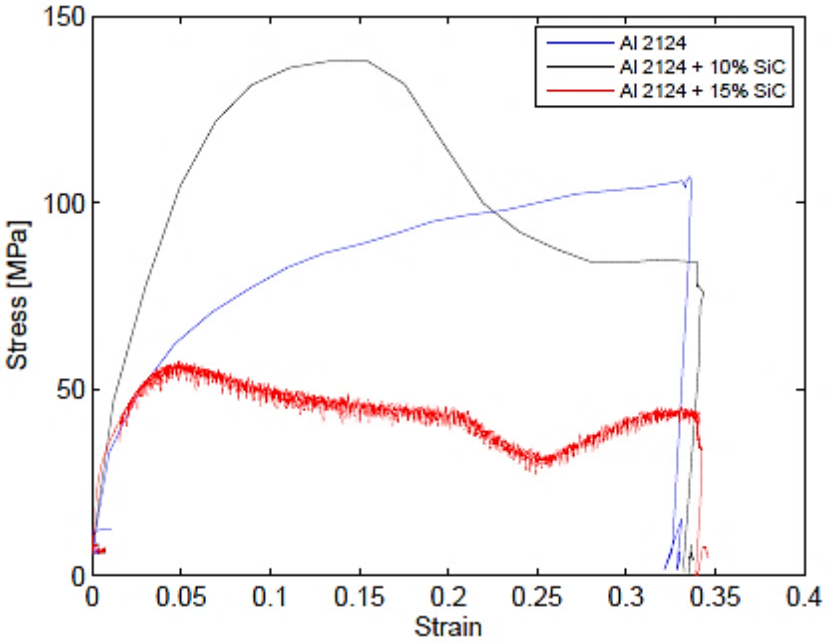

Figure 80: Engineering stress-strain data at 5 s^{-1} generated by Gleeble compression at 280°C for sintered unreinforced 2124-Al (blue curve), 2124-Al with 10% SiC (black curve) and 2124-Al with 15% SiC (red curve).

A material model was fitted to the data to calculate the material compressive behaviour during the simulation. The material model had to account for the elasticity, plasticity and damage observed in the data. The three regions are shown in Figure 81 where: line *a*-*b* is the elastic region, line *b*-*c* is the plastic region and line *d*-*e* is the damage region. The solid curve *c*-*e* in Figure 81 is the damaged response and the dotted line is the undamaged

response of the material. σ_{y0} is the yield stress and $\underline{\varepsilon_0}^{-pl}$ is the equivalent plastic strain at the point of damage initiation. Point *c* is the point of damage initiation where the overall damage parameter $D = 0$. $\underline{\varepsilon_f}^{-pl}$ is the equivalent plastic strain at failure ($D = 1$) which depends on the characteristic length of the element. The overall damage parameter *D* accounts for the combined effect of all the active damage mechanisms. Damage can be due to a number of mechanisms, such as ductile damage due to void coalescence, or shear damage due to shear band formation (Simulia, 2007).

More information on the damage behaviour of the three billet materials was required to include damage evolution in the finite element model (FEM). However, ductile damage initiation is defined for this study. The stiffness is not degraded if there is no damage evolution defined, but the output variable DUCTCRT can be used to indicate if the damage criterion has been met in an element.

The linear elasticity and isotropic hardening Abaqus material models were used in this analysis. Smooth data can be supplied to Abaqus, which then uses the data to fit the material models. The stress-strain data at 5 s^{-1} was smoothed and divided into elastic, plastic and damage data ranges (except for 2124-Al), as shown in Figure 82.

Static yield stress is the stress required to initiate flow in a material from a point of rest (Galindo-Rosales *et al*., 2010). The static yield stress is required as a reference point when strain rate dependent plasticity data is supplied (Simulia, 2007). As this data was not available, it was approximated by using the stress-strain data at 0.01 s^{-1} and perfect plasticity was assumed at 0 s^{-1}. The approximated static yield stress is given in Table 7.

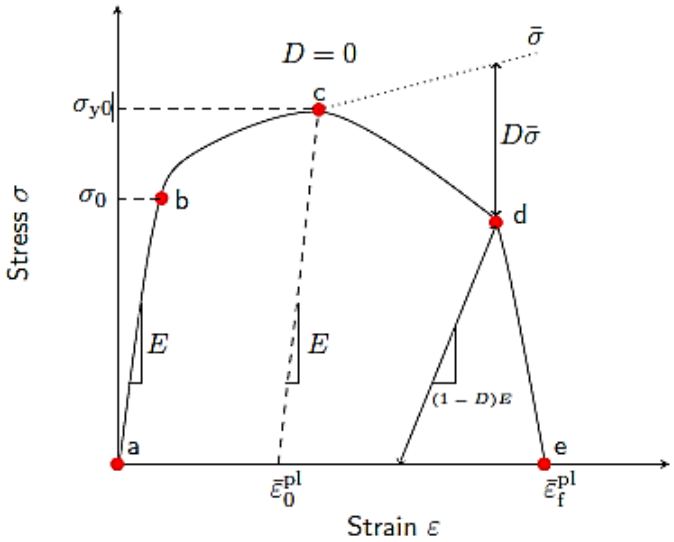

Figure 81: Typical uniaxial stress-strain response of a metal specimen undergoing damage (Simulia, 2007).

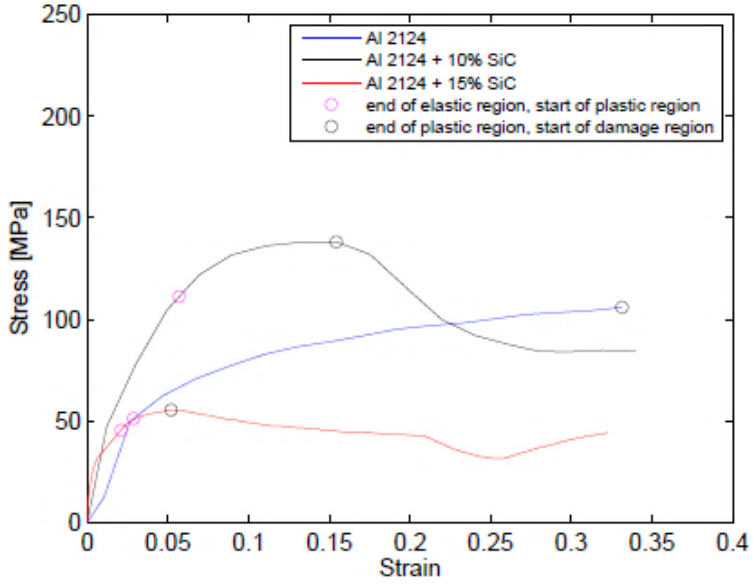

Figure 82: Engineering stress-strain data after smoothing at 5 s^{-1} for unreinforced 2124-Al (blue curve), 2124-Al with 10% SiC (black curve) and 2124-Al with 15% SiC (red curve).

Table 7: Approximated static yield stress of unreinforced 2124-Al, 2124-Al with 10% SiC and 2124-Al with 15% SiC.

Material	Static yield stress [Pa]
Unreinforced 2124-Al	66.8×10^6
2124-Al with 10%SiC	141.7×10^6
2124-Al with 15%SiC	14.8×10^6

The properties of the hot-worked W302 steel die with Rockwell hardness 42-46 HRC are listed in Table 8. The die can withstand a maximum temperature of 640°C before tempering occurs (Böhler Steel Africa, 2011; Boyer & Gall, 1985)

Table 8: Die material properties (Bohler Steel Africa, 2011; Boyer & Gall, 1985).

Material property	**Hot worked W302 steel**
Density [$kg.m^{-3}$]	7800
Thermal conductivity [$W.m^{-1}.K^{-1}$]	26.1
Inelastic heat fraction	0.9
Specific heat [$J.kg^{-1}.K^{-1}$]	460
Young's Modulus [Pa]	$215x10^9$
Poisson's ratio	0.29
Coefficient of Expansion [K^{-1}]	$12.2x10^{-6}$

Each finite element analysis consisted of three fully-coupled transient thermal displacement steps which are described in Table 9. The duration of Step 2 was calculated as the distance that the billet has to travel from its initial position divided by the extrusion speed. The duration of Step 2 would, for example, be 10 s if the billet has to travel 100 mm to be outside the die, if the extrusion speed is set to 10 $mm.s^{-1}$.

Table 9: Analysis steps

Step	Duration [s]	Description
1	1	Establish contact between billet and die
2	10*	Extrusion
3	0.1	Remove contact pairs

* displacement/speed

Mechanical and thermal interactions between the forming billet and the die are described in Table 10. The analysis steps to which the interactions apply are also given in Table 10. There is heat generation between the die and billet due to friction and plastic work dissipation (Selvan *et al*., 2010). Cooling down of the billet was not investigated in this study because appropriate heat transfer coefficient data could not be found.

Table 10: Thermal and mechanical interactions.

Type	**Interaction**	**Properties**	**Applicable steps**
Mechanical	Contact between the *vertical* face of the billet and the die.	Isotropic tangential behaviour: ● Penalty formulation ● Friction coefficient=0.1*	1 and 2
Mechanical	Contact between the *horizontal* face of the billet and the die.	Isotropic tangential behaviour: ● Penalty formulation ● Friction coefficient=0.1*	1 and 2
Thermal	Contact between the *vertical* face of the billet and the die	Heat generation: ● Fraction of dissipated energy converted to heat = 0.5 ● Weighting factor for the distribution of heat between interacting surfaces=0.5	1 and 2
Thermal	Contact between the *horizontal* face of the billet and the die.	Isotropic tangential behaviour: ● Penalty formulation Friction coefficient=0.1*	1 and 2

The displacement and thermal boundary conditions applied to the billet and die are described in Table 11. The analysis steps to which these conditions apply are also given. U_1, U_2 and U_3 are the displacement in the radial, vertical and tangential directions, respectively.

Table 11: Boundary conditions

Type	Boundary condition	Reason	Applicable steps
Displacement	U_1=0, U_2=0 and U_3=0 applied to die reference point.	Prevent rigid body movement	1 to 3
Displacement	U_1=0 applied to inner edge of billet	Axisymmetric condition	1 to 3
Displacement	U_2= -0.000125 applied to top of billet	To establish contact between billet and die	1
Displacement	U_2= -0.1 applied to top of the billet	Extrusion	2 to 3
Thermal	T_i= 280°C for billet	Initial temperature field of billet	1 to 3
Thermal	T_i = 280°C for die	Initial temperature field of die	1 to 3

4.8.2 FEA model: effect of extrusion speed

The extrusion speeds investigated were 1 to 10 mm.s^{-1} and the friction coefficient was set to 0.1. The effect of increasing extrusion speed on the contact pressure can be observed in Figure 83. The maximum contact pressure on unreinforced 2124-Al and 2124-Al with 15% SiC billets increased slightly with increasing extrusion speed. For the 15% SiC billet there was an increase in maximum contact pressure of 36% from 1 to10 mm.s^{-1}. The maximum contact pressure on the unreinforced 2124-Al, 10% SiC and 15% SiC billets at 10 mm.s^{-1} was 179.4 MPa, 343.8 MPa and 68.1 MPa, respectively. This is 8.3, 4.3 and 22 times less, respectively, than the maximum pressure (1500 MPa) that the die can withstand.

These results show that during extrusion the highest contact pressure can be expected in 10% SiC compact and can be attributed to better consolidation in this compact, which may have improved its load bearing capacity. Based on the simulation results it was expected that the die would be able to withstand pressures exerted on it during extrusion of all three materials since the contact pressures found are much lower than the maximum pressure that the die can withstand.

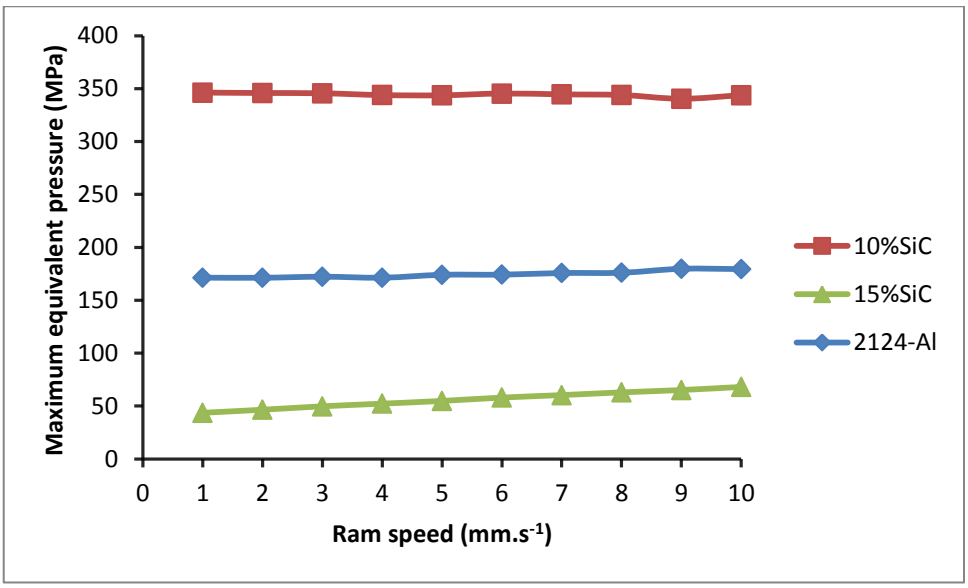

Figure 83: Maximum contact pressure in the die at different extrusion speeds.

The maximum temperature of the die increases slightly with increase in extrusion speed (Figure 84). This may be due to increased heat generation as a result of increased friction and deformation work inside the die (Saha, 2000). This result gives insight into heat generation during extrusion and information that the die temperature may differ slightly for different extruded materials at the same speed, which may assist more effective interpretation of results.

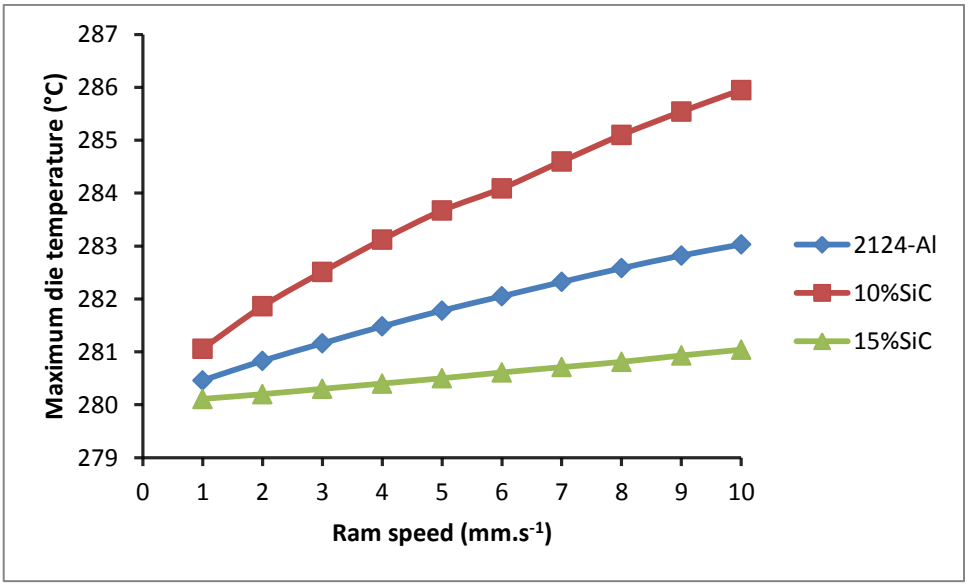

Figure 84: Maximum temperature in the die at the different extrusion speeds investigated.

The effect of increasing extrusion speed on the maximum temperature of the billets can be observed in Figure 85. The maximum temperature of the billet increases only a few degrees with an increase in extrusion speed from 1 – 10 mm.s^{-1}. The 2124-Al with 10% SiC billet shows the largest increase in temperature from 280°C to 312.7°C which is an increase of 11.6%. A comparison of results, shown in Figures 84 and 85, depicts that the billet temperature is affected more than the die by an increase in extrusion speed. This suggests that most of the heat generated during extrusion is absorbed by the billet. It can be seen that while we might do our best in ensuring that the initial temperature of the die assembly and billets is 280°C, the temperature may not stay constant during extrusion.

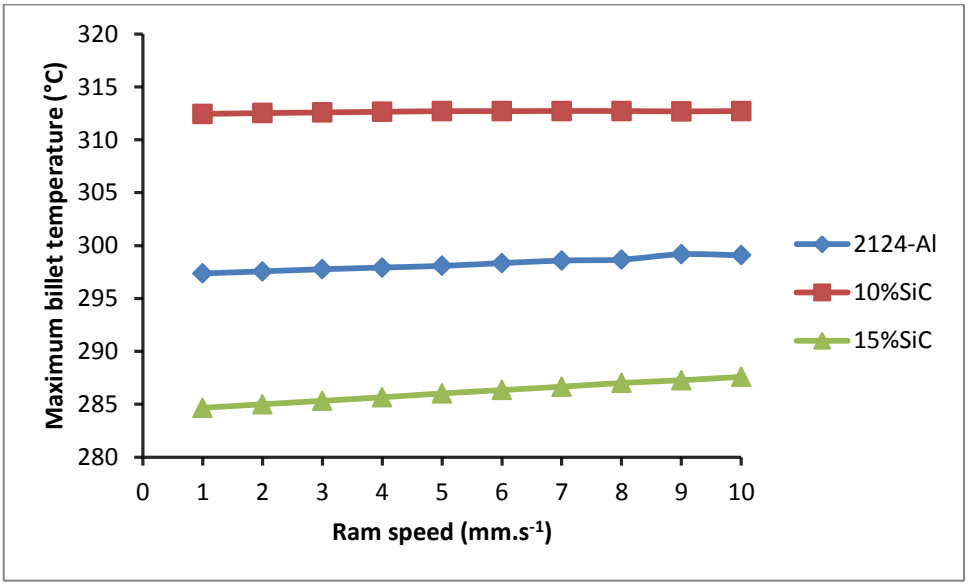

Figure 85: Maximum temperature in the billet at the different extrusion speeds investigated.

A linear trend line was fitted to FEA results to show the relationship between the maximum equivalent (von Mises) strain rate and extrusion speed (Figure 86). The maximum equivalent (Von Mises) strain rate in the billet increases with increasing extrusion speed. The results from the uniaxial compression tests showed that a better quality of deformed samples was obtained at a strain rate of 5 s^{-1} than 0.01 s^{-1}, hence 5 s^{-1} was used for the extrusion process. To operate as close as possible to a strain rate of 5 s^{-1}, an extrusion speed of 7 mm.s^{-1} would have to be used. At a speed of 7 mm.s^{-1} results showed that the strain rate in the unreinforced 2124-Al and 2124-Al with 10% SiC was ~5s^{-1} and in the 2124-Al with 15% SiC it was slightly above 5 s^{-1}.

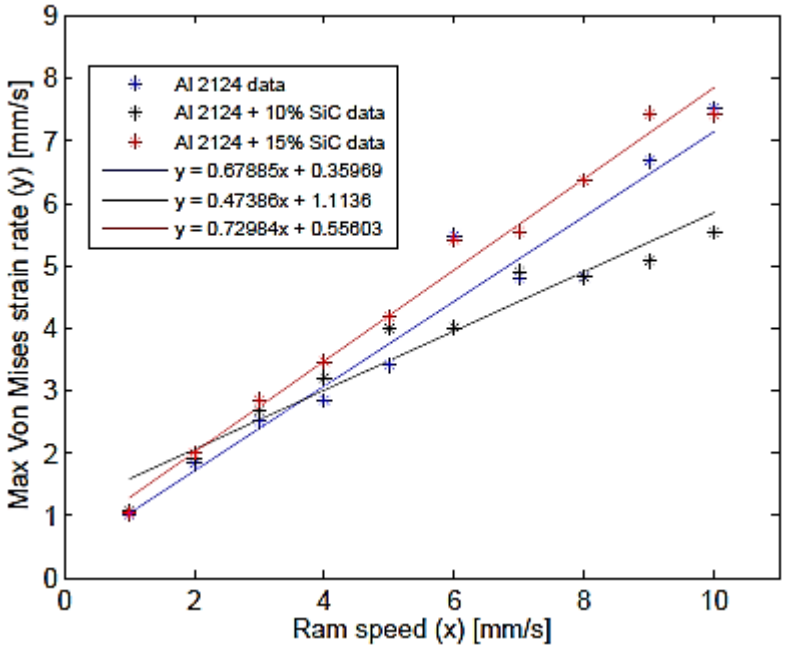

Figure 86: The effect of the extrusion speed on the maximum equivalent strain rate for un-reinforced 2124-Al (blue curve), 2124-Al with 10%SiC and 2124-Al with 15%SiC.

When the output variable DUCTCRT > 1, the ductile damage criterion is satisfied (Simulia, 2007). These DUCTCRT-values only give an indication that damage may have occurred in the billet. More information on the damage behaviour of the three billet materials is required for more realistic FEA damage results. The DUCTCRT-values shown in Figure 87 indicate that some damage may occur in the extruded samples since they are larger than one. The damage does not seem to vary much with increasing extrusion speed. This seems unrealistic (Prasad *et al.*, 2001), and may be due to a lack of strain rate dependent damage data. So, according to the results shown in Figure 87 one should not be surprised if the extruded parts exhibit some degree of damage but one would have to run extrusion experiments at the different extrusion speeds to determine how much the degree of damage in the deformed billets is influenced by extrusion speed. Another alternative for determining the influence of extrusion speed on degree of damage in the deformed billets would be to get more strain rate dependent damage data. Figure 87 also shows that the likelihood of damage increases with an increase in volume fraction of SiC. This coincides with the result from uniaxial compression as Figure 59 shows that the SiC reinforced MMCs had surface cracks and the cracking worsened with an increase (from 10 to 15%) in SiC volume fraction.

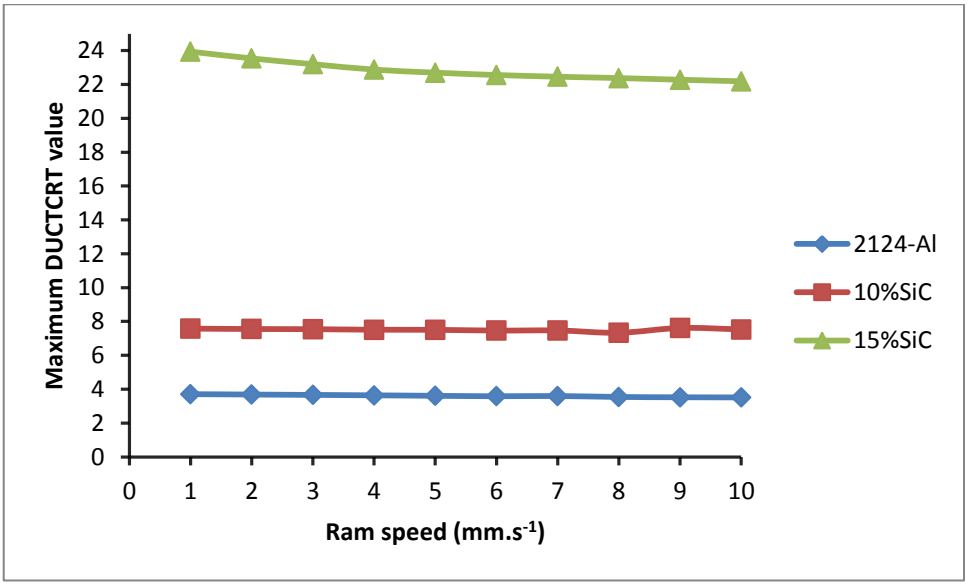

Figure 87: Maximum DUCTCRT-value of the formed billet at different extrusion speeds investigated.

4.8.3 Summary

From the finite element analysis done in Abaqus the maximum contact pressures for the billets at the highest extrusion speed of 10 $mm.s^{-1}$ were: 179.4 MPa for unreinforced 2124-Al, 343.8 MPa with 10% SiC and 68.1 MPa with 15% SiC. This is 8.3, 4.3 and 22 times less than the maximum pressure of 1500 MPa the die can withstand. This suggests that the extrusion experiments can be carried out at any extrusion speed up to 10 $mm.s^{-1}$ without damaging the die.

The results from the uniaxial compression tests showed that the best quality of deformed samples was obtained at a strain rate of 5 s^{-1}, so this strain rate was used for the extrusion process. The extrusion speed which gave a strain rate of ~5 s^{-1} in the billets was 7 $mm.s^{-1}$.

The effect of extrusion speed on die and billet temperature was also investigated. There was a higher increase in temperature in the billets than in the die, so a slight increase in temperature should be expected during extrusion. DUCTCRT-values for all the billets indicated the possibility of damage in the extruded billets and the degree of damage is expected to increase with an increase in SiC volume fraction in Al-alloy matrix.

The simulation results showed that the extrudability of SiC reinforced MMCs at warm working temperatures is possible but with some degree of damage expected in the extruded billets. The fact that the simulations crashed at extrusion speeds larger than 2 $mm.s^{-1}$ for the Al_2O_3 reinforced MMNC suggests that the extrudability of the Al_2O_3 reinforced

MMNC at warm working temperatures is likely to be poorer. This result coincides with the results from the uniaxial compression tests performed on the Gleeble since it was shown that at a strain rate of 5 s^{-1}(equivalent to ~7 $mm.s^{-1}$), the SiC reinforced MMCs had higher values for flow stress than the Al_2O_3 reinforced MMNC; indicating better formability.

Thus far it has been shown that:

1. Uniaxial compression tests performed on a Gleeble 3500® thermomechanical simulator can be used to study the deformation behaviour of Al low-micron MMCs and MMNCs.
2. Results obtained from uniaxial compression tests performed on a Gleeble can be used to simulate an extrusion process using software such as Abaqus and give important information regarding pressure, extrusion speed, strain rate and temperature which can assist in a more informed design and understanding of an extrusion process.
3. Uniaxial compression and extrusion of SiC reinforced MMCs can be done at warm working temperatures.

The results obtained from the uniaxial compression tests performed on a Gleeble and simulations of an extrusion process on Abaqus were then validated by laboratory scale extrusion experimental trials.

4.9 Laboratory scale extrusion experimental trials

The extrusion experiments were used to validate the physical results obtained from the uniaxial compression tests and the FEA results; thus evaluating whether a thermomechanical simulator such as a Gleeble can be used to design an extrusion experiment.

It can be observed that only the unreinforced 2124-Al sample extruded well (Figure 88a) while the extrusion of the the Al_2O_3 or SiC reinforced composites failed as only a small portion of the samples was extruded (Figures 88b and 89). The whole length of the unreinforced 2124-Al sample was extruded and the targeted reduction of 30% was achieved. The targeted reduction of 30% was not achieved in the Al_2O_3 or SiC reinforced samples. This result was expected for the 2124-Al with 5% Al_2O_3 sample since in the FEA analysis (Section 4.8) it was mentioned that this sample could not be extruded at speeds

greater than 2 $mm.s^{-1}$ and this sample had fractured during uniaxial compression (Section 4.7). Metallographic evaluations, at various processing steps (Figures 44, 45, and 67), on the 2124-Al with 5 %Al_2O_3 showed that there were Al_2O_3 particles concentrated on Al alloy grain boundaries which possibly limited deformation and bonding. X-ray mapping on 2124-Al with 5% Al_2O_3 (Figure 45) also showed that there were Al_2O_3 particles which were dispersed within the 2124-Al alloy grains. These particles may have also contributed to poor deformation since they may have limited plastic flow by restricting mobility of dislocations, grains and grain boundaries during deformation (Zhang & Chen, 2006). It was thus inferred that the extrudability of the 2124-Al with 5% Al_2O_3 was poor due to a lack of ductility and limited plastic flow. It was thought that the deformation conditions used in this work were not suitable for deforming the Al_2O_3 reinforced samples. Figure 88b shows that the small extruded portion of the 2124-Al with 5% Al_2O_3 sample fractured. This fracturing is indicative of poor bonding in the 2124-Al with 5% Al_2O_3 sample. A good distribution of Al_2O_3 reinforcing particles in the Al alloy matrix was achieved after blending (Figures 15 & 17) but the processing steps used in this work seem to not be suitable for this material. The desire is to maintain the uniform distribution of Al_2O_3 particles in the Al alloy matrix achieved after blending thus it was thought that it may be beneficial in future work to explore other parameters and forming processes for the 2124-Al with 5% Al_2O_3.

Results obtained from uniaxial compression tests (Section 4.7) and FEA (Section 4.8) showed that SiC reinforced MMCs could be deformed successfully at 280°C and strain rate of 5 s^{-1} but with minor surface defects. The extrusion results for the SiC reinforced MMCs do not coincide with the results from the uniaxial compression tests and FEA. It was thought that this was due to a lack of lubrication. The friction coefficient used in the FEM analysis to simulate the extrusion process was 0.1. This friction coefficient may have been underestimated and the friction during extrusion may have actually been higher. The MMCs and MMNC were more difficult to extrude than the unreinforced 2124-Al alloy because they have a higher resistance to deformation as a result of the harder, stiffer reinforcing particles which do not deform easily (Turner & Ashby, 1993). So, the lack of lubrication could have made deformation of MMCs and MMNCs even more difficult due to higher friction (therefore increased resistance to deformation) and reduced material flow. Lubrication improves material flow by reducing friction during metal forming processes. The improved metal flow also results in lower loads since the material becomes easier to deform in the lubricated condition (Kim *et al.*, 2006). Thus, the poorer

extrudability of the SiC reinforced MMCs may be improved by the use of lubrication. The effect of lubrication on extrudability of 2124-Al alloy composites will be explored in future work. The fact that the unreinforced 2124-Al alloy sample was extruded successfully shows that the design of the extrusion process was successful and the extrusion process works.

From Figure 90 it can be observed that the unreinforced 2124-Al alloy extruded well and plastically deformed. The sudden increase in stress that can be seen on the blue curve showing deformation behaviour of unreinforced 2124-Al alloy was attributed to a lack of lubrication where friction between the die and sample became too high. This increased resistance to deformation and therefore stress. The reinforced materials (2124-Al with 5% Al_2O_3, 2124-Al with 10% SiC and 2124-Al with 15% SiC) have the same maximum compressive stress of 900 MPa. The shapes of the curves showing deformation behaviour of Al_2O_3 or SiC reinforced materials during extrusion also show that the reinforced materials did not plastically deform since there was a sharp decrease once the maximum stress was reached. This shows that material flow was poor during extrusion and ultimately indicates that extrudability of the reinforced materials was poor.

The shape of the curves for the SiC reinforced samples (curve 3&4 in Figure 90) are similar which suggests that the materials behaved in a similar manner during extrusion, regardless of the difference in vol. % of SiC (10 vs. 15%). This result is similar to that obtained when 2124-Al with 10% SiC and 212-Al with 15% SiC green compacts were uniaxially compressed at 280°C at a strain rate of 5 s^{-1} (Figure 57b). It was expected that the shapes of the curves showing deformation behaviour of extruded samples would be similar to the curves in Figures 62 and 63 since the same parameters were used (280°C, 5s^{-1} and 20 minutes soaking time) in the extrusion process. This result shows that using a soaking time of 20 minutes prior to extrusion did not improve deformation behaviour of SiC reinforced MMCs as in the uniaxial compression tests.

In the laboratory scale extrusion experiments, the compressive stresses of the unreinforced 2124-Al and reinforced materials were found to be ~790 MPa and 900 MPa respectively (Figure 90). In the uniaxial compression tests these compressive stresses were much lower (Section 4.7). It was thought that this was due to the fact that there was more resistance to deformation during extrusion because the samples were enclosed in a die. Enclosing a sample in a die generates more friction which is why resistance to deformation increases. A higher resistance to deformation results in higher compressive stresses. The fact that the

die was not lubricated may have also played a role since it may have increased friction (therefore resistance to deformation) even further (Saha, 2000). This result shows that there is a need to for lubrication.

It was inferred that the results obtained in the lab scale extrusion experimental trials did not coincide with results obtained in uniaxial compression because of a difference in friction coefficients. The fact that the unreinforced 2124-Al alloy was extruded successfully shows that the extrusion process was designed successfully using the information obtained from the uniaxial compression tests and FEA. However, the uniaxial compression tests cannot help in determining friction effects since in the uniaxial compression tests the samples are exposed to less friction than in the extrusion process. The FEA analysis assumed a lower friction coefficient because the uniaxial compression setup was being considered. So, to improve correlation between results obtained from uniaxial compression tests, FEA and lab scale extrusion experiments careful attention has to be paid to friction effects. Ultimately, this highlights that to effectively design an extrusion process using uniaxial compression tests and FEM, the friction conditions in the extrusion process have to be matched (as closely as possible) to those in the uniaxial compression tests. Lubrication therefore has to be used during extrusion to reduce friction.

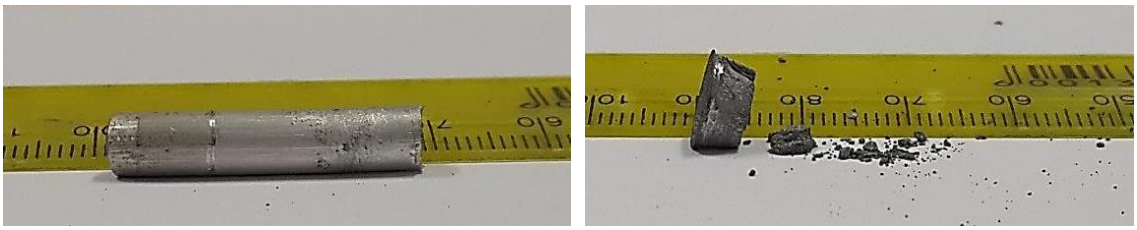

a b

Figure 88: a) unreinforced 2124-Al and b) 2124-Al with 5% Al_2O_3 samples after extrusion at 280°C, extrusion speed of 7 $mm.s^{-1}$ and strain of 0.3.

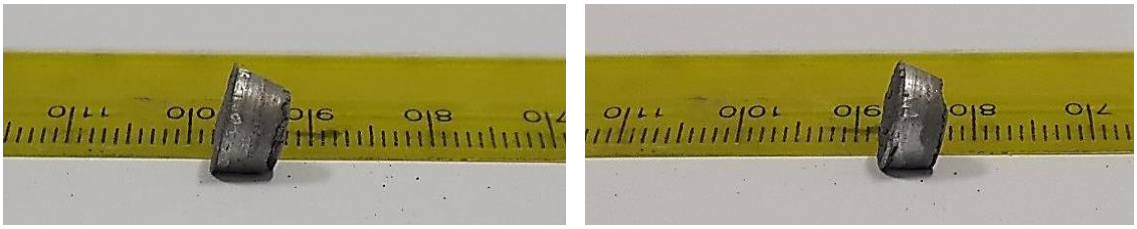

a b

Figure 89: a) 2124-Al with 10% SiC and b) 2124-Al with 15% SiC samples after extrusion at 280°C, extrusion speed of 7 $mm.s^{-1}$ and strain of 0.3.

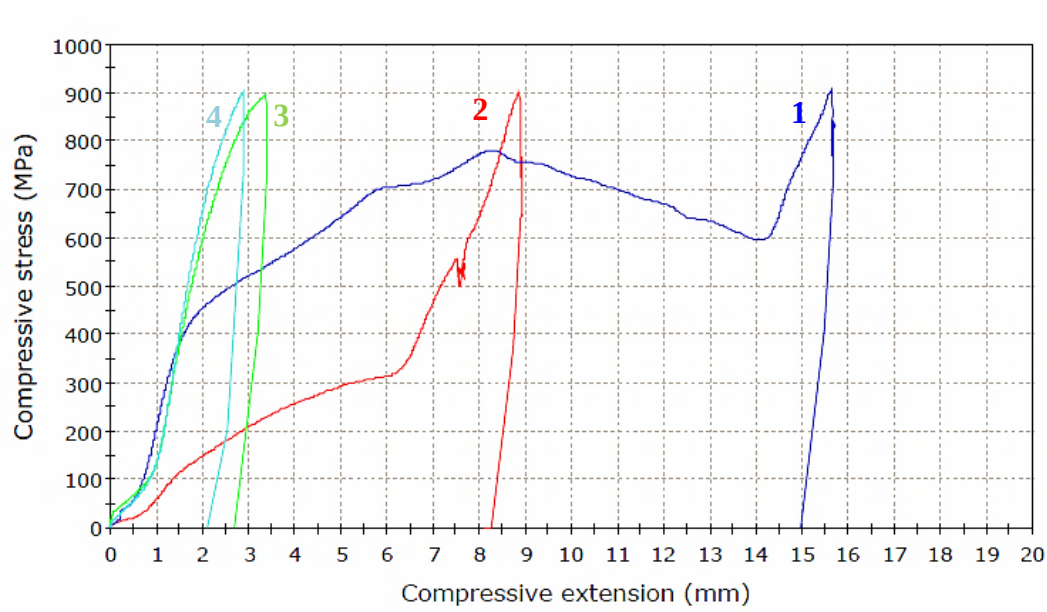

Figure 90: Compression stress (MPa) vs. compressive extension (mm) for 1) unreinforced 2124-Al 2) 2124-Al with 5% Al_2O_3 3) 2124-Al with 10% SiC and 4) 2124-Al with 15% SiC after extrusion.

4.9.1 Metallographic evaluation of extruded samples

Figures 88b and 89 showed that extrusion of the Al_2O_3 reinforced MMNC and SiC reinforced MMCs was unsuccessful as only a small portion of the samples was extruded. The deformation at the surface and core of the samples could not be analysed and compared since only a small portion of the samples was actually extruded. All the extruded samples (Figures 88 & 89) were sectioned along their axes of symmetry, in the extrusion direction, and analysed.

Figure 91 shows that in the unreinforced 2124-Al sample, the grains deformed and changed shape. There seems to be good bonding between the 2124-Al alloy grains but there are a lot of micro voids as well. These micro voids are mostly found on the grain boundaries and it was inferred that they formed due to particle debonding during deformation.

There seems to have been some deformation achieved in the 2124-Al with 5% Al_2O_3 MMNC since the 2124-Al grains changed shape due to extrusion (Figure 92). The Al_2O_3 particles concentrated on the 2124-Al alloy grain boundaries could have limited plastic flow by limiting movement of 2124-Al grains and grain boundaries (Casati & Vedani, 2014). The slight fracturing observed in the 2124-Al with 5% Al_2O_3 extruded sample (Figure 88b) could have been caused by the agglomeration of Al_2O_3 particles on grain

boundaries since these Al_2O_3 particles could have made grain boundaries brittle and therefore susceptible to fracture.

In the 2124-Al with 10% SiC extruded sample, the 2124-Al grains deformed due to extrusion and this deformation can be seen by the elongation of 2124-Al grains (Figure 93). Figure 93 shows that the SiC particles have formed small bands in the extrusion direction but there are some areas where 2124-Al grains have bonded and there are a few SiC particles distributed inside the deformed grains. A low reduction in area of 8.12% was achieved in the 2124-Al with 10% SiC MMC. Figure 93 illustrates that extrusion could potentially improve deformation and distribution of SiC particles inside the 2124-Al grains, however higher deformation (i.e. higher reduction in area) has to be achieved.

Figure 94 shows that the grains in the 2124-Al with 15% SiC sample deformed due to extrusion. The higher vol. % of SiC led to higher amount of SiC particles concentrated on grain boundaries. The deformation in the extruded 2124-Al with 15% SiC is fairly consistent with that of the uniaxially compressed surface of the 2124-Al with 15% SiC sample (Figure 71). When one analyses Figure 94 one can see that the 2124-Al grains elongated due to deformation but there are virtually no SiC particles dispersed in the deformed region. It was deduced that, much like in the uniaxially compressed sample, the deformation was restricted to some extent by the high amount of SiC on grain boundaries. So there was more resistance to the applied force in the 2124-Al with 15% SiC such that only grains were deformed but there was no evidence of deformation achieved leading to some improvement in distribution of SiC particles.

Overall, microstructures obtained from extrusion are consistent with those obtained in uniaxial compression (Sections 4.7.8 and 4.9.1). Figures 65 and 91 show that good deformation was achieved in the unreinforced 2124-Al sample, but there was porosity. The uniaxially compressed unreinforced 2124-Al seems to be more porous than the extruded sample. This could be attributed to slightly better deformation achieved in the extruded sample. In the 2124-Al with 5% Al_2O_3 it was observed that some deformation was achieved but there were a lot of Al_2O_3 particles situated on grain boundaries (Figure 67 and 92). Figures 58b and 88b showed that deformation of 2124-Al with 5% Al_2O_3 was accompanied by fracturing and this was attributed to the agglomeration of Al_2O_3 particles at grain boundaries causing poor bonding and brittleness. In the 2124-Al with 10% SiC MMC it was observed that in areas where deformation had occurred there were some SiC particles inside deformed grains (Figures 68, 69 and 93). Extrusion showed potential to

improve distribution of SiC particles in 2124-Al grains; however more deformation is required.

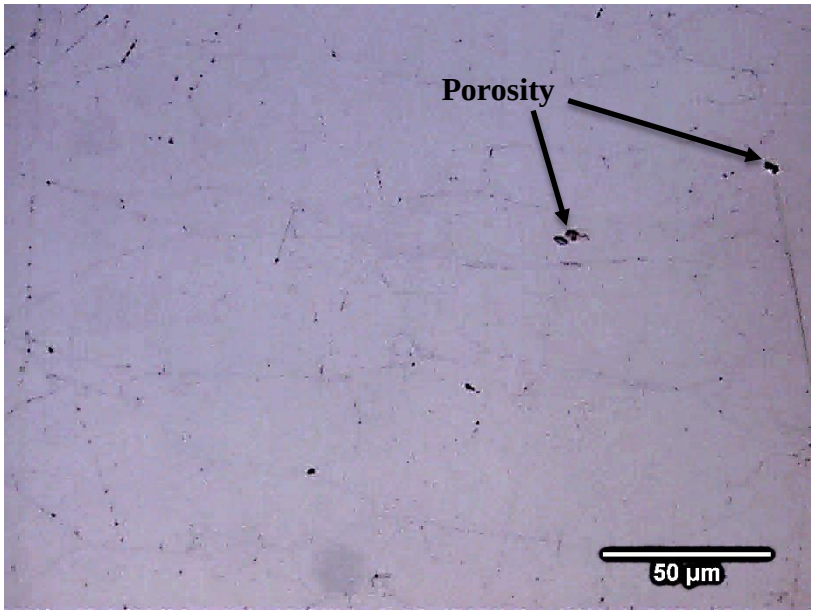

Figure 91: Optical micrograph showing deformation in the unreinforced 2124-Al sample after extrusion at 280°C (scale bar = 50 µm).

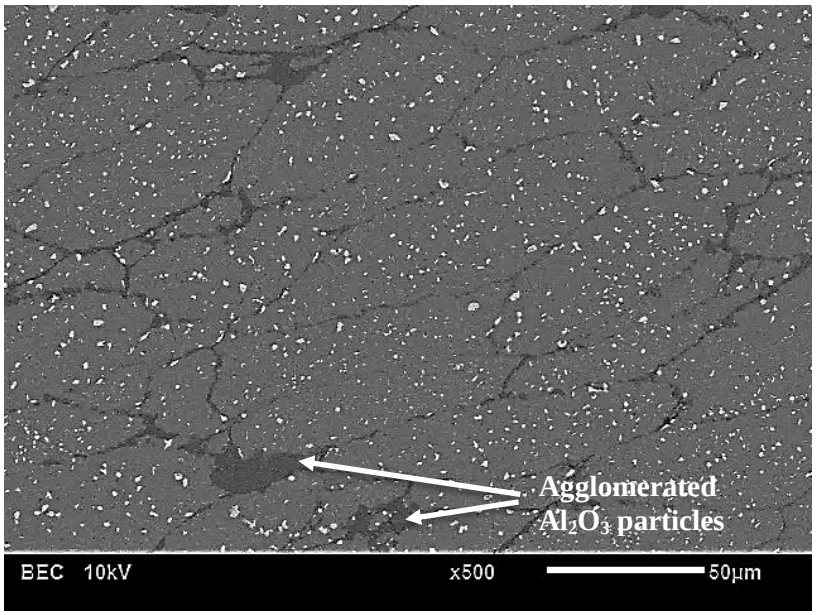

Figure 92: SEM BSE micrograph showing deformation in 2124-Al with 5% Al_2O_3 after extrusion at 280°C (scale bar=50 µm).

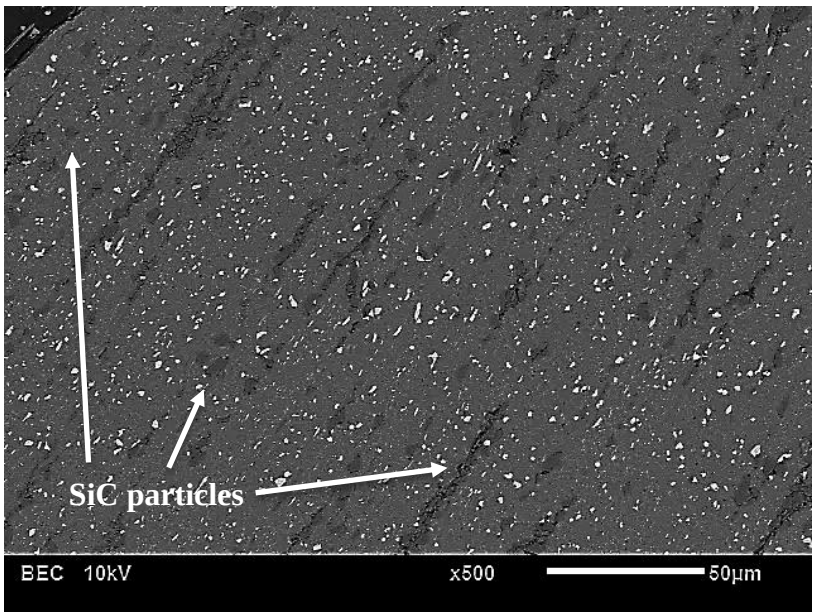

Figure 93: SEM BSE micrograph showing deformation in 2124-Al with 10 %SiC after extrusion at 280°C (scale bar=50 µm).

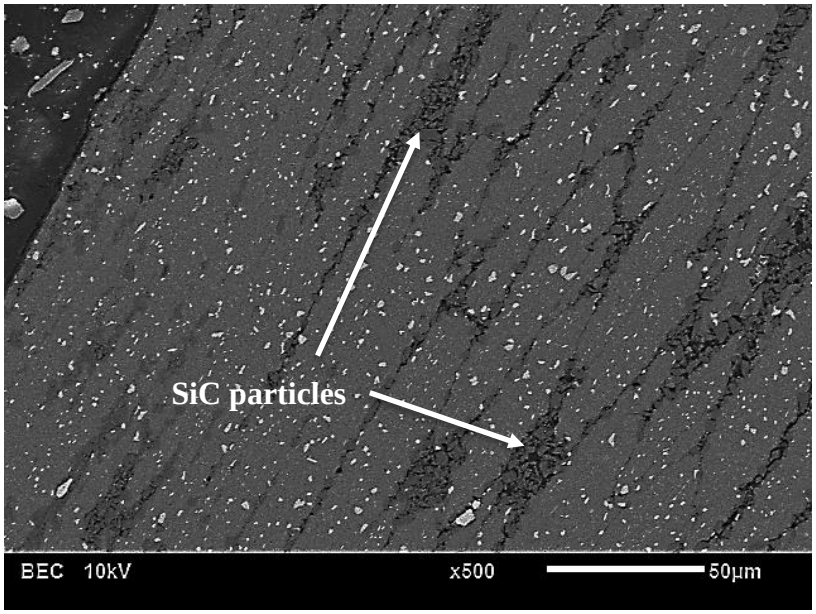

Figure 94: SEM BSE micrograph showing deformation in 2124-Al with 15% SiC after extrusion at 280°C (scale bar=50 µm).

4.9.2 Effect of extrusion on density

When the uniaxially compressed and extruded samples are compared it can be observed that the relative densities of the unreinforced 2124-Al and 2124-Al with 5% Al_2O_3 increased due to extrusion. However, extrusion led to a decrease in density in the SiC reinforced MMCs (Figure 95).

When compared, Figures 65 and 91 show that the unreinforced 2124-Al had less porosity in the extruded condition. It was inferred that the reduction in porosity together with improved bonding contributed to the increase in density in the extruded 2124-Al sample. When Figure 67 is compared to Figure 92, it can be observed that more deformation was achieved in the 2124-Al with 5% Al_2O_3 during extrusion. The grains in the extruded 2124-Al with 5%Al_2O_3 (Figure 92) are more elongated; showing more deformation. Thus, the increase in density in the 2124-Al with 5% Al_2O_3 after extrusion was attributed to improved deformation and bonding.

Figures 93 and 94 show that deformation was achieved in the SiC reinforced MMCs. However, the reduction in area achieved during extrusion of the SiC reinforced MMCs was only ~8%. It was deduced that the low reduction in area achieved resulted in poorer deformation and bonding during extrusion which in turn led to a lower density.

These results show that the degree of deformation achieved during extrusion had an influence on density. From the unreinforced 2124-Al sample it was seen that extrusion decreased porosity and increased density and poorer extrudability of SiC reinforced MMCs decreased density.

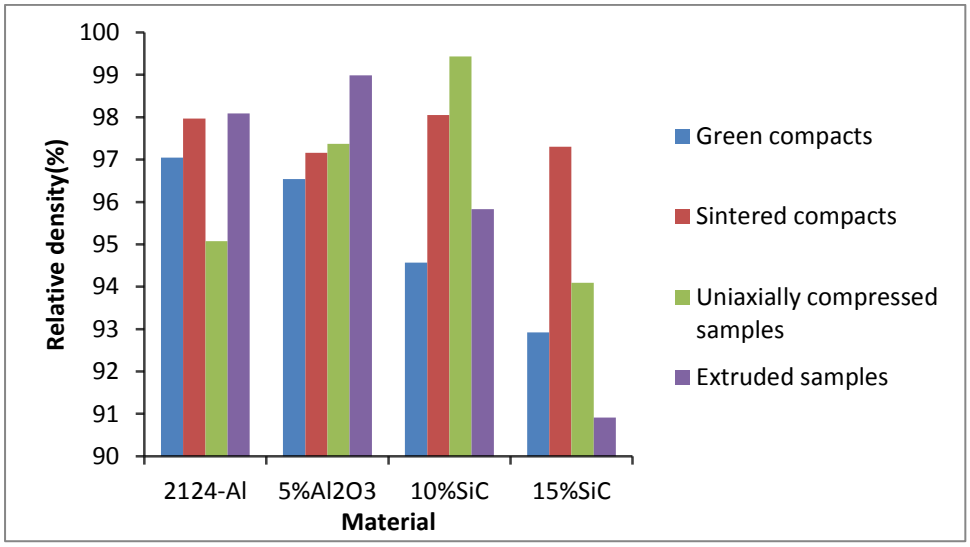

Figure 95: Relative densities of green compacts, sintered compacts, uniaxially compressed and extruded samples.

4.9.3 Hardness of extruded samples

Figure 96 shows that, in the extruded condition, the Al_2O_3 reinforced MMNC and SiC reinforced MMCs had higher hardness values when compared to the unreinforced 2124-Al. This result can be attributed to the strengthening effect of reinforcing particles. The

hardness values for the 5% Al_2O_3, 10% SiC and 15% SiC samples were found to be 60.01 $HV_{0.1}$, 74.14 $HV_{0.1}$ and 73.84 $HV_{0.1}$ respectively. It was also observed that SiC had a better strengthening effect in the extruded condition since the SiC reinforced samples (10 or 15 vol. %SiC) both had higher hardness values than the 2124-Al with 5% Al_2O_3.

Figure 95 shows that relative densities of the unreinforced 2124-Al and 2124-Al with 5%Al_2O_3 samples were similar after extrusion (2124-Al=98.09%, 5%Al_2O_3=98.99%) but the 2124-Al with 5%Al_2O_3 had a higher hardness (60.01 $HV_{0.1}$) when compared to the unreinforced 2124-Al (43.27 $HV_{0.1}$). This result further highlights the strengthening effect of reinforcing particles. It was thought that the presence of Al_2O_3 reinforcing particles increased the 2124-Al alloy's resistance to deformation since the Al_2O_3 particles can strengthen the alloy by restricting movement of dislocations, grains and grain boundaries (Casati & Vedani, 2014). X-ray mapping on the 2124-Al with 5%Al_2O_3 extruded sample showed that while the Al_2O_3 particles were concentrated on 2124-Al grain boundaries, some Al_2O_3 particles were also situated inside the 2124-Al grains (Figure 97). The Al_2O_3 particles inside the grains may have acted as obstacles to dislocations and increased resistance to deformation; thus increasing hardness.

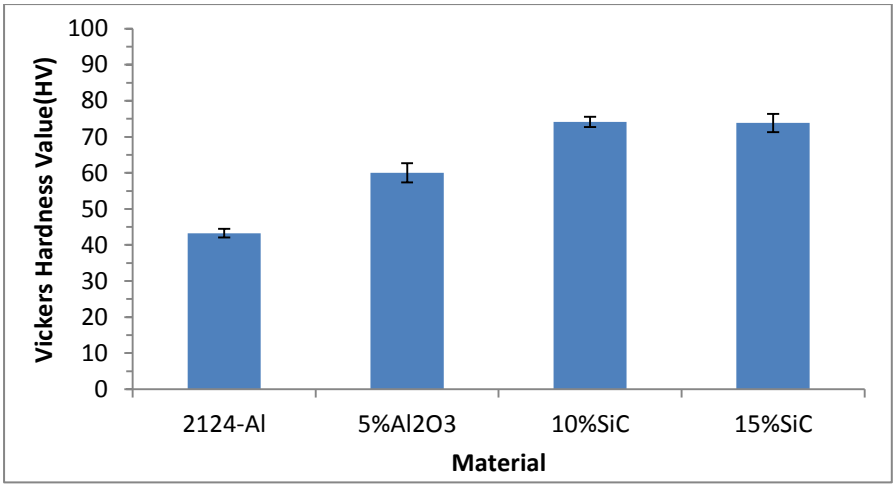

Figure 96: Hardness of extruded samples.

The 2124-Al with 10% SiC MMC had the highest hardness of 74.14 $HV_{0.1}$ after extrusion. Figure 95 shows that although this sample did not have the highest relative density after extrusion, its relative density was relatively high (*i.e.* 95.83%); indicating good densification. Figure 75 shows that the 10% SiC sample also had the highest hardness after uniaxial compression, where its surface and core had hardness values of 85.73 $HV_{0.1}$ and 97.96 $HV_{0.1}$ respectively. It can be observed that hardness was lower in the extruded

condition (74.14 $HV_{0.1}$). This was attributed to better deformation and densification achieved during uniaxial compression since the relative density of the 2124-Al with 10% SiC sample was higher after uniaxial compression (Figure 95).

When Figures 75 and 96 are compared it can be seen that, for all the materials, extrusion resulted in lower hardness values than uniaxial compression. For the unreinforced 2124-Al this result was unexpected since Figure 95 shows that the relative density achieved for the unreinforced 2124-Al after extrusion was higher than that achieved due to uniaxial compression. A comparison of Figures 91 (as-extruded) and 65 (uniaxially compressed) showed that extrusion led to a decrease in porosity; further supporting the notion of improved densification due to extrusion. The FEA (Section 4.8) showed the possibility of a slight increase in temperature during the extrusion process. Figure 85 shows that for the unreinforced 2124-Al, at a speed of 7 $mm.s^{-1}$, the temperature of the billet was expected to be ~298.58°C (*i.e.* slightly higher than selected temperature of 280°C). This increase in temperature was based on a friction coefficient of 0.1. Figures 88b and 89 showed that extrudability of MMNCs and MMCs was poor and this was attributed to lack of lubrication. This means that the friction coefficient may have been higher than 0.1 during extrusion. It was therefore thought that if the samples experienced more friction during extrusion, the temperature of the unreinforced 2124-Al sample may have been higher than 298.58°C and had an overageing effect on the unreinforced 2124-Al sample (making it softer), which would explain the lower hardness achieved after extrusion. The lower hardness values obtained after extrusion are indicative of poor extrudability. The use of a lubricant may improve extrudability of the MMNCs and MMCs and possibly improve hardness as well.

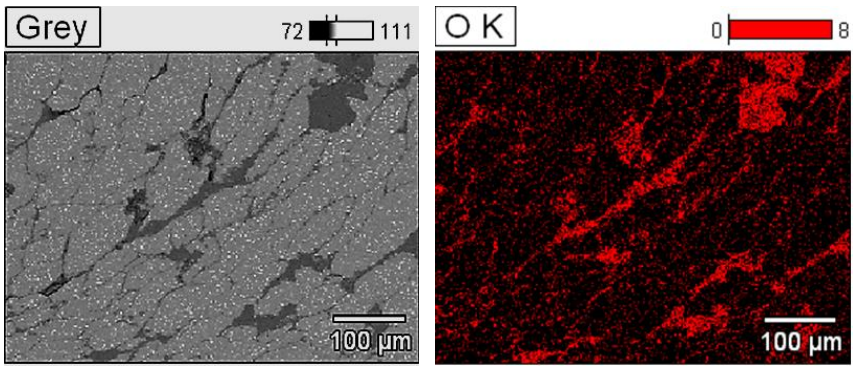

a b

Figure 97: X-ray mapping of Al_2O_3 reinforced MMNC after extrusion.

5 Conclusions

Uniaxial compression tests performed on a Gleeble 3500® were used to study the deformation behaviour of an Al_2O_3 reinforced (5 vol. %) MMNC and SiC reinforced (10 or 15 vol. %) MMCs within the warm working temperature range (i.e. 170 - 280°C). The results from the uniaxial compression tests were used as input data for a Finite Element analysis (FEA) on Abaqus. The uniaxial compression test results and FEA were used to design a warm temperature extrusion process. The extrudability of the MMNC and MMCs as well as the effect of deformation (in uniaxial compression and extrusion) on the distribution of reinforcing particles was evaluated. The following conclusions were drawn:

1. Uniaxial compression tests performed on a Gleeble 3500® can be used to study deformation behaviour of an Al_2O_3 reinforced MMNC and SiC reinforced MMCs at warm working temperatures and design a warm temperature extrusion process.

2. Extrudability of unreinforced 2124-Al was good while the Al_2O_3 reinforced MMNC and SiC reinforced MMCs had poorer warm temperature extrudability. Lack of lubrication was cited as the main contributing factor to poor extrudability.

3. Results from lab scale extrusion experimental trials for SiC reinforced MMCs did not coincide with results from uniaxial compression tests and FEA on Abaqus. Uniaxial compression tests and FEA showed that SiC reinforced MMCs can be successfully deformed and extruded at 280°C (although with minor defects e.g. surface cracks) while extrusion of SiC reinforced MMCs was unsuccessful.

4. To effectively design an extrusion process, using uniaxial compression tests and FEA, and improve the correlation between results obtained from uniaxial compression, FEA and lab scale extrusion experimental trials; friction conditions in the extrusion process have to be matched, (as closely as possible) to those in the uniaxial compression tests. Therefore highlighting need for lubrication during extrusion.

5. Engineering stress-strain curves showed that an increase in temperature (from ambient to 280°C) and strain rate (0.01 to $5s^{-1}$) improved the deformation behaviour of SiC reinforced MMCs.

6. The temperature and strain rate that resulted in uniaxially compressed samples with the best integrity were 280°C and 5 s^{-1} respectively.

7. Engineering stress-strain curves showed that deformation behaviour improved significantly when sintered MMC compacts were uniaxially compressed at 280°C and strain rate of 5 s^{-1} using a soaking time of 20 minutes.

8. The best deformation (*i.e.* good ductility; shown by large plastic region and high flow stress) was achieved in the 2124-Al with 10% SiC MMC because it plastically deformed at the highest stress (~153 MPa) up to the maximum total strain of 0.3.

9. A good distribution of Al_2O_3 reinforcing particles in 2124-Al alloy matrix was achieved after blending but this uniform distribution of Al_2O_3 particles was not maintained by cold compaction, uniaxial compression and extrusion. Thus highlighting that an alternate processing route is required for the Al_2O_3 reinforced MMNCs.

10. The distribution of SiC particles in 2124-Al with 10% SiC was improved slightly by deformation during uniaxial compression. SiC particles only dispersed inside slightly deformed 2124-Al grains, illustrating that deformation can improve distribution of SiC particles in Al alloy matrix.

11. Extrusion showed potential to improve distribution of SiC particles in 2124-Al grains; however more deformation is required.

12. Due to the nature of the cold compaction process (*i.e.* limited plastic flow), concentration of reinforcing particles (Al_2O_3 or SiC) at 2124-Al alloy grain boundaries occurred even in cases where a uniform distribution of reinforcing particles was achieved in the blending step.

13. Powder blending in a high energy ball mill produced a more uniform distribution of reinforcement phase in 2124-Al with nano-sized Al_2O_3 than 2124-Al with micron-sized SiC.

14. The morphology and size of the 2124-Al powder and distribution of Al_2O_3 or SiC on Al alloy particles were consistent over three batches.

6 Recommendations

To address some of the issues highlighted in this study, the following recommendations are made:

6.1 Improving the blending achieved in SiC reinforced MMCs

The poorer blending achieved in the SiC reinforced MMCs than Al_2O_3 MMNCs was attributed to poorer surface interaction between the SiC and Al alloy particles. Cheng *et al.* (2009) reported that SiC particles often contain impurities such as SiO_2, Al_2O_3 and Fe_2O_3 due to exposure to high temperatures when SiC is formed by baking. The amount of these impurities on SiC particle surfaces is small but they may act as barriers and hinder bonding between SiC and other materials. So, the surface interaction between the SiC and Al alloy particles was poor due to the probable presence of impurities on SiC particle surfaces. The bonding between SiC and Al alloy particles may be improved if the SiC particles are subjected to surface treatments (Cheng *et al*., 2009). It is thus recommended that the SiC particles be subjected to surface treatments prior to blending to improve surface interaction between SiC and Al alloy particles.

More blending experiments could also be done for SiC reinforced powders, to find alternative blending parameters for SiC reinforced MMCs.

6.2 Minimising agglomeration and concentration of reinforcing particles (Al_2O_3 or SiC) at 2124-Al grain boundaries

It was concluded that due to the nature of the cold compaction process (*i.e.* limited plastic flow), concentration of reinforcing particles (Al_2O_3 or SiC) at 2124-Al alloy grain boundaries occurred even in cases where a uniform distribution of reinforcing particles was achieved in the blending step. It is thus recommended that different consolidation techniques which will result in more plastic flow, such as spark plasma sintering (SPS), be explored to retain uniform distribution of Al_2O_3 reinforcing particles achieved during blending and reduce agglomeration. SPS may be effective in consolidating the blended powders with lower amount of agglomeration due its ability to apply pressure and heat simultaneously (Sweet *et al.*, 2015). So there will be more plastic flow than in cold compaction which may result in less agglomeration of reinforcing particle at grain boundaries.

Deformation at higher strains should also be explored.

6.3 Improving warm temperature extrudability of SiC reinforced MMCs

Uniaxial compression tests and FEA showed that it is possible to deform SiC reinforced MMCs in the warm working temperature range but extrusion of SiC reinforced MMCs failed. It was thought that this was due to higher friction during extrusion than during uniaxial compression. Thus it is recommended that lubrication be used during extrusion to decrease friction, making MMCs easier to deform and possibly improving extrudability.

6.4 Further work to determine the cause of shallow exothermic peaks identified in DSC study

Shallow exothermic peaks between 496 and 518°C were identified in the DSC study. Several literature studies on DSC analysis of Al-Cu-Mg alloys were consulted and none of the studies reported the presence of exothermic peaks between 496 and 518°C (Wang & Starink, 2007; Paul, 2014). In fact, no exothermic peaks were reported at temperatures above 340°C. It is recommended that an in-depth analysis on these exothermic peaks be done in future work.

6.5 Add more detail to analysis of microstructures of deformed samples

Evidence supporting the occurrence of DRX was not found in the microstructures of the SiC reinforced MMCs. It is recommended that, in future work, further analysis be done on these microstructures using transmission electron microscopy (TEM).

6.6 Improving extrudability of MMCs and MMNCs

It was observed that the extrudability of MMCs and MMNCs was poor. It is recommended that the die be lubricated to reduce friction and improve material flow.

7 References

Agarwal, B. D., Broutman, L. J. & Chandrashekhara, K. (2006).Composite materials. In *Analysis and Performance of Fiber Composites*.(3rd edn).New Dehli:John Wiley & Sons,Inc.

Aghajanian, M. K., Rocazella, M. A., Burke, J. T. & Keck, S. D. (1991). The fabrication of metal matrix composites by a pressureless infiltration technique. *Journal of Materials Science*, *26*(2), 447–454. http://doi.org/10.1007/BF00576541

Ahamed, H. & Senthilkumar, V. (2012). Hot deformation behavior of mechanically alloyed Al6063/0.75Al_2O_3/0.75Y_2O_3 nano-composite—A study using constitutive modeling and processing map. *Materials Science and Engineering: A*, *539*, 349–359. http://doi.org/10.1016/j.msea.2012.01.109

Angelo, P. & Subramanian, R. (Eds.). (2009). Stages in solid state sintering. *Powder Metallurgy:Science,Technology and Applications* (2nd Edn)., 132–134. New Dehli: PHI Learning Private Limited.

Arif, A. F. M., Sheikh, A. K. & Qamar, S. Z. (2003). A study of die failure mechanisms in aluminum extrusion. *Journal of Materials Processing Technology*, *134*(3), 318–328. http://doi.org/10.1016/S0924-0136(02)01116-0

Asadipanah, Z. & Rajabi, M. (2015). Production of Al–ZrB2 nano-composites by microwave sintering process. *Journal of Materials Science: Materials in Electronics*. http://doi.org/10.1007/s10854-015-3195-9

ASTM B962-17(2017), Standard Test Methods for Compacted and Sintered Powder Metallurgy (PM) Products using Archimedes' Principle, ASTM International, Westt Conshohocken,PA.

ASTM E92-17 (2017), Standard Test Methods for Vickers Hardness and Knoop Hardness of Metallic Materials, ASTM International, West Conshocken, PA.

Babu, N. K., Kallip, K., Leparoux, M., AlOgab, K. A., Reddy, G. M. & Talari, M. K. (2016). Characterization of microstructure and mechanical properties of friction stir welded AlMg5- Al_2O_3 nanocomposites. *Materials Science and Engineering A*, *658*, 109–122. http://doi.org/10.1016/j.msea.2016.01.102

Benbow, J. (1983). Mechanisms of compaction. *Enalrgement and Compaction of Particulate Solids* (1st Edn). Great Britain: Butterworth & Co Ltd.

Bohler Steel Africa. (2011). *Boehler W302 - Hot work tool steel*. Retrieved from http://www.bucorp.com/media/BOHLER_W302ISOBLOC.pdf

Borgonovo, C. & Apelian, D. (2011). Manufacture of Aluminum Nanocomposites: A Critical Review. *Materials Science Forum*, *678*, 1–22. http://doi.org/10.4028/www.scientific.net/MSF.678.1

Boyer, H. E. & Gall, T. L. (1985). Aluminium 2124. *ASM Aerospace Specification Metals Inc.* http://www.matweb.com/search/GetReference.aspx?matid=8913

Brush Wellman Inc. (2010). Strain Hardening & Strength. *Technical Tidbits*,(17),2-3.

Butrymowicz, D. B., Manning, J. R. & Read, M. E. (1973). Diffusion in Copper and Copper Alloys. *Journal of Physical and Chemical Reference Data*. http://doi.org/10.1063/1.3253129

Campbell, F.(2010). Secondary Processing of Discontinous MMCs. *Structural Composite Materials*. Ohio: ASM International.

Campbell, F.(Ed.)(2013). Powder Metallurgy Part Defects. *Inspection of Metals: Understanding the Basics*. Ohio: ASM International.

Casati, R. & Vedani, M. (2014). Metal Matrix Composites Reinforced by Nano-Particles—A Review. *Metals*, *4*(1), 65–83. http://doi.org/10.3390/met4010065

Cavaliere, P. (2002). Hot and warm forming of 2618 aluminium alloy. *Journal of Light Metals*, *2*(4), 247–252. http://doi.org/10.1016/S1471-5317(03)00008-7

Chaubey, A., Konda Gokuldoss, P., Wang, Z., Scudino, S., Mukhopadhyay, N. & Eckert, J. (2016). Effect of Particle Size on Microstructure and Mechanical Properties of Al-Based Composite Reinforced with 10 Vol.% Mechanically Alloyed Mg-7.4%Al Particles. *Technologies*, *4*(4), 37. http://doi.org/10.3390/technologies4040037

Chen, W. C., Davies, C. H. J., Samarasekera, I. V., Brimacombe, J. K. & Hawbolt, E. B. (1996). Mathematical modeling of the extrusion of 6061/Al_2O_3/20p composite. *Metallurgical and Materials Transactions A*, *27*(12), 4095–4111. http://doi.org/10.1007/BF02595658

Cheng, N. P., Li, C. M., Hui, Q. & Chen, Z. Q. (2009). Effect of particle surface treatment on the microstructure and property of SiCp/AA6066 composite produced by powder metallurgy. *Materials Science and Engineering A*, *517*(1-2), 249–256. http://doi.org/10.1016/j.msea.2009.04.005

Chu-ming, L., Shu-nong, J. & Xin-ming, Z. (2005). Continuous dynamic recrystallization and discontinuous dynamic recrystallization in 99.99% polycrystalline aluminium hot compression. *Transactions of Nonferrous Metals Society of China.*, *15*(1), 82–86. http://doi.org/1003-6326(2005)01-0082-05

Daniel, J. & Granholt, D.A. (2012). Masters thesis : Precipitate Structure Changes during Overaging in an Al-Mg-Si Alloy (June) from Norwegian University of Science & Technology.

Dasgupta, R., Das, S., Chaturvedi, S. & Jha, A. K. (2010). Effect of extrusion on properties of Al-based composite. *Transactions of Nonferrous Metals Society of China (English Edition)*, *20*(12), 2229–2233. http://doi.org/10.1016/S1003-6326(10)60633-4

Dasgupta, R., Jha, A. K. & Das, S. (2014). Effect of Addition of Fine SiC Particles on the Dry Sliding Wear Behaviour of Extruded 2014 Al-Alloy.International Scholarly Research Notices,2013 (2013),1-9..

Dash, K., Chaira, D. & Ray, B. C. (2013). Synthesis and characterization of aluminium-alumina micro- and nano-composites by spark plasma sintering. *Materials Research Bulletin*, *48*(7), 2535–2542. http://doi.org/10.1016/j.materresbull.2013.03.014

De Jonghe, L. C. & Rahaman, M. N. (2003). Sintering of Ceramics. *Handbook of Advanced Ceramics: Materials, Applications, Processing and Properties*. London : Elsevier Inc.http://doi.org/10.1016/B978-012654640-8/50006-7

Dieter, G. E. (1986). Mechanical Metallurgy.Metallurgy and Metallurgical Engineering series.USA: Mc-Graw-Hill Book Company,Inc.

Dieter, G. E., Kuhn, H. A. & Semiatin, S. L. (Eds.). (2003). *Handbook of Workability and Process Design*. United States of America: ASM International. http://doi.org/10.1361/hwpd2003p003

Doherty, R. D., Hughes, D. A., Humphreys, F. J., Jonas, J. J., Jensen, D. J., Kassner, M. E. & Rollett, A.D. (1997). Current issues in recrystallization: a review. *Materials Science and Engineering: A*, *238*(2), 219–274. http://doi.org/10.1016/S0921-5093(97)00424-3

Ezatpour, H. R., Torabi-Parizi, M. & Sajjadi, S. A. (2013). Microstructure and mechanical properties of extruded Al/Al_2O_3 composites fabricated by stir-casting process. *Transactions of Nonferrous Metals Society of China*, *23*(5), 1262–1268. http://doi.org/10.1016/S1003-6326(13)62591-1

Falticeanu, C., Chang, I. T., Kim, J. & Cook, R. (2006). *Sintering behaviour of Al-Cu-Mg-Si blends*. Busan,Korea. Retrieved from https://dspace.lboro.ac.uk/dspace-jspui/bitstream/2134/11228/6/Sintering.pdf

Fard, R. R. & Akhlaghi, F. (2007). Effect of extrusion temperature on the microstructure and porosity of A356-SiCp composites. *Journal of Materials Processing Technology*, *187-188*, 433–436. http://doi.org/10.1016/j.jmatprotec.2006.11.077

Faridmehr, I., Hanim Osman, M., Bin Adnan, A., Farokhi Nejad, A., Hodjati, R. & Amin Azimi, M. (2014). Correlation between Engineering Stress-Strain and True Stress-Strain Curve. *American Journal of Civil Engineering and Architecture*, *2*(1), 53–59. http://doi.org/10.12691/ajcea-2-1-6

Fleck, N., Hutchinson, J. & Tvergaard, V. (1989). Softening by void nucleation and growth in tension and shear. *Journal of Mechanics and Physics of Solids*, *37*(4), 515–540.

Fransson, C. (2009). Masters thesis : Accelerated aging of aluminum alloys (March) from Karlstads Universiteit.

Galindo-Rosales, F. J. & Rubio-Hernandez, F. J. (2010). Static and dynamic yield stresses of aerosil® 200 suspensionsin polypropylene glycol. *Applied Rheology*, *20*(2), 1–10. http://doi.org/10.3933/ApplRheol-20-22787

Garcia, W. (2015). Characteristics and Applications of Ti-alloy powders produced via Electrode Induction-Melting Gas Atomization.*Titanium Europe 2015*,May 11-13,Birmingham,UK.

Genders, R. (1954). US2675125A Direct and Indirect Extrusion of Metals. England: United States Patent Office. Retrieved from https://www.google.com/patents/US2675125

German, R. M. (1994). Compaction.*Powder Metallurgy Science* (2nd Edn). New Jersey: Metal Powder Industries Federation.

Giannelis, E. P. (1992). A new strategy for synthesizing polymer-ceramic nanocomposites. *Journal of Materials*, *44*(3), 28–30. http://doi.org/10.1007/BF03222789

Glass, S. J. & Ewsuk, K. G. (1995). Ceramic powder compaction. *American Ceramic Society International Symposium on Manufacturing Practices and Technology*. http://doi.org/10.1557/S0883769400034709

Govindarajan, R. & Aravas, N. (1994). Deformation Processing of Metal Powders. *International Journal of Mechanical Science*, *36*(4), 359–372.

Guo, R. Q., Rohatgi, P. K. & Nath, D. (1997). Preparation of aluminium – fly ash particulate composite by powder metallurgy technique. *Journal of Manufacturing Science*, *32*(15), 3971–3974. http://doi.org/10.1023/A:1018625118090

Guo-zheng, Q. (2013). Characterization for Dynamic Recrystallization Kinetics Based on Stress-Strain Curves. *Recent Developments in the Study of Recrystallization*, 61 – 64. http://doi.org/10.5772/54285

Gxowa, Z., Camagu, S. T., Govender, G. & Pereira, M. F. (2015). Reinforcement of 2124 Al alloy with low micron SiC and nano Al_2O_3 via solid-state forming. In H. K. Chikwanda & S. Chikosha (Eds.), *Light Metals Technology Conference 2015* (pp. 172–178). Port Elizabeth,South Africa: Trans Tech Publications Ltd. http://doi.org/10.4028/www.scientific.net/MSF.828-829.172

Hafizpour, H. R., Khoeini, M. & Branch, S. (2011). Compaction of Aluminum Matrix composites reinforced with nano/micro scale SiC Particulates. *Journal of American Science*, *7*(7), 753–759.

Hallberg, H., Wallin, M. & Ristinmaa, M. (2010). Simulation of discontinuous dynamic recrystallization in pure Cu using a probabilistic cellular automaton. *Computational Materials Science*, *49*(1), 25–34. http://doi.org/10.1016/j.commatsci.2010.04.012

Hao, S. M., Xie, J. P., Wang, A. Q., Wang, W. Y., Li, J. W. & Sun, H. L. (2014). Hot deformation behaviors of 35%SiCp/2024Al metal matrix composites. *Oral Oncology*, *50*(10), 2468–2474. http://doi.org/10.1016/S1003-6326(14)63372-0

Harris, C., Li, Q. & Jolly, M. R. (2004). Prediction of extruded microstructures using experimental and numerical. *La Metallurgia Italiana*, 31–35.

Hashim, J., Looney, L. & Hashmi, M. S. J. (1999). Metal matrix composites: production by the stir casting method. *Journal of Materials Processing Technology*, *92-93*, 1–7. http://doi.org/10.1016/S0924-0136(99)00118-1

Heckel, R. W. (1961). Density-Pressure Relationships in Powder Compaction. *Transactions of the Metallurgical Society of AIME*, *221*, 671–675.

Hesabi, R. Z., Hafizpour, H. R. & Simchi, A. (2007). An investigation on the compressibility of aluminum/nano-alumina composite powder prepared by blending and mechanical milling. *Materials Science and Engineering: A*, *454-455*, 89–98. http://doi.org/10.1016/j.msea.2006.11.129

Hirianiah, C. S. R. A., Harishanad, K. S. & Noronha, N. P. (2012). A review on hot extrusion of Metal Matrix Composites. International Journal of Engineering and Science, *1*(10), 30–35.

Hofmann, H. & Bowen, P. (2011). Part II: Compaction BT - Powder Metallurgy Science. *Powder Metallurgy Science*, 1–25.

Horiba Scientific. (2010). A Guidebook To Particle Size Analysis. *Distribution*. https://www.horiba.com/fileadmin/uploads/Scientific/eMag/PSA/Guidebook/pdf/PSA_Guidebook.pdf

Humphreys, F. & Hatherly, M. (Eds.). (1995). Softening by dynamic recovery. *Recrystallization and Related Annealing Phenomena* (1st Edn). Netherlands: Elsevier Science Ltd.

Jang, J. H., Nam, D. G., Park, Y. H. & Park, I. M. (2013). Effect of solution treatment and artificial aging on microstructure and mechanical properties of Al-Cu alloy. *Transactions of Nonferrous Metals Society of China (English Edition)*, *23*(3), 631–635. http://doi.org/10.1016/S1003-6326(13)62509-1

Jensrud, O. (1998). Warm-Deformation and the Age Hardening Response in Two Aluminium Alloys. *Advanced Light Alloys and Composites*. Dordrecht: Springer Netherlands. http://doi.org/10.1007/978-94-015-9068-6_54

Jiang, J., Collado, C., Keeley, D. & Dodd, B. (1995). Room temperature formability of particle- reinforced metal matrix composites: forging, extrusion and deep drawing. *Composites*, *26*(11), 785–789.

Jiang, J. & Dodd, B. (1995). Matrix composites in cold compression. *Composites*, *26*(March 1994), 62–66.

Jung, H. K., Cheong, Y. M., Ryu, H. J. & Hong, S. H. (1999). Analysis of anisotropy in elastic constants of SiCp/2124 Al metal matrix composites. *Acta Metallurgica*, *41*(12), 1261–1267.

Kaygısız, Y. & Maraşlı, N. (2015). Microstructural, mechanical and electrical characterization of directionally solidified Al–Si–Mg eutectic alloy. *Journal of Alloys and Compounds*, *618*(4), 197–203. http://doi.org/10.1016/j.jallcom.2014.08.056

Khan, I. N., Starink, M. J. & Yan, J. L. (2008). A model for precipitation kinetics and strengthening in Al-Cu-Mg alloys. *Materials Science and Engineering A*, *472*(1-2), 66–74. http://doi.org/10.1016/j.msea.2007.03.033

Kim, S. H., Chung, S. W. & Padmanaban, S. (2006). Investigation of lubrication effect on the backward extrusion of thin-walled rectangular aluminum case with large aspect ratio. *Journal of Materials Processing Technology*, *180*(1-3), 185–192. http://doi.org/10.1016/j.jmatprotec.2006.06.003

Klar, E. & Samal, P. K. (Eds.). (2007). Compacting and Shaping. *Powder Metallurgy Stainless Steels*. United States of America: ASM International.

Klimowicz, T. F. (1994). The Large-Scale Commercialization of Aluminum-Matrix Composites. *Journal of Materials*, *46*(11), 49–53.

Ko, B. C., Park, G. S. & Yoo, Y. C. (1999). Effects of SiC particle volume fraction on the microstructure and hot workability of SiCp/AA 2024 composites. *Journal of Materials Processing Technology*, *95*(1-3), 210–215. http://doi.org/10.1016/S0924-0136(99)00292-7

Ko, B.C. & Yoo, Y. C. (2000). Processing Map for Hot Working AA2024 Composites Reinforced with SiC Particle. *Materials Science Forum*, *331-337*(6), 1139–1144. http://doi.org/10.4028/www.scientific.net/MSF.331-337.1139

Koli, D. K. (2013). Properties and Characterization of Al-Al_2O_3 Composites Processed by Casting and Powder Metallurgy Routes (Review). *Composites*, *2*(4), 486–496.

Kunin, N. F. & Yurchenko, B. D. (1968). Net compaction pressure of metal powders. *Soviet Powder Metallurgy and Metal Ceramics*, *7*(8), 604–609. http://doi.org/10.1007/BF00780216

Li, L. X., Wang, G., Liu, J. & Yao, Z. Q. (2014). Flow softening behavior and microstructure evolution of Al-5Zn-2Mg aluminum alloy during dynamic recovery. *Transactions of Nonferrous Metals Society of China (English Edition)*, *24*(1), 42–48. http://doi.org/10.1016/S1003-6326(14)63026-0

Li, X., Liu, C. & Al-Samman, T. (2011). Microstructure and mechanical properties of Mg - 2Gd-3Y-0.6Zr alloy upon conventional and hydrostatic extrusion. *Materials Letters*, *65*(11), 1726–1729. http://doi.org/10.1016/j.matlet.2011.02.073

Li, Y. Y., Ngai, T. L., Zhang, D. T., Long, Y. & Xia, W. (2002). Effect of die wall lubrication on warm compaction powder metallurgy. *Journal of Materials Processing Technology*, *129*(1-3), 354–358. http://doi.org/10.1016/S0924-0136(02)00648-9

Liang, X., Earthman, J. C., Wolfenstine, J., & Lavernia, E. J. (1992). A comparison of techniques for determining the volume fraction of particulates in metal matrix composites. *Materials Characterization*, *28*(4), 173–178. http://doi.org/10.1016/1044-5803(92)90079-W

Lieblich, M., González-doncel, G., Ibáñez, J., Fernández, R., Rey, P., Vázquez, A. & Castro, G. (2006). Extrusion of Ingot and Powder Metallurgy Aluminum Matrix Composites Profiles. *(CENIM)Communicaciones Congresos*, 1–12.

Lim, C. Y., Lim, S. & Gupta, M. (2003). Wear behaviour of SiCp-reinforced magnesium matrix composites. In P. Blau & R.Bayer (Eds.), *14th International Conference on Wear Materials* (p. 636). Washington D.C: Elsevier B.V.

Lim, S. & Gupta, M. (1997). Friction and wear characteristics of Al–Cu/C composites synthesized using partial liquid phase casting process. *Materials & Design*, *18*(3), 161–166. http://doi.org/10.1016/S0261-3069(97)00095-2

Lima, F. M. S. (2012). Using surface integrals for checking Archimedes' law of buoyancy. *European Journal of Physics*, *33*(1), 101–113. http://doi.org/10.1088/0143-0807/33/1/009

Lindroos, V. K. & Talvitie, M. J. (1995). Recent advances in metal matrix composites. *Journal of Materials Processing Technology*, *53*(1-2), 273–284. http://doi.org/10.1016/0924-0136(95)01985-N

Liu, Y. B., Lim, S. C., Lu, L. & Lai, M. O. (1994). Recent development in the fabrication of metal matrix-particulate composites using powder metallurgy techniques. *Journal of Materials Science*, *29*(8), 1999–2007. http://doi.org/10.1007/BF01154673

Llorca, J. (2002). Fatigue of particle-and whisker-reinforced metal-matrix composites. *Progress in Materials Science*, *47*(3), 283–353. http://doi.org/10.1016/S0079-6425(00)00006-2

Long, B. D., Othman, R., Zuhailawati, H. & Umemoto, M. (2014). Comparison of two powder processing techniques on the properties of Cu-NbC composites. *Advances in Materials Science and Engineering*, *2014*. http://doi.org/10.1155/2014/160580

Lu, G. Q. & Shi, X. (1994). Computer-Simulation of Isostatic Powder Compaction By Random Packing of Monosized Particles. *Journal Of Materials Science Letters*, *13*(23), 1709–1711. http://doi.org/10.1016/j.jinorgbio.2011.09.033

Mason, J. & Ritchie, R. (1997). Fatigue crack growth resistance in SiC particulate and whisker reinforced P/M 2124 aluminum matrix composites. *Materials Science and Engineering: A*, *231*(1-2), 170–182. http://doi.org/10.1016/S0921-5093(97)00086-5

Mazen, A. A. & Emara, M. M. (2004). Effect of Particle Cracking on the Strength and Ductility of Al-SiCp Powder Metallurgy Metal Matrix Composites. *Journal of Materials Engineering and Performance*, *13*(1), 39–46. http://doi.org/10.1361/10599490417579

McQueen, H. J. & Bourell, D. L. (1987). Hot Workability of Metals and Alloys. *Journal of Materials*, *39*(9), 28–35. http://doi.org/10.1007/BF03257647

McWilliams, B., Ramesh, K. & Yen, C. (2012). Effect of Particle Size Distribution on the Response of Metal Matrix Composites. In V. Chalivendra, B. Song, & D. Casem

(Eds.), *Dynamic Behaviour of Materials*. New York: Springer Berlin Heidelberg. http://doi.org/10.1007/978-1-4614-4238-7

Meluch, L. (2009). PhD thesis : Warm Compaction of Aluminium Alloy Alumix 123, University of Birmingham.

Mimica, R. (2015). *Hardness versus time dependency during artificial ageing of AlMgSi$_{0.5}$ aluminium* alloy (Vol. 5). Croatia. Retrieved from hrcak.srce.hr/file/220540

Moghadam, A. D., Schultz, B. F., Ferguson, J. B., Omrani, E., Rohatgi, P. K. & Gupta, N. (2014). Functional metal matrix composites: Self-lubricating, self-healing, and nanocomposites-an outlook. *Journal of Materials*, *66*(6), 872–881. http://doi.org/10.1007/s11837-014-0948-5

Morse, M. B. (2011). Masters thesis : Effects of Grain Boundary Character on Dynamic Recrystallization Using a Modified Monte Carlo Method. (December) from Boise State University.

Nair, F. & Karamis, M. B. (2010). An investigation of the tribological interaction between die damage and billet deformation during MMC extrusion. *Tribology International*, *43*(1-2), 347–355. http://doi.org/10.1016/j.triboint.2009.06.018

Nazarenko, O. B., Amelkovich, Y. A. & Sechin, A. I. (2014). Characterization of aluminum nanopowders after long-term storage. *Applied Surface Science*, *321*, 475–480. http://doi.org/10.1016/j.apsusc.2014.10.034

Nestler, D., Siebeck, S., Podlesak, H., Wagner, S., Hockauf, M. & Wielage, B. (2011). Powder Metallurgy of Particle-Reinforced Aluminium Matrix Composites (AMC) by Means of High-Energy Ball Milling. *Integrated Systems, Design and Technology 2010* (pp. 93–107). Berlin, Heidelberg: Springer Berlin Heidelberg. http://doi.org/10.1007/978-3-642-17384-4_9

Norris, S. D. & Wilson, I. (1999). Application of 3D numerical modelling for thermal profile optimization on the Gleeble thermomechanical simulator. *Modelling and Simulation in Materials Science and Engineering*, *7*(3), 297–309. http://doi.org/10.1088/0965-0393/7/3/301

Oberacker, R. (2012). Powder Compaction by Dry Pressing. In R. Riedel & I.W. Chen (Eds.), *Ceramics Science and Technology*. Germany: Wiley-VCH.

Olson, G. B., Mescall, J. F. & Azrin, M. (1982). Adiabatic deformation and strain localisation. In : Meyers M.A, Murr,L.E (eds). *Shock Waves and High-Strain-Rate Phenomena in Metals.* Springer : Boston, MA

Orbulov, I. N. & Ginsztler, J. (2012). Compressive behaviour of metal matrix syntactic foams. *Acta Polytechnica Hungarica*, *9*(2), 43–56. http://doi.org/10.4028/www.scientific.net/MSF.729.68

Osakada, K. (1997). Effects of strain rate and temperature in forming processes of metals. *Le Journal de Physique IV*, *07*, 37–44. http://doi.org/10.1051/jp4:1997302

Ozkan, N. & Briscoe, B. J. (1997). Characterisation of Die-Pressed Green Compacts. *Journal of the European Ceramic Society*, *17*(5), 697–711. http://doi.org/10.1016/S0955-2219(96)00090-8

Ozturk, F., Ece, R. E., Polat, N., Koksal, A., Evis, Z. & Sheikh-Ahmad, J. Y. (2016). Application of Electric Resistance Heating Method on Titanium Hot Forming at Industrial Scale. *Arabian Journal for Science and Engineering*. http://doi.org/10.1007/s13369-016-2159-6

Pakdel, A., Farhangi, H. & Emamy, M. (2007). Effect of extrusion process on ductility and fracture behaviour of SiCp/aluminium-alloy composites. *8th International Fracture Conference*, 460–469.

Palumbo, G. (1998). US5817193A Metal alloys having improved resistance to intergranular stress corrosion cracking. United States Patent Office.

Parel, T. S., Wang, S. C. & Starink, M. J. (2010). Hardening of an Al-Cu-Mg alloy containing Types I and II S phase precipitates. *Materials and Design*, *31*(SUPPL. 1), S2–S5. http://doi.org/10.1016/j.matdes.2009.12.048

Park, B. G., Crosky, A. G. & Hellier, A. K. (2001). Material characterisation and mechanical properties of Al_2O_3-Al metal matrix composites. *Journal of Materials Science*, *36*(10), 2417–2426. http://doi.org/10.1023/A:1017921813503

Paul, C. (2014). Masters thesis : Effect of alumina particle additions on the aging kinetics of 2014-aluminum matrix composites. Naval Postgraduate School.

Perry, R. E., Ansel, G. & Dietrich, R. L. (1953). US2639809A Extrusion of continuous metal articles. United States of America: United States Patent Office.

Prasad, V. V. B., Bhat, B. V. R., Mahajan, Y. R. & Ramakrishnan, P. (2001). Effect of Extrusion Parameters on Structure and Properties of 2124 Aluminum Alloy Matrix Composites. *Materials and Manufacturing Processes*, *16*(6), 841–853. http://doi.org/10.1081/AMP-100108703

Prasad, Y. V. R., Rao, K. & Sasidhara, S. (Eds.). (2015). *A Compendium of Processing Maps* (second). Ohio: ASM International.

Qangule, L. (2015). Maters thesis : The influence of process route on mechanical property development in sintered commercially pure and blended elemental titanium. University of Cape Town.

Radomysel'skii, D. & Serdyuk, G. (1970). Use of viscoplastic porous solid model for solution of hpt plastic working problems. *Theory and Technology of the Component Formation Process*24 (2),96-101.

Rahimian, M., Ehsani, N., Parvin, N. & Baharvandi, H. R. (2009). The effect of particle size, sintering temperature and sintering time on the properties of Al-Al_2O_3 composites, made by powder metallurgy. *Journal of Materials Processing Technology*, *209*(14), 5387–5393. http://doi.org/10.1016/j.jmatprotec.2009.04.007

Rahimian, M., Ehsani, N., Parvin, N. & Baharvandi, H. R. (2009). The effect of sintering temperature and the amount of reinforcement on the properties of Al-Al_2O_3 composite. *Materials and Design*, *30*(8), 3333–3337. http://doi.org/10.1016/j.matdes.2008.11.027

Rahman, M. M., Ariffin, A. K., Nor, S. S. M. & Rahman, H. Y. (2011). Powder material parameters establishment through warm forming route. *Materials and Design*, *32*(1), 264–271. http://doi.org/10.1016/j.matdes.2010.05.058

Rajamuthamilselvan, M. & Ramanathan, S. (2012). Development of processing map for 7075 Al/20% SiCp composite. *Journal of Materials Engineering and Performance*, *21*(2), 191–196. http://doi.org/10.1007/s11665-011-9871-x

Ramesh, B. & Senthilvelan, T. (2010). Formability Characteristics of Aluminium Based Composites-A Review. *International Journal of Engineering and Technology*, *2*(1), 1–6. http://doi.org/10.7763/IJET.2010.V2.91

Rao, B. K., Khadar, M. S. A & Srinivasan, K. (1999). High temperature compression testing and determination of warm working temperature for commercial purity aluminium. *Bulletin of Materials Science*, *22*(1), 17–20. http://doi.org/10.1007/BF02745670

Ravichandran, M. & Dineshkumar, S. (2014). Synthesis of Al-TiO_2 Composites through Liquid Powder Metallurgy Route. *SSRG International Journal of Mechanical Engineering*,*1*(1).

Razavi-Tousi, S. S., Yazdani-Rad, R. & Manafi, S.A. (2011). Effect of volume fraction and particle size of alumina reinforcement on compaction and densification behavior of Al-Al_2O_3 nanocomposites. *Materials Science and Engineering A*, *528*(3), 1105–1110. http://doi.org/10.1016/j.msea.2010.09.085

Rdzawski, Z. (2010). Thermomechanical processing of CuTi4 alloy. Journal of Achievements in Materials and Manufacturing,*42*, 9–25.

Reti, A. M. (1970). Masters thesis : Thermomechanical Processing of Aluminium Alloys. Massachusetts Institute of Technology.

Robbins, P. (2012). Aluminum Extrusion as a Maturing Industry. *Light Metal Age*, (June),82-83.

Roy, A. (2014). Powder metallurgy. *Valery Marinov, Manufacturing Technology*, (1), 40–43.

Roylance, D. (2001). Stress-Strain Curves. Mechanics of materials,1-14.

Ryu, H. J. & Hong, S. H. (2000). Load transfer mechanism and mechanical properties of SiCw/Al metal matrix composites. *Metals and Materials*, *6*(1), 33–38. http://doi.org/10.1007/BF03026342

Sadanandam, J., Bhikshamaiah, G., Gopalakrishna, B., Suryanarayana, S. V, Mahajan, Y. R. & Jain, M. K. (1992). Effect of different reinforcements on the thermal expansion

of 2124 aluminium metal-matrix composites. *Journal of Materials Science Letters*, *11*, 1518–1520.

Saha, P. (2000). *Aluminium Extrusion Technology*. United States of America: ASM International.

Samanta, S. K. (1972). A new die profile with high process efficiency. *Applied Scientific Research*, *25*(1), 54–64. http://doi.org/10.1007/BF00382284

Saravanan, L. & Senthilvelan, T. (2015). Investigations on the Hot Workability Characteristics and Deformation Mechanisms of Aluminium alloy-Al_2O_3 Nanocomposite. *Materials & Design*, *79*, 6–14. http://doi.org/10.1016/j.matdes.2015.04.024

Selig, S. G. (2012). Masters thesis : Finite element simulation of the compaction and springback of an aluminium powder metallurgy alloy. Dalhousie University.

Sellars, C. M. (1985). Computer modelling of hot-working processes. *Materials Science and Technology*, *1*(April), 325–332. http://doi.org/10.1533/9781845699949.1.86

Selvan, R. M. & Ramanathan, S. (2013). Effect of silicon carbide volume fraction on the hot workability of 7075 aluminium-based metal-matrix composites. *International Journal of Advanced Manufacturing Technology*, *67*(5-8), 1711–1720. http://doi.org/10.1007/s00170-012-4604-3

Selvan, R. M., Ramanathan, S. & Karthikeyan, R. (2010). Processing map for hot working of SiCp/7075 Al composites. *Transactions of Nonferrous Metals Society of China (English Edition)*, *20*(4), 668–674. http://doi.org/10.1016/S1003-6326(09)60196-5

Serafini, T. T., Mcdanels, D. L. & Lewis, R. (1986). Polymer, Metal, and Ceramic Matrix Composites for Advanced Aircraft Engine Applications. *American Society for Metals*, *8*(1), 80–91.

Shao, J. C., Xiao, B. L., Wang, Q. Z., Ma, Z. Y., Liu, Y. & Yang, K. (2010). Constitutive flow behavior and hot workability of powder metallurgy processed 20vol.%SiCP/2024Al composite. *Materials Science and Engineering A*, *527*(29-30), 7865–7872. http://doi.org/10.1016/j.msea.2010.08.080

Sheikh, A. K., Qamar, S. Z. & Raza, M. K. (2002). Product Defects in Aluminum Extrusion and Their Impact on Operational Cost. *6th Saudi Engineering Conference* (Vol. 5). Dhahran, Saudi Arabia.

Shen, P., Elgallad, E. & Chen, X. (2013). On the aging behaviour of AA2618 DC cast alloy. In B. Sadler (Ed.), *Light Metals* (pp. 373–376). New Jersey: John Wiley & Sons, Ltd.

Sheppard, T., Tunnicliffe, P. J. & Patterson, S. J. (1982). Direct and indirect extrusion of a high strength aerospace alloy (AA 7075). *Journal of Mechanical Working Technology*, *6*(4), 313–331. http://doi.org/10.1016/0378-3804(82)90031-6

Shi, C., Lai, J. & Chen, X. G. (2014). Microstructural evolution and dynamic softening mechanisms of Al-Zn-Mg-Cu alloy during hot compressive deformation. *Materials*, *7*(1), 244–264. http://doi.org/10.3390/ma7010244

Simulia. (2007). Extrusion of a cylindrical metal bar with frictional heat generation. In *Abaqus Example Problems Manual* (pp. 75–94). United States of America: Abaqus Inc.

Singh, C. & Singh, J. (2014). Synthesis of Al- SiC Composite Prepared By Mechanical Alloying, *11*(3), 12–17. http://doi.org/10.9790/1684-11341217

Sjolander, E. & Seifeddine, S. (2010). The heat treatment of Al-Si-Cu-Mg casting alloys. *Journal of Materials Processing Technology*, *210*(10), 1249–1259. http://doi.org/10.1016/j.jmatprotec.2010.03.020

Skiba, J., Pachla, W., Mazur, A., Przybysz, S., Kulczyk, M., Przybysz, M. & Wróblewska, M. (2014). Press for hydrostatic extrusion with back-pressure and the properties of thus extruded materials. *Journal of Materials Processing Technology*, *214*(1), 67–74. http://doi.org/10.1016/j.jmatprotec.2013.07.014

Sri, T. S., Al-hajri, M., Smith, C. & Petraroli, M. (2009). The tensile response and fracture behaviour of 2009 aluminum alloy metal matrix composite, *346*(2003), 91–100.

Sridhar, I. & Fleck, N. A. (2000). Yield behaviour of cold compacted composite powders. *Acta Materialia*, *48*(13), 3341–3352. http://doi.org/10.1016/S1359-6454(00)00151-8

Srivatsan, T. S., Ibrahim, I. A., Mohammed, F. A. & Lavernia, E. J. (1991). Particulate reinforced metal matrix composites - a review. *Journal of Materials Science*, *26*, 1137–1156. http://doi.org/10.1007/BF01113872

Sundaresh, S. (2014). Masters thesis : A mesoscopic approach towards modelling of compaction process in powder metallurgy. The Ohio State University.

Suresh, K., Mahendran, S., Krupashankara, M. & Avinash, L. (2015). Influence of Powder Composition & Morphology on Green Density for Powder Metallurgy Processes. *International Journal of Innovative Research in Science, Engineering and Technology*, *04*(01), 18629–18634. http://doi.org/10.15680/IJIRSET.2015.0401037

Sweet, G.A., Brochu, M., Hexemer, R. L., Donaldson, I. W. & Bishop, D. P. (2015). Consolidation of aluminum-based metal matrix composites via spark plasma sintering. *Materials Science and Engineering: A*, *648*, 123–133. http://doi.org/10.1016/j.msea.2015.09.027

Syu, D. G. & Ghosh, A. (1993). The effect of temperature on the fracture mechanism in 2014/15vol.%Al_2O_3 composite. *Materials Science and Engineering*, *184*(1994), 27–35.

Taya, M. & Arsenault, R. J. (1989). Introduction. In *Metal Matrix Composites* (pp. 1–8). Elsevier. http://doi.org/10.1016/B978-0-08-036984-6.50006-5

Tekmen, C., Ozdemir, I., Cocen, U. & Onel, K. (2003). The mechanical response of Al-Si-Mg/SiCp composite: Influence of porosity. *Materials Science and Engineering A*, *360*(1-2), 365–371. http://doi.org/10.1016/S0921-5093(03)00461-1

Tian, B., Lind, C., Schafler, E. & Paris, O. (2004). Evolution of microstructures during dynamic recrystallization and dynamic recovery in hot deformed Nimonic 80a. *Materials Science and Engineering A*, *367*(1-2), 198–204. http://doi.org/10.1016/j.msea.2003.10.226

Tisza, M. (Ed.). (2002). Dynamic recrystallization. *Physical Metallurgy for Engineers* (2nd Edn). Ohio: Freund Publishing House Ltd.

Tiwari, S., Rajput, P. & Srivastava, S. (2012). Densification Behaviour in the Fabrication of Al-Fe Metal Matrix Composite Using Powder Metallurgy Route. *ISRN Metallurgy*, *2012*, 1–8. http://doi.org/10.5402/2012/195654

Tjong, S. (2000). Microstructural and mechanical characteristics of in situ metal matrix composites. *Materials Science and Engineering: R: Reports*, *29*(3-4), 49–113. http://doi.org/10.1016/S0927-796X(00)00024-3

Torralba, M. & Caruana, G. (1997). Extrudability of PM 2124/SiCp aluminium matrix composite. *Journal of Materials Science Letters*, *16*(9), 726–728. http://doi.org/10.1023/A:1018572812599

Totten, G., Howes, M. & Inoue, T. (Eds.). (2002). Powder Metallurgy Parts Manufacturing. In *Handbook of Residual STress and Deformation of Steel* (p. 398). ASM International.

Tumanov, A. & Portnoi, K. (1972). Composite materials. *Metal Powder Report*. http://doi.org/10.1016/S0026-0657(02)80648-8

Turenne, S., Godere, C., Thomas, Y. & Mongeon, P. E. (1999). Evaluation of friction conditions in powder compaction for admixed and die wall lubrication. *Powder Metallurgy*, *42*(3), 263–268. http://doi.org/10.1179/003258999665611

Turner, C. & Ashby, M. (1993). Experimental and Theoretical Modelling of the Isostatic Pressing of Composite Powders. In L. Delaey & H. Tas (Eds.), *Hot Isostatic Pressing* (pp. 3–14). Netherlands: Elsevier B.V.

Unal, R. & Dean, B. E. (1991). Taguchi approach to design optimization for quality and cost : an overview. *Annual Conference of the International Society of Parametric Analysts*.

Upadhyaya, G. (Ed.). (2002). Metal Powder Compaction. *Powder Metallurgy Technology* (1st Edn). Cambridge,United Kindgdom: Cambridge International Science Publishing.

Van Tyne, C. J. (2004). Design of Forming Processes:Bulk Forming. In L. Xie, K. Funatani & G. E. Totten (Eds.), *Handbook of Metallurgical Process Design* (pp. 1–22). Colorado: CRC Press.

Wang, J., Yang, H. T., Wang, X. G. & Xiao, H. (2015). A new mathematical model for predicting flow stress up to the critical strain during hot deformation. *Materials & Design*, *65*, 637–643. http://doi.org/10.1016/j.matdes.2014.09.072

Wang, S. C. & Starink, M. J. (2007). Two types of S phase precipitates in Al-Cu-Mg alloys. *Acta Materialia*, *55*(3), 933–941. http://doi.org/10.1016/j.actamat.2006.09.015

Wang, Z., Song, M., Sun, C., Xiao, D. & He, Y. (2010). Effect of extrusion and particle volume fraction on the mechanical properties of SiC reinforced Al-Cu alloy composites. *Materials Science and Engineering A*, *527*(24-25), 6537–6542. http://doi.org/10.1016/j.msea.2010.07.017

Yadav, D. & Bauri, R. (2012). Effect of friction stir processing on microstructure and mechanical properties of aluminium. *Materials Science and Engineering A*, *539*, 85–92. http://doi.org/10.1016/j.msea.2012.01.055

Yadav, P. T., Yadav, M. & Singh, P. D. (2012). Mechanical Milling: a Top Down Approach for the Synthesis of Nanomaterials and Nanocomposites. *Nanoscience and Nanotechnology*, *2*(3), 22–48. http://doi.org/10.5923/j.nn.20120203.01

Yamaoglu, R. & Olevsky, E. A. (2015). Consolidation of Al-nanoSiC Composites by Spark Plasma Sintering. *International Journal of Materials, Mechanics and Manufacturing*, *4*(2), 119–122. http://doi.org/10.7763/IJMMM.2016.V4.237

Yang, Y., Zhang, Z. & Zhang, X. (2012). Processing map of Al_2O_3 particulate reinforced Al alloy matrix composites. *Materials Science and Engineering: A*, *558*(0), 112–118. http://doi.org/10.1016/j.msea.2012.07.092

Yavuz, N. (1996). Mechanics of Dynamic Powder Compaction. *Journal of Engineering Sciences*, *2*(2), 129–136.

Zhang, J. & Di, H. (2016). Deformation heating and flow localization in Ti–15–3 metastable β titanium alloy subjected to high Z deformation. *Materials Science and Engineering A*, *676*, 506–509. http://doi.org/10.1016/j.msea.2016.09.011

Zhang, P., Li, F. & Wan, Q. (2010). Constitutive equation and processing map for hot deformation of SiC particles reinforced metal matrix composites. *Journal of Materials Engineering and Performance*, *19*(9), 1290–1297. http://doi.org/10.1007/s11665-010-9611-7

Zhang, Z. & Chen, D. (2006). Consideration of Orowan strengthening effect in particulate-reinforced metal matrix nanocomposites: A model for predicting their yield strength. *Scripta Materialia*, *54*(7), 1321–1326. http://doi.org/10.1016/j.scriptamat.2005.12.017

Zhou, J., Druzdzel, A. & Duszczyk, J. (1999). The effect of extrusion parameters on the fretting wear resistance of Al-based composites produced via powder metallurgy. *Journal of Materials Science*, *34*(20), 5089–5097.

Zhou, J., Li, L. & Duszczyk, J. (2004). Computer simulated and experimentally verified isothermal extrusion of 7075 aluminium through continuous ram speed variation.

Journal of Materials Processing Technology, *146*(2), 203–212. http://doi.org/10.1016/j.jmatprotec.2003.10.018

Zolotorevsky, V., Belov, N. & Glazoff, M. (2007). The Al-Cu-Mg system. *Casting Aluminum Alloys* (1st Edn). Great Britain: Elsevier.

Zonta, M. L. (2013). The efect of sintering temperature on microstructure and properties of Al-SiC composites. *Archives of Metallurgy and Materials*, *20*(1), 65–68. http://doi.org/10.2478/v10172-012-0148-7

8 Appendix A- Proof for equation used to calculate density of mixtures using wt %

To prove that $\frac{1}{\rho_{mix}} = \frac{x_A}{\rho_A} + \frac{x_B}{\rho_B} + \cdots$ the following procedure was used:

The first thing that should be noted is that the $x_A \; and \; x_B$ in the equation above are in wt%. If two components (A and B) are mixed to form a mixture, their mass fractions in the mixture would be expressed as:

$$wt.\%\; of\; component\; A = x_A = \frac{M_A}{M_{mix}} \quad [1]$$

And

$$wt.\%\; of\; component\; B = x_B = \frac{M_B}{M_{mix}} \quad [2]$$

The mixture is fabricated via a powder metallurgical processing route and it can be assumed that A and B do not react with each other and therefore masses and volumes are additive.

$$M_{mix} = M_A + M_B \quad [3]$$

And

$$V_{mix} = V_A + V_B \quad [4]$$

Equations [1] and [2] have to represent the mixture so variables that do not pertain to or describe the mixture (i.e. M_A and M_B) must be cancelled out. To do this, these two equations can be divided by density (ρ).Therefore equation [1] becomes :

$$\frac{x_A}{\rho_A} = \frac{(\frac{M_A}{M_{mix}})}{\rho_A}$$

It is known that $\rho_A = \frac{M_A}{V_A}$

Therefore:

$$\frac{x_A}{\rho_A} = \frac{M_A}{M_{mix}} * \frac{V_A}{M_A}$$

$$\frac{x_A}{\rho_A} = \frac{V_A}{M_{mix}} \quad [5]$$

The same procedure was followed for equation [2] and equation [6] becomes:

$$\frac{x_B}{\rho_B} = \frac{V_B}{M_{mix}} \quad [6]$$

Adding Equation [5] and [6] gives:

$$\frac{x_A}{\rho_A} + \frac{x_B}{\rho_B} = \frac{(V_A + V_B)}{M_{mix}} \quad [7]$$

Substituting Equation [4] into equation [7] gives:

$$\frac{x_A}{\rho_A} + \frac{x_B}{\rho_B} = \frac{V_{mix}}{M_{mix}} \quad [8]$$

$\frac{V_{mix}}{M_{mix}}$ Is in fact ρ inverse($\frac{1}{\rho_{mix}}$), therefore equation [8] becomes:

$$\frac{x_A}{\rho_A} + \frac{x_B}{\rho_B} = \frac{1}{\rho_{mix}} \quad [9]$$

9 Appendix B- Derivation of equation used to calculate densities of compacted, sintered, uniaxially compressed and extruded MMCs and MMNCs

Appendix A showed that the density of the 2124-Al alloy was calculated using equation 9.

$$\frac{1}{\rho_{mix}} = \frac{x_A}{\rho_A} + \frac{x_B}{\rho_B} + \cdots \quad [9]$$

where: ρ_{mix} = density of the 2124 aluminium alloy (g/cm^3)

x_x = mass fraction of element *x* in alloy

ρ_x = density of element *x* (g/cm^3)

When the reinforcement phase is added to the matrix the composite that is formed has a different density to the reinforcement phase and matrix. Equation 9 can only be used when the fraction (*x*) of a material is in terms of weight percent. In this work, the fraction of the reinforcement phase in the matrix was expressed in terms of volume percent. This meant that Equation 9 could not be used to calculate the densities of the composites that were fabricated. Thus an equation that could be used to calculate the densities of the composites was derived by referring to the proof of Equation 9 which is shown in Appendix A.

The derivation of the equation to calculate densities of composites in this work follows. If two components (e.g. A and B) are mixed together to form a mixture and the volumes of the components are known, the volume of the mixture can be calculated if it is assumed that volumes are additive since the components do not react in the mixture. The volume fractions of the components in the mixture can be expressed as:

$$Vol.\%\ of\ component\ A = Y_A = \frac{V_A}{V_{mix}} \quad [10]$$

and

$$Vol.\%\ of\ component\ B = Y_B = \frac{V_B}{V_{mix}} \quad [11]$$

Equations 10 and 11 have two terms for volume (V_x and V_{mix}) and to get rid of the volume terms pertaining to the individual components so that V_{mix} is the only volume term.

Equations 10 and 11 can be multiplied by the densities of components A and B, becoming:

$$Y_A\rho_A = \frac{V_A}{V_{mix}} * \rho_A \quad [12]$$

$$\rho_A = \frac{M_A}{V_A} \quad [13]$$

Substituting Equation [13] into [12]:

$$Y_A\rho_A = \frac{V_A}{V_{mix}} * \frac{M_A}{V_A}$$

Therefore:

$$Y_A\rho_A = \frac{M_A}{V_{mix}} \quad [14]$$

The same is done for Equation [11] and it becomes:

$$Y_B\rho_B = \frac{M_B}{V_{mix}} \quad [15]$$

Now [14] + [15] gives:

$$Y_A\rho_A + Y_B\rho_B = \frac{M_A}{V_{mix}} + \frac{M_B}{V_{mix}}$$

$$Y_A\rho_A + Y_B\rho_B = \frac{(M_A+M_B)}{V_{mix}} \quad [16]$$

The sum of the masses of components A and B equal to the mass of the mixture thus:

$$M_A + M_B = M_{mix} \quad [17]$$

Substituting [17] into [16]:

$$Y_A\rho_A + Y_B\rho_B = \frac{M_{mix}}{V_{mix}}$$

Therefore:

$$Y_A\rho_A + Y_B\rho_B = \rho_{mix} \quad [18]$$

Equation 18 was then used to calculate the theoretical densities of the unreinforced aluminium alloy, SiC reinforced MMCs and Al_2O_3 reinforced MMNC. This was useful in determining relative densities once densities of the compacts had been determined using Archimedes' principle.